How mitochondrial DNA mutations affect the growth of MCF-7 clones

A thesis submitted in partial fulfillment of the

requirements for the Degree of

Master of Science

in

Cellular and Molecular Biology

in the School of Biological Sciences, University of Canterbury,

New Zealand

Angie Yuan Yan, Sin

2006

THIS THESIS IS DEDICATED TO ALL MITOCHONDRIAL DISEASES PATIENTS.

TABLE OF CONTENTS

LIST OF FIGURES ..... **IV**

LIST OF TABLES ..... **VI**

ABSTRACT ..... **VIII**

CHAPTER 1: INTRODUCTION

1.1. The mitochondrion **1**

1.1.1. Background 1
1.1.2. Structure 2
1.1.3. Functions 3
1.1.4. Mitochondrial DNA (mtDNA) 5

1.2. Mitochondrial disorders **9**

1.2.1. Mitochondrial diseases 9
1.2.2. mtDNA mutation and male infertility 11
1.2.3. Mitochondria in aging and neurodegeneration 11
1.2.4. Mitochondrial DNA in human malignancy 12

1.3. Effect of extracellular ATP on cell proliferation **14**

1.4. Other effect of ATP **177**

1.5. MCF-7 cell line **18**

1.6. Hypothesis **18**

1.7. Aims of research **19**

CHAPTER 2: MATERIAL AND METHODS

2.1. Materials **20**

2.2. Methods **20**

2.2.1. Cell culture 20
2.2.2. Single cell clone isolation 21
2.2.3. Growth rate and doubling time 24
2.2.4. DNA extraction 24
2.2.5. Polymerase chain reaction (PCR) 25
2.2.6. Purification of PCR products 27
2.2.7. mtDNA sequencing and analysis 28

2.2.8. Sensitivity of heteroplasmy detection 29
2.2.9. Mutational analysis 29
2.2.10. Isolation of mitochondria 30
2.2.11. Quantitation of mitochondria (Bradford assay) 31
2.2.12. Enzyme assays 31
2.2.13. Effect of extracellular adenosine 5'-triphosphate (ATP) on cell proliferation 35
2.2.14. RNA extraction from cell cultures 36
2.2.15. Quantitation and visualisation of RNA 36
2.2.16. Reverse transcription of RNA 37
2.2.17. Statistical analysis 39

CHAPTER 3: RESULTS

3.1. Morphology and characteristics of the clone cells 40

3.2. Growth curve and doubling time 40

3.3. DNA extraction 44

3.4. PCR amplification and purification 45

3.5. mtDNA mutation analysis 49

3.6. Sensitivity of heteroplasmy detection 55

3.7. RNA secondary structure prediction 56

3.8. Amino acid sequence analysis 56

3.8.1. A4137G heteroplasmic mutation in D9 58
3.8.2. C9527T heteroplasmic mutation in B12 59
3.8.3. C11496T homoplasmic mutation in D4 60
3.8.4. C14263G heteroplasmic mutation in B12 61

3.9. Enzyme assays 62

3.10. Effect of extracellular ATP on cell proliferation 66

3.11. RNA extraction from cell cultures 69

3.12. Comparative reverse-transcription PCR (RT-PCR) 70

CHAPTER 4: DISCUSSION

4.1. Cell morphology and growth characteristics 73

4.2. Mutational analysis 74

4.2.1. Amino acid change in ND1 74
4.2.2. Amino acid change in COX III 76
4.2.3. Amino acid change in ND4 77
4.2.4. Amino acid change in ND6 79

4.2.5. RNA secondary structure prediction 80

4.3. Enzyme assays 81

4.4. Effect of extracellular ATP on cell proliferation 84

4.5. Comparative RT-PCR analysis 86

4.6. Future directions 87

4.7. Conclusions 88

ACKNOWLEDGEMENTS 89

REFERENCES 91

APPENDICES

Appendix 1: Abbreviations 101
Appendix 2: Recipes 102
Appendix 3: Raw data of results 104

LIST OF FIGURES

Figure 1.1.	Electron micrograph and diagram showing the structure of a mitochondrion.	2
Figure 1.2.	Mitochondrial respiratory chain.	4
Figure 1.3.	Human mitochondrial genome.	7
Figure 1.4.	Alteration in cancer cell function by different modes of action of P2 receptor subtypes.	17
Figure 2.1.	Preparation of conditioned medium.	22
Figure 2.2.	Dilution cloning method.	23
Figure 3.1.	Growth morphology and characteristics of MCF-7 clones in culture.	41
Figure 3.2.	Growth curve of the six single cell clones.	42
Figure 3.3.	Analytical gel showing DNA extracted from the three clones of MCF-7 cells.	44
Figure 3.4.	PCR amplification of mtDNA isolated from three single clones (Primer pairs A and B).	45
Figure 3.5.	PCR amplification of mtDNA isolated from three single clones (Primer pairs C and D).	46
Figure 3.6.	PCR amplification of mtDNA isolated from three single clones (Primer pairs E and F).	46
Figure 3.7.	PCR amplification of mtDNA isolated from three single clones (Primer pairs G and H).	47
Figure 3.8.	PCR amplification of mtDNA isolated from three single clones (Primer pairs I and J).	47
Figure 3.9.	PCR amplification of mtDNA isolated from three single clones (Primer pairs K and L).	48
Figure 3.10.	PCR amplification of mtDNA isolated from three single clones (Primer pair M).	48
Figure 3.11.	Sequencing patterns of the mutation sites in mitochondrial 16S rRNA gene from the three clones.	52

Figure 3.12.	Identification of C9527T mutation in the mitochondrial COX III gene.	53
Figure 3.13.	Identification of C14263G mutation in the mitochondrial ND6 gene.	53
Figure 3.14.	Identification of A4137G mutation in the mitochondrial ND1 gene.	54
Figure 3.15.	Identification of C11496T mutation in the mitochondrial ND4 gene.	54
Figure 3.16.	Detection of A2520T mtDNA heteroplasmy.	55
Figure 3.17.	Secondary structures prediction of 16S rRNA by the RNAfold software.	57
Figure 3.18	nnpredict secondary structure prediction for ND1 at amino acid residue 277.	58
Figure 3.19.	nnpredict secondary structure prediction for COX III at amino acid residue 107.	59
Figure 3.20.	nnpredict secondary structure prediction for ND4 at amino acid residue 246.	60
Figure 3.21.	nnpredict secondary structure prediction for ND6 at amino acid residue 138.	61
Figure 3.22.	Citrate synthase activity in B12, D4 and D9.	63
Figure 3.23.	Respiratory chain biochemistry in MCF-7 clones.	64
Figure 3.24.	Growth morphology and characteristic showing the effect of extracellular ATP on cultured cells.	67
Figure 3.25.	Effect of the extracellular ATP on growth rate.	68
Figure 3.26.	Representative gel image of total RNA.	69
Figure 3.27.	Representative results of RT-PCR analysis.	71
Figure 3.28.	Graphical representation of the comparative RT-PCR.	72
Figure 4.1.	The effect of mtDNA mutations on oxidative phosphorylation.	82

LIST OF TABLES

Table 1.1.	Composition of the respiratory chain and oxidative phosphorylation system.	8
Table 1.2.	Differences in genetic code between mitochondrial genome and nuclear genome.	8
Table 1.3.	Proposed subclassification of P2 purinoceptors.	15
Table 2.1.	Primer pairs used for the PCR amplification of mtDNA.	26
Table 2.2.	Additional mtDNA primers used for ABI sequencing.	28
Table 2.3.	mtDNA primers used in RT-PCR.	38
Table 3.1.	Doubling time of six cell clones.	43
Table 3.2.	Tukey HSD test of six single cell clones.	43
Table 3.3.	The purity and concentration of DNA from three clones.	44
Table 3.4.	Common mutations in MCF-7 clones with respect to human mtDNA sequence.	50
Table 3.5.	Summary of the single nucleotide polymorphisms (SNPs) detected in three clones.	51
Table 3.6.	Hydropathicity and polarity analysis of amino acid residue 277 of ND1.	58
Table 3.7.	Hydropathicity and polarity analysis of amino acid residue 107 of COX III.	59
Table 3.8.	Hydropathicity and polarity analysis of amino acid residue 246 of ND4.	60
Table 3.9.	Hydropathicity and polarity analysis of amino acid residue 138 of ND6.	61
Table 3.10.	Mitochondrial OXPHOS enzyme-specific activities in MCF-7 clones.	63
Table 3.11.	Statistical significance analysis of citrate synthase (CS) and the normalised mitochondrial respiratory enzyme activities in B12, D4 and D9 clones.	65
Table 3.12.	Doubling time of B12 (at different ATP concentration) and D4 (without ATP).	66

Table 3.13.	Tukey HSD test of B12 (at different ATP concentration) and D4 (without ATP).	69
Table 4.1.	Amino acid homology showing comparison of residue 277 between species.	75
Table 4.2.	Amino acid homology showing comparison of residue 107 between species.	77
Table 4.3.	Amino acid homology showing comparison of residue 246 between species.	78
Table 4.4.	Amino acid homology showing comparison of residue 138 between species.	79

ABSTRACT

Mitochondria are the main sites for adenosine triphosphate (ATP) generation within most cells. Structural and functional alterations of mitochondria due to genetic abnormalities of mitochondria can cause respiratory chain dysfunction. In this study, the important role of mitochondria in energy metabolism was determined by comparing the effect of mitochondrial DNA (mtDNA) mutations on growth patterns and oxidative phosphorylation (OXPHOS) enzyme activities of six isolated clones (B5, B12, D4, D9, E1 and E8); as well as the effect of ATP supplement to culture using the slowest growing clone. The isolated clones had shown distinct growth pattern and morphology. The difference in proliferation rates among the clones was ascertained by the doubling times (B5=26.4h. B12=43.2h. D4=25.7h. D9=33.6h. E1=26.9h and E8=28.8h). The clone's slow growth rate was likely the result of mitochondrial mutations in the 16S rRNA gene, ND1, ND4, ND6 and COX III. Five heteroplasmic mutations were found in clone B12 (G2480T, C2513G, A2520T, C9527T and C14263G), one heteroplasmic mutation in clone D9 (A4137G) and one homoplasmic mutation in clone D4 (C11496). The mutations in clone B12 appeared to be deleterious to the cell by disrupting mitochondrial OXPHOS activities and reducing energy output. Additionally, extracellular ATP supplement to OXPHOS deficient clone B12 facilitated cell growth and enhances the gene expression. Increased expression of mtDNA-encoded respiratory chain complexes observed in clone B12 compared to clone D4 may reflect mitochondrial genomic adaptation to perturbations in cellular energy requirements. The stimulation of mitochondrial biogenesis may be a cellular response in compensation for defects in OXPHOS associated with mtDNA mutations. My data support the hypothesis that the variability in functional manifestations of mtDNA is attributed to the nature of the mutation, number of mutation and the gene specifically affected. These results will help to further our understanding of the relationship between mitochondrial mutation and cellular function.

Keywords: MCF-7, cell doubling time, mitochondrial DNA mutation, OXPHOS defect, ATP, gene expression

1.1. The mitochondrion

Mitochondria have been extensively studied in the past decades. These membrane-bound cytoplasmic organelles have received ample interest from researchers from different scientific fields due to their function and remarkably unique properties. Mitochondria have a pivotal role in cellular energy metabolism, being the major site of ATP synthesis via oxidative phosphorylation (OXPHOS). This chapter will briefly review current understanding of the structure and function of mitochondria, as well as the effect of mitochondrial DNA (mtDNA) mutation on their oxidative potential and ATP production which ultimately lead to a myriad of diseases.

1.1.1. Background

According to the endosymbiotic theory of Gray *et al*. (1999), double-membraned mitochondria are evolved from facilitated aerobic bacteria. Their closest living relatives, based on ribosomal RNA comparisons are the α-proteobacteria (in particular Rickettsia). Gray *et al*. (1999) suggested that mitochondria originated as separate prokaryotic organisms, which were engulfed by a nucleus-containing host cell without being digested. When they became incorporated into the cytoplasm, the mitochondria developed a symbiotic relationship with the host cell. The outer membrane represents the plasma membrane of the ancestral feeder host cell; the inner membrane corresponds to the plasma membrane of the ancestral endosymbiont. Several lines of evidence supporting the theory include: (1) The genome of mitochondria reside within a single, circular DNA molecule that is devoid of histone proteins, which resemble bacterial genophores. (2) Mitochondrial ribosomes are about the same size as those in bacteria. (3) Mitochondria reproduce asexually in a manner resembling binary fission in bacteria. (4) As in bacteria, mitochondrial genomes encode rRNA and tRNA for their own protein synthesis.

1.1.2. Structure

Mitochondria are bounded by two membranes separated by a narrow fluid-filled space. The outer membrane contains specialised transport proteins called porins, which allow passage of molecules with molecular weights as high as 10,000 dalton into the intermembrane space. The inner membrane is highly impermeable to small ions due to the high concentration of a phospholipid, cardiolipin. The inner membrane is highly folded into irregular series of partitions called cristae. The cristae protrude into the central space of the mitochondrion, the matrix (Fig. 1.1). The cristae increase the surface area for reactions that depend upon the creation of a proton gradient across the cristae. They are the sites of the enzymes of aerobic respiration and ATP production. The matrix consists of numerous compounds such as proteins, lipid and nucleic acid. All mitochondria contain multiple copies of their genomes in the matrix (Campbell and Reece, 2002).

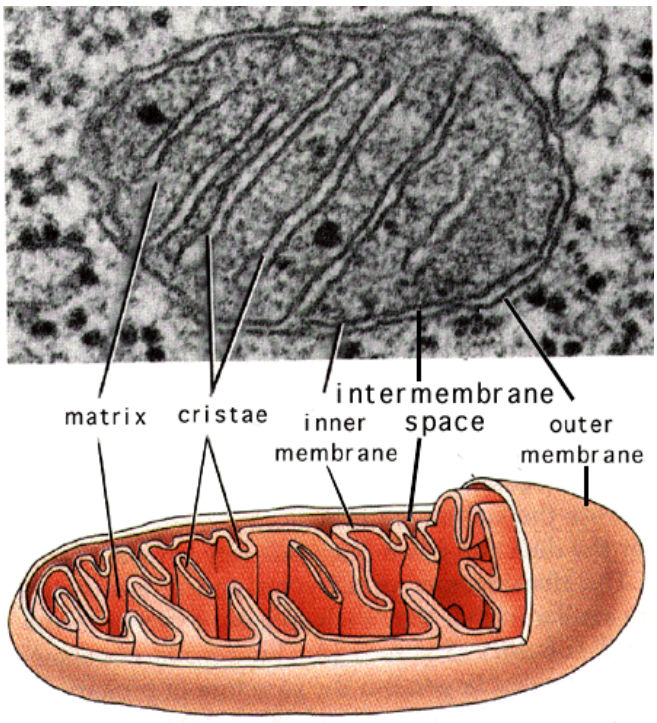

Figure 1.1. Electron micrograph and diagram showing the structure of a mitochondrion. Adapted from Purves *et al*. (1994).

There are several unique characteristics of mitochondria that could contribute to the pathogenesis of diseases associated with defects in mitochondrial genome. Current understanding of mitochondrial genetics include: (1) maternal inheritance, (2) mitotic segregation, (3) high mutation rate in mtDNA, (4) heteroplasmy, (5) threshold effect in phenotypic expression of mutant mtDNA, and (6) accumulation of somatic mtDNA mutations in aging and degenerative diseases (Schon, 2000; Pulkes and Hanna, 2001).

1.1.3. Functions

Mitochondria generate cellular energy in the form of adenosine triphosphate (ATP) via the process of oxidative phosphorylation (OXPHOS). The energy-producing pathway consists of the proton-translocating respiratory chain complexes I, III and IV, the proton-utilising ATP synthase (complex V), and a set of accessory complexes that supply electrons to coenzyme Q (ubiquinone), including complex II, the electron-transfer flavoprotein-ubiquinone oxidoreductase (ETF-QO), and dihydroorotate dehydrogenase (Smeitink *et al*., 2006) (Fig. 1.2). These OXPHOS components are located within the mitochondrial inner membrane.

Pyruvate, which is generated by glycolysis in the cytosol, enters mitochondria when oxygen is available. It is then enzymatically converted to acetyl coenzyme A (acetyl CoA) and carbon dioxide. Acetyl CoA enters the Krebs cycle in the matrix of mitochondria. Coenzymes such as flavin adenine dinucleotide (FAD) and nicotinamide adenine dinucleotide (NAD) serve as electron carriers, which transfer electrons to ubiquinone in the respiratory chain. Together with cytochromes, they make up an electron transport chain. This coupled series of oxidation-reduction (redox) reactions passes electrons from hydrogen atoms along the membrane-bound carrier molecules. Most of the energy decrease at each of the three redox steps of the electron cascade of mitochondria is used to synthesise ATP, whereas the remainder energy is lost as heat. Oxygen is the final acceptor of hydrogen ions and electrons; water is the end product of this electron cascade. Several molecules of ATP are synthesised from

ADP along this pathway. The net energy yield from oxidative respiration may be as high as 38 ATP molecules per molecule of glucose (two each by substrate-level phosphorylation during glycolysis and the Krebs cycle; 34 from oxidative phosphorylation via the electron transport chain).

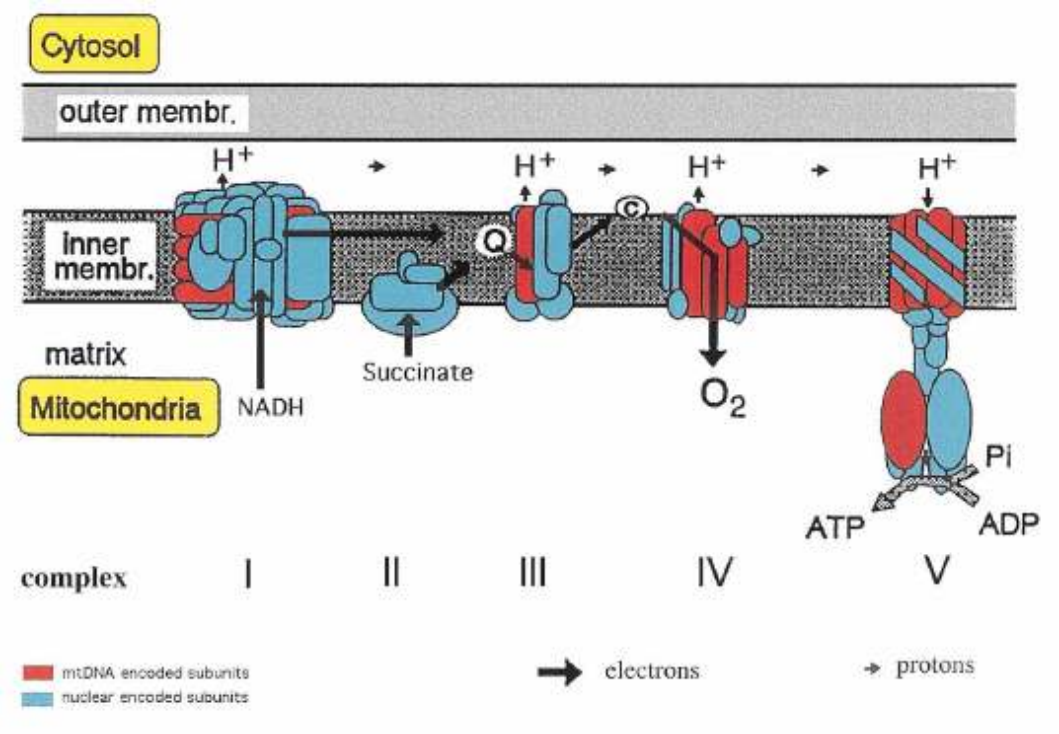

Figure 1.2. Mitochondrial respiratory chain. NADH, reduced form of nicotinamide adenine dinucleotide; Q, coenzyme Q (ubiquinone); c, cytochrome c; H^+, proton; ADP, adenosine diphosphate; ATP, adenosine triphosphate. The direction of protons and electron flux and are indicated by arrows. All five enzymatic multi-heteromeric complexes (I, II, III, IV and V) are embedded in the inner membrane of mitochondria. Reducing equivalents from the tricarboxylic acid cycle are transferred to OXPHOS as NADH (at complex I), or reduced flavins (entering at complex II). Coenzyme Q and cytochrome c serve as electron shuttles between the complexes. Adapted from Hanna and Nelson (1999).

The respiratory chain transfers electrons from reduced substrates down a stepwise energy gradient, finally to molecular oxygen to form water. The energy released is used by complexes I, III and IV to pump protons (H^+) out of the mitochondrial matrix into the intermembrane space. A proton electrochemical potential gradient is generated across the inner mitochondrial membrane. This proton motive force (PMF) is harnessed by complex V (ATP synthase), which is essentially an ATP-hydrolysing pump, to synthesise adenosine triphosphate (ATP) from adenosine diphosphate (ADP) and inorganic phosphate (Pi) (Chinnery and Schon, 2003). Some of the matrix ATP is used for the mitochondrion's own needs, but most of it is transported outside the organelle by the adenine nucleotide translocator (ANT) and used for diverse cell functions (Hatefi, 1985).

1.1.4. Mitochondrial DNA (mtDNA)

(i) Structure and functions

The human mitochondrial genome is a circular molecule consisting of 16,569 base pairs (bp) of nucleotides. There are multiple copies of mitochondrial DNA (mtDNA) in each mitochondrion. They are located in the mitochondrial matrix. All of the coding sequences are contiguous with each other, and the coding regions have no introns. There is a non-coding region of 1124 bp, the displacement-loop (D-loop), which contains regulatory sequences controlling both transcription and replication of mtDNA (Anderson *et al*., 1981). The D-loop, the hypervariable region, is most prone to mutation. There are two complementary DNA strands the heavy (O_H) and light (O_L) strands, which can be distinguished by their density. The O_L strand is rich in cytosines, and the O_H strand is rich in guanines. The origin of replication of the heavy strand (O_H) is located in the D-loop, whereas the origin of replication of the light strand (O_L) is located farther on the genome. Transcription takes place in opposite directions for the two strands starting from their respective promoters (Baggetto, 1993). The O_L strand serves as the template for the continuous synthesis of a new O_H strand, an origin of replication site that corresponds to a transcriptional promoter on the light chain (Klug

and Cummings, 2000). The O_H strand gives polycistronic RNAs that are subsequently matured by endonucleolytic cleavages upstream and downstream of the tRNA sequences (Tan *et al*., 2002). Ribosomal RNAs are then modified post-transcriptionally by the addition of short adenyl stretches, whereas the mitochondrial mRNAs are polyadenylated by a mitochondrial poly(A) polymerase during or immediately after cleavage (Ojala *et al.,* 1981). As mtDNA uses a different genetic code from nuclear DNA, mitochondrial mRNA cannot be translated in the cytosol (Anderson *et al.,* 1981).

The mtDNA encodes for 37 genes that are involved in cellular energy production. These 37 genes include 13 of the ~85 polypeptides comprising the OXPHOS complexes (subunits of complexes I, III, IV, and V), along with two rRNAs and 22 tRNAs that are required for their translation (Anderson *et al*., 1981) (Fig. 1.3). Complex I or NADH-ubiquinone oxidoreductase, which accomplishes the oxidation of NADH derived by the oxidation of pyruvate, contains seven subunits (ND1-ND6 and ND4L) and at least 30 nuclear-encoded subunits (Smeitink *et al*., 2001). Complex II or succinate-ubiquinone oxidoreductase, which accomplishes the oxidation of $FADH_2$ derived from fatty acid and the Krebs' cycle, is composed of four nuclear-encoded subunits. Complex III or ubiquinol-ferricytochrome c oxidoreductase, which catalyses the transfer of two electrons from ubiquinol to ferricytochrome c, holds one mtDNA encoded subunit (cytochrome b) and 10 subunits encoded by the nuclear genome. Complex IV or cytochrome c oxidase (COX) catalyses electron transfer from cytochrome c to molecular oxygen and pumps protons to the intermembrane space. Complex IV consists of three mtDNA encoded subunits (COX I-III) and other 10 by nuclear DNA. Complex V or ATP synthase (ATPase) acts as a rotary motor coupled proton gradient generated by the respiratory chain to phosphorylate matrix ADP. Complex V is composed of two mtDNA encoded subunits (ATPase 6 and 8), plus 14 nuclear DNA encoded subunits (Zeviani and Di Donato, 2004). Table 1.1 summarises the composition of the five mitochondrial membrane-bound enzyme complexes that are involved in OXPHOS. The degree of impairment of the complexes usually matches their content of mitochondrially encoded components: complex I > complex IV > complex V > complex III (James and Murphy, 2002). In addition, the other OXPHOS polypeptides, and proteins involved in mtDNA maintenance and expression are all

encoded by the nuclear genome. These components are synthesised in the cytoplasm and imported into the mitochondria (Chinnery and Schon, 2003).

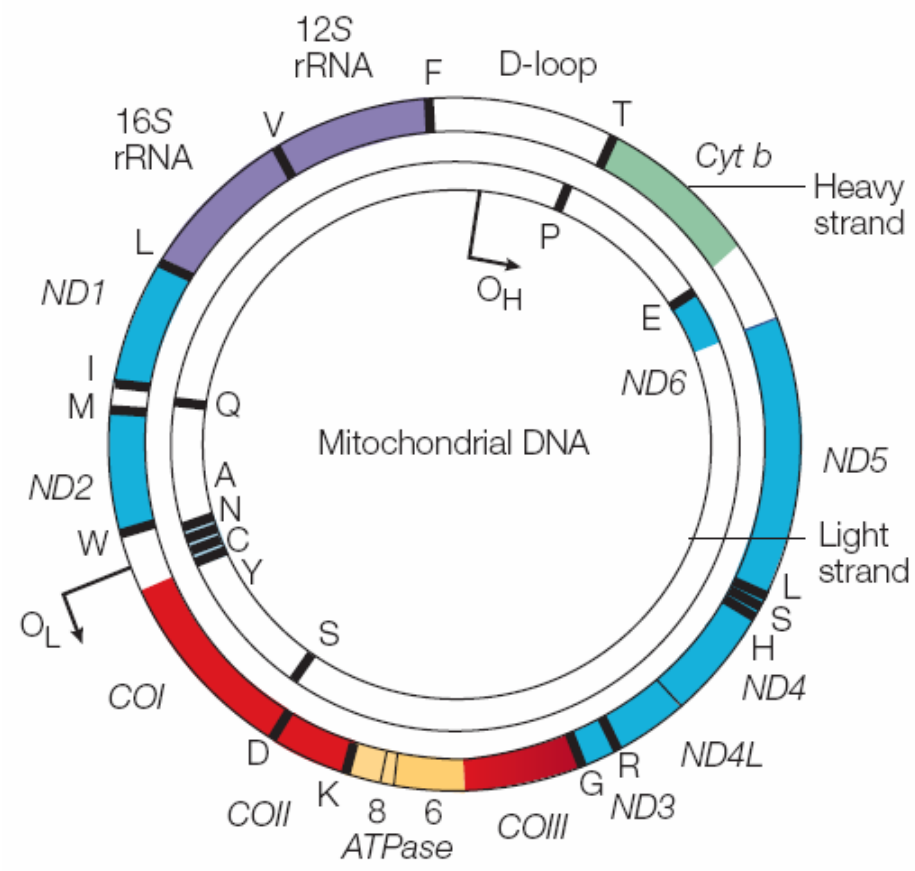

Figure 1.3. Human mitochondrial genome. Protein-coding genes: seven subunits of NADH dehydrogenase-CoQ oxidoreductase (ND); one subunit of CoQ-cytochrome c oxidoreductase (Cyt b); three subunits of cytochrome c oxidase (COX); and two subunits of ATP synthase (A). Protein synthesis genes: 12S, 16S rRNAs and tRNAs (indicated by black lines and denoted by their single letter code). Mitochondrially encoded subunits are shown in different colours: complex I = blue; complex III = green; complex IV = red; complex V = yellow; 12S and 16S rRNA = purple. O_H and O_L, the origins of heavy and light strand mtDNA replication. Adapted from Taylor and Turnbull (2005).

Table 1.1. Composition of the respiratory chain and oxidative phosphorylation system. Adapted from Penta *et al.* (2001).

Complex	Total no. subunits	No. subunits encoded by mtDNA
I	43	7 (ND 1-6, ND4L)
II	4	0
III	11	1 (cytochrome b)
IV	13	3 (COX I, II, III)
V	16	2 (ATPase 6 and 8)

(ii) Differences from nuclear DNA

The genetic code of mitochondrial differs slightly from the nuclear genetic code (Table 1.2). Mitochondrial genes, which lack a termination codon, are overcome by the insertion of UAA at the transcriptional level. Since the mtDNA genetic code differs from the universal code, expression of mtDNA genes must rely upon mitochondrion-specific protein synthesis, which is carried out through the interplay of nuclear-encoded transcriptional, and translational factors with rRNAs and tRNAs synthesised from the corresponding mitochondrial genes (Zeviani and Di Donato, 2004).

Table 1.2. Differences in genetic code between mitochondrial genome and nuclear genome.

Codon	Mitochondrial genome	Nuclear genome
AGA	STOP	Arginine
AGG	STOP	Arginine
AUA	START (Methionine)	Isoleucine
UGA	Tryptophan	STOP

Unlike nuclear DNA replication that occurs only during the S phase, replication of mitochondrial DNA is not restricted to the S phase of the cell cycle, but can occur during all stages of interphase ($G_1 \rightarrow S \rightarrow G_2$). It replicates rapidly without efficient proofreading, DNA repair mechanisms, and the protection of DNA-binding proteins such as histones (Brown and Wallace, 1994; Klug and Cummings, 2000). These factors are thought to contribute to the high mutation rate of mtDNA, which is about 10 times higher than that of nuclear DNA (cited in Snustad and Simmons, 2003). However, recent studies have shown that mtDNA do have proofreading ability through human DNA polymerase gamma (Ropp and Copeland, 1996; Longley *et al*., 2001).

1.2. Mitochondrial disorders

1.2.1. Mitochondrial diseases

Mutations of the mitochondrial genome causing respiratory dysfunction are responsible for a wide variety of mitochondrial diseases (Schon *et al*., 1997). Because the mtDNA mutation rate is high, mtDNA diseases appear to be common. These diseases may be present at any time from the neonatal period to late adult life. The phenotypic effects of mitochondrial mutations reflect the extent to which a tissue relies on oxidative metabolism. Therefore, mitochondrial disorders most commonly manifest themselves in tissues such as the brain, the heart, skeletal muscle, nerves, renal and the endocrine systems that are highly dependent on biological energy (Wallace, 1999, 2000; Pulkes and Hanna, 2001). The majority of patients with mitochondrial disease have significant neuropathology, with the most common features being spongiform degeneration, neuronal loss and gliosis, as well as loss of vision, hearing impairment, epilepsy, deficiencies of skeletal and cardiac muscle function or diabetes (Pulkes and Hanna, 2001). Furthermore, OXPHOS defects may also affect various cellular properties, such as mitochondrial membrane potential in myoclonus epilepsy with ragged red fibres (MERRF); mitochondrial encephalopathy, lactic acidosis and stroke like episodes (MELAS) (James *et al.,* 1996); ATP/ADP ratio (James *et al.,* 1999), reactive oxygen species (ROS) production (Luo *et al*., 1997) and mitochondrial calcium homeostasis (Brini *et al*., 1999).

Each human cell contains numerous mitochondria and each mitochondrion contains approximately 10 to 100 mtDNA molecules (Schuster *et al*., 1988). Variant mixtures of mutant or partially deleted mitochondria often exist in cells that also contain normal mitochondria: a state known as heteroplasmy. Pathogenic mtDNA mutations are expressed according to a threshold effect. There may be a mixture of respiratory competent and deficient cells within a tissue, in which a threshold mutation level is required to develop a biochemical respiratory chain defect in individual cells (Taylor and Turnbull, 2005). For instance, in wild-types, when their mutation tolerance levels fall below a critical value, at which point they can no longer compensate for the effect of the mutation, impairment of mitochondrial function is likely to occur. The precise threshold for biochemical expression varies from mutation to mutation, and from tissue to tissue. Retrospective studies have shown that the percentage level of mutated mtDNA in clinically relevant tissues does correlate with the severity of disease (Chinnery *et al*., 1997).

Rossignol *et al.* (2003) postulated that, in the absence of mutations, there is an excess of mRNAs, tRNAs and active respiratory chain complexes compared with what is required to permit `normal' respiration. Genetic and functional complementation can occur at different levels of gene expression in mitochondria depending on the gene affected by the mutation in mtDNA. They suggested that the effect of a mutation can be complemented at either transcription or translation level; during OXPHOS enzyme activity and ATP synthesis; or even cell growth.

The OXPHOS system is under dual genetic control, thus, mutations in either mitochondrial or nuclear genomes can lead to mitochondrial dysfunction. However, due to the high mutation rate of mtDNA and the vast number of nuclear genes involved, molecular diagnosis of mtDNA disorders has been focused on mtDNA mutation. There are two main types of mtDNA mutations, those that affect mitochondrial protein synthesis and those in protein-coding genes (DiMauro and Schon, 2001). Thus, five criteria are required to prove that a mtDNA mutation is pathogenic: (1) The mutation must be specific and not associated with other disease-causing mutations. (2) The mutation results in a change of a conserved nucleotide base or amino acid residue, which alters a functional protein. (3) Deleterious mutations are

usually heteroplasmic. (4) The mutation segregates with the disease clinically. (5) The mutation segregates with the disease biochemically (Riordan-Eva and Harding, 1995; Chinnery and Schon, 2003). In the past 18 years, more than 100 point mutations or large scale rearrangements (deletions and duplications) of mtDNA have been associated with human mitochondrial disease (e.g. Wallace, 2000; Chinnery *et al*., 2000a).

1.2.2. mtDNA mutation and male infertility

Mitochondria also play an important role in spermatozoa functionality due to the high ATP demand of these cells. Previous findings suggest that mtDNA mutations are associated with diminished fertility and motility of human spermatozoa (Frank and Hurst 1996; Kao *et al*., 1995, 1998; Ruiz-Pesini *et al*., 1998, 2000; Holyoake *et al*., 1999; St. John *et al*., 2000). Single nucleotide polymorphisms (SNPs) can also compromise semen quality (Holyoake *et al.,* 2001). There may be many descriptions of pathophysiological changes as a result of mtDNA mutation. But little is known about its relevance to sperm number and sperm function. The human testis manufactures over 100 million sperm cells daily. The process of spermatogenesis is divided into three stages: mitosis, meiosis and spermiogenesis. All these stages require ATP to ensure efficient cell replication as cells need the energy to divide. Thus, it has been hypothesised that mtDNA mutation affects ATP production and can lead to a reduction in sperm count.

1.2.3. Mitochondria in aging and neurodegeneration

Mitochondrion is increasingly recognised as playing an important role in both aging and neurodegenerative diseases. Previous studies have shown that the accumulation of mtDNA mutations accelerates normal aging, results in oxidative damage to nuclear DNA, thus, impairing gene transcription. There is considerable

evidence from studies of animal models that mitochondrial dysfunction may contribute to the pathogenesis of neurodegenerative diseases, such as Alzheimer's disease, Parkinson's disease, Huntington's disease, amyotrophic lateral sclerosis, hereditary spastic paraplegia, and cerebellar degenerations (for review see Beal, 2005). For example, oxidative damage to lipids has been shown to precede β-amyloid deposition in Alzheimer's disease in transgenic mice (Pratico *et al*., 2001). The mitochondria generate most of the cellular reactive oxygen species (ROS) as a toxic by-product of OXPHOS, resulting in oxidative damage to mitochondrial and cellular proteins, lipids, and nucleic acids (Chance *et al*., 1979; Floyd and Carney, 1992). Brain is particularly susceptible to oxidative damage because it is enriched in the more easily peroxidisable fatty acids, and has a relative deficit of antioxidant defence systems (Floyd, 1999). In Parkinson's disease, mutation in DJ-1, a protein that participates in the oxidative stress response in mitochondria, renders nerve cells more vulnerable to oxidative damage (Taira *et al.,* 2004).

1.2.4. Mitochondrial DNA in human malignancy

Alterations in the enzymatic complexes which impede the OXPHOS system have been reported in solid tumours such as breast, colon, stomach, liver, kidney, bladder, prostate, lung, head and neck, and in hematologic malignancies such as leukaemia, myelodysplastic syndrome (MDS) and lymphoma (for review see Penta *et al*., 2001). Although the exact mechanism is still not well-documented, there is considerable evidence suggesting that mitochondria may serve as contributors to carcinogenesis (Shay and Werbin, 1987; Baggetto, 1993; Cavelli and Liang, 1998). Thus, an increasing number of laboratories have investigated mtDNA as a potential marker for tumourigenesis in various types of tissues (Sanchez-Cespedes *et al.,* 2001; Wong *et al*., 2003).

Oxidative damage has been implicated in human carcinogenesis (Poulsen *et al.,* 1998). It is believed that mtDNA mutations and respiratory dysfunction may be linked directly to carcinogenesis via ROS and apoptotic-mediated pathways

(Cavalli and Liang, 1998). mtDNA is located in the mitochondrial matrix in close proximity to the electron transport system where ROS, such as superoxide anions, hydrogen peroxide and hydroxyl radicals, are continuously generated. Mutations in mtDNA may lead to a decreased efficiency of the electron transport chain and an increased leakage of electrons at this site. This may result in increased generation of mitochondrial and cellular ROS, creating oxidative stress and damaging to lipid membranes and other cellular constituents, thereby favouring the neoplastic process (Sawyer and Van Houten, 1999). Moreover, most mtDNA mutations occur in coding sequences because mtDNA lacks introns. Also, due to the lacking of protective histones and effective DNA repair capabilities, the mitochondrial genome is highly susceptible to oxidative damage and ultimately leads to mutations (Mecocci *et al*., 1993). It is proven that mutations induced by oxidative damage contribute significantly to genetic instability in tumours and thereby promote a higher propensity for tumour progression (Zienolddiny *et al*., 2000). Hence, there is a higher possibility that the high mutation rate of mtDNA may worsen oxidative stress or vice versa.

In addition, Shay and Werbin (1987) proposed that a mitochondrial factor in combination with a nuclear gene, code for a suppressor of tumorigenicity. A gradual reduction in the number of mitochondria during the progression stage of carcinogenesis would lead to a simultaneous reduction in the cytoplasmic suppressor. As a result, there is a gradual activation of a mutated oncogene and the onset of the tumorigenic phenotype.

Recent studies have also demonstrated a relationship between nucleus-encoded mitochondrial succinate dehyrogenase (SDH) and cancer (Selak *et al*., 2005). SDH is a component of the OXPHOS complexes I-IV and tricarboxylic acid cycle (TCA), as well as a tumour suppressor. Deficiency of SDH may lead to the accumulation of succinate intramitochondrally. The increased concentration of succinate will inhibit prolyl hydroxylases (PHD), hence the degradation of hypoxia-inducible factor (HIF-1α). The elevated HIF activity may induce the transcription of nuclear genes that facilitate angiogenesis, metastasis, and glycolysis, ultimately leading to tumour progression.

1.3. Effect of extracellular ATP on cell proliferation

ATP is a physiological compound present in all cells. ATP can be released in the extracellular space by many cell types, such as platelets, adrenal chromaffin, endothelial cells and injured cells, via secretory exocytosis and carrier-mediated mechanisms. Extracellular ATP can influence many biological processes including platelet aggregation, vascular tone, neurotransmission, skeletal and smooth muscle contraction, endocrine/exocrine secretion, inflammation, wound healing, immune response, pulmonary and cardiac function, and cell growth (for review see Gordon, 1986). Extracellular ATP functions by interacting with plasma membrane nucleotide receptors (Rathbone *et al.,* 1992; Abbracchio and Burnstock, 1994). In addition to its many intracellular functions, ATP may act as a potent extracellular messenger, mediating the coupling of purinergic (P2) receptors to different pathophysiological functions such as cell proliferation, differentiation and apoptosis (White and Burnstock, 2006). The term 'purinoceptor' is now generally used for such nucleotide receptors.

Several studies using pharmacological approach have recently demonstrated a close relationship between ATP and the proliferative activities of mammalian cultured cells, such as rat astrocytes (Hindley *et al*., 1994), mouse fibroblast (Huang *et al*., 1989), human astrocytoma, porcine aortic smooth muscle cells (Wang *et al*., 1992), rat renal mesangial cells (Schulze-Lohoff *et al*., 1992, 1995, 1996, 1998; Huwiler and Pfeilschifter, 1994), rat proximal tubule epithelial cells (Paller *et al*., 1998), human ovarian cancer cells (Popper and Batra, 1993; Batra and Fadeel, 1994; Schultze-Mosgau *et al*., 2000), breast cancer cells (Dixon *et al*., 1997), human intestinal epithelial cancer cells (Coutinho-Silva *et al.,* 2005), and human endometrial cancer cells (Katzur *et al.,* 1999). Abbracchio and Burnstock (1994) proposed that there are three major P2 purinoceptor classes based on agonist selectivity and signaling properties: ionotropic P2X, metabotropic P2Y and P2Z (Table 1.3). Each of these classes of receptors is composed of several subtypes. P2Z is later known as $P2X_7$. Currently, seven P2X and eight P2Y receptor subtypes have been characterized (White and Burnstock, 2006).

The P2X purinoreceptors are ATP-regulated non-selective cation channels permeable to Na^+, K^+ and Ca^{2+} (Bean, 1992). On prolonged exposure of cultured mesangial cells to high concentration of ATP, the cation channel can be converted to a large nonselective transmembrane pore allowing the passage of larger molecules, facilitating apoptosis and necrosis (Schulze-Lohoff *et al*., 1998). This effect is associated with apoptosis mediated through the caspase enzyme system (Humphreys *et al.*, 2000).

Table 1.3. Proposed subclassification of P2 purinoceptors. Adapted from Abbracchio and Burnstock (1994).

Name	P2X	P2Y	P2Z
Type	Ligand-gated channel (Na^+, K^+, Ca^{2+})	G-protein coupled ($[Ca^{2+}]_I$, IP_3, DAG)	Non-selective pore
General agonist	ATP/ADP/UTP	ATP/ADP/AMP/UTP	ATP

P2Y has been predicted to possess characteristics of G-protein-coupled receptors: an N-terminal extracellular domain with two consensus sites for N-linked glycosylation, seven hydrophobic putative transmembrane α-helices, and a large C-terminal intracellular domain containing several consensus phosphorylation sites. (Barnard *et al*., 1994). P2Y modulates a primary signal transduction pathway through activation of phospholipase C (PLC), which leads to the formation of inositol 1,4,5-trisphosphate (IP_3) and diacyle-glycerol (DAG) generation (Cusack, 1993), as well as regulating mobilisation of intracellular Ca^{2+} from the endoplasmic reticulum (White *et al*., 2005). P2Y is also involved in secondary signalling pathways including the inhibition and stimulation of adenylyl cyclase (AC) (White and Burnstock, 2006).

ATP also appears to co-ordinately regulate protein synthesis, DNA synthesis, and expression of immediate-early genes. It has been shown previously that

extracellular ATP stimulated phosphorylation and activation of mitogen-activated protein kinase (MAPK) and increased expression of the immediate early genes, which include proto-oncogenes *c-fos*, *c-jun* and *Egr-1* via specific P2Y receptors (Huwiler and Pfeilschifter, 1994; Schulze-Lohoff *et al*., 1996). Soltoff *et al.* (1998) further demonstrated that the activation of G-protein-coupled P2Y2 receptors by extracellular ATP and UTP stimulated MAPK by a mechanism that was dependent on the elevation of intracellular Ca^{2+} and the activation of related adhesion focal tyrosine kinase (RAFTK) and protein kinase C (PKC).

P2Z receptors are present on mast cells, macrophages, and fibroblasts. Falzoni *et al*. (1995) reported that the P2Z receptor was expressed during macrophage differentiation and upregulated by an inflammatory cytokine such as IFN-y. These findings suggested that P2Z receptors may have an important role in macrophage physiology. Additionally, Saribas *et al*. (1993) reported that exogenous ATP could alter the membrane permeability of mouse fibroblasts through the interaction with P2Z receptors. Activation of the P2Z receptor could also promote apoptosis via the opening of large plasma membrane pores (Pizzo *et al.,* 1992). Nevertheless, the function of P2Z is still less well understood.

Recent researches have presented evidence on the functional roles of P2Y and P2X receptors on carcinoma cells from different tissues. Rapaport (1983) demonstrated that low levels of extracellular ATP significantly inhibit the growth of human tumor cells (CAPAN-1, a pancreatic adenocarcinoma; HT29, a colon adenocarcinoma) *in vitro*. Such antiproliferative actions of ATP were also observed in endometrial cancer cells (Katzur *et al.,* 1999) and human ovarian cancer cells (Schultze-Mosgau *et al*., 2000). Conversely, ATP can also exert mitogenic effect on many cancer cells through the stimulation of P2Y receptors (Wang *et al*., 1992; Schulze-Lohoff *et al*., 1992, 1995, 1996; Popper and Batra, 1993; Hindley *et al*., 1994; Huwiler and Pfeilschifter, 1994; Dixon *et al*., 1997; Paller *et al*., 1998; Wagstaff *et al*., 2000; White *et al*., 2005). It is likely that these actions depend on the receptor subtype in a particular tissue and the activated intracellular signalling pathways. Figure 1.4 summarises the possible modes of action of P2 receptors on cancer cells.

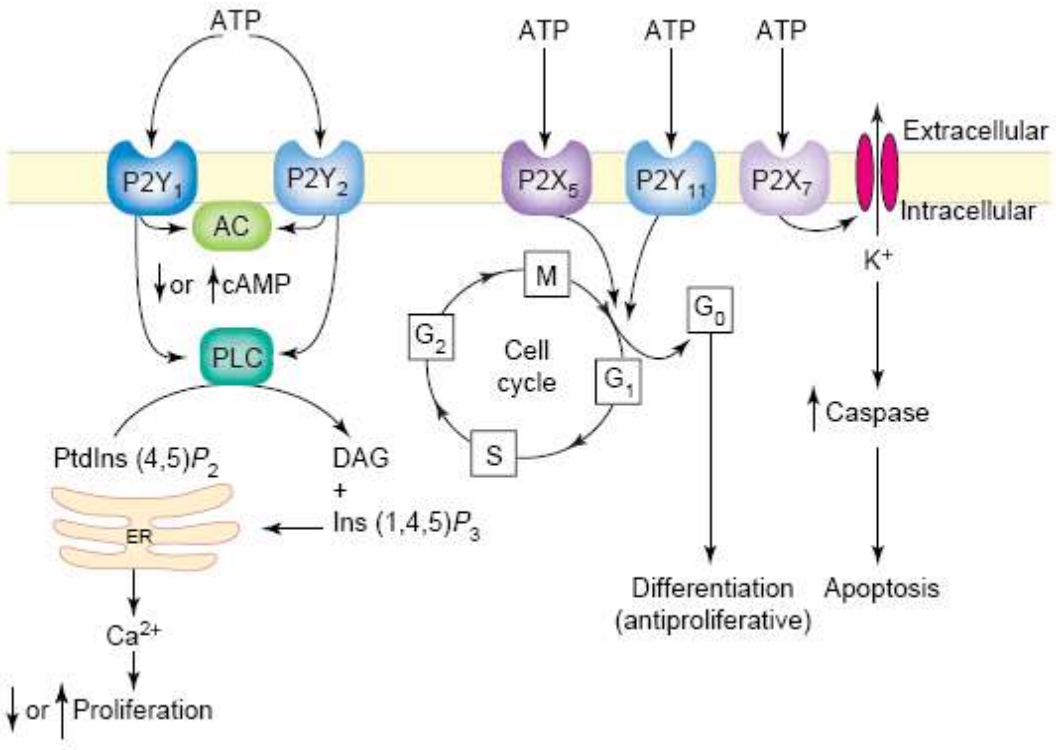

Fig. 1.4. Alteration in cancer cell function by different modes of action of P2 receptor subtypes. Adapted from White and Burnstock (2006). Abbreviations: AC, adenylyl cyclase; DAG, diacylglycerol; Ins(1,4,5)P3, inositol (1,4,5)-trisphosphate; PLC, phospholipase C; PtdIns(4,5)P2, phosphatidylinositol (4,5)-bisphosphate.

1.4. Other effect of ATP

Sperm mitochondria play an important role in spermatozoa because of the high ATP demand of these cells. Therefore, any alterations in mtDNA may have consequences for normal fertilisation. This is supported by the findings of Díez-Sánchez *et al*. (2003), which demonstrated a marked increase of mtDNA copy number per cell volume during spermatogenesis. It is also reported previously that oxidative phosphorylation activity is variable depending on the mitochondrial genetic background and is correlated with sperm motility (Ruiz-Pesini *et al*., 1998, 2000).

These observations lead to the question of how mtDNA variability could affect sperm function. Additionally, ATP is a potent inducer of acrosome reaction and capacitation in human spermatozoa (Foresta *et al*., 1992, 1996c). Sperm incubation with extracellular ATP induced a significant increase of fertilization rate in *in vitro* fertilisation for male factor infertility (Rossato *et al*., 1999).

1.5. MCF-7 cell line

MCF-7 cell line was established from the pleural effusion of a patient who was diagnosed with adenocarcinoma of the breast (Soule *et al.* 1973). This cell line has been shown by Resnicoff *et al*. (1987) to be highly heterogeneous with the ability to generate clonal variability. These findings showed an existence of several sublines which possessed different properties including growth rate and gene expression. On the other hand, Wagstaff *et al*. (2000) demonstrated that extracellular ATP potentiates growth factor-induced *c-fos* expression in MCF-7 cells resulted from P2Y receptor activation, which induced multiple signaling pathways. Cell proliferation is associated with ATP and mediated by a complex intracellular signaling network whose disruption is strongly linked to neoplastic transformation. However, there is little known about the relevance of mtDNA mutation in the performance of OXPHOS enzymes and on MCF-7 growth characteristics. Thus, MCF-7 cells will provide an excellent *in vitro* model system for research into the relationship between mitochondrial mutations and biochemical changes that may attribute to the growth characteristics of different sublines of MCF-7. The present study aims to improve our understanding of the effect of mtDNA mutation on MCF-7 cell line that is previously not well established.

1.6. Hypothesis

On the basis of the aforementioned genetics and biochemical functions of mitochondria, it is evident that normal mitochondrial function is vital for cell

function. The aim of this study was to investigate the relationship between mitochondrial mutation and cell proliferation. In this study, it is proposed that any mutation that alters a functional gene in mtDNA is likely to affect OXPHOS and ATP production, and the number of mutations may be associated with the severity of the respiratory chain impairment. It is also purported that extracellular ATP supplement to OXPHOS deficient cells may facilitate cell growth and enhances the gene expression. Such a model promises to recapitulate the genetic and physiological variation seen in mitochondrial diseases and may ultimately provide important new insights into the role of mitochondrial defects in a spectrum of progressive diseases.

1.7. Aims of research

(1) To use a breast cancer cell line MCF-7, as a model to study the basic function of mitochondria, the pathogenetic mechanisms that underlie normal and abnormal respiratory chain functions.

(2) To identify mutations in genes encoded by mtDNA and characterise these mutations by DNA sequencing.

(3) To investigate the effect of mitochondrial mutation on the enzymes of oxidative phosphorylation and establish a relationship between OXPHOS function and growth pattern.

(4) To investigate the effect of extracellular ATP on cell growth and gene activation.

2.1. Materials

The chemicals used in this study were of analytical grade. The chemicals with suppliers and abbreviations are listed in the text. All chemicals were obtained from BDH Chemicals (Poole, England) unless otherwise indicated. The water used in all experiments was purified by a NANOpure ultra-filtration system (Millipore, USA). Then the water was sterilised by autoclaving before use, and expressed as ddH_2O. The recipes for some preparations are shown in Appendix 2.

2.2. Methods

2.2.1. Cell culture

An MCF-7 cell line (passage 138), a stable cell line derived by pleural effusion from human adenocarcinoma, was purchased from the American Type Culture Collection (ATCC) (Rockville, MD). The cells were cultured in Dulbecco's modified Eagle's medium (DMEM) (pH 7.4) containing Phenol Red^+ and supplemented with 10% fetal bovine serum (FBS), 2 mM L-glutamine and 50 U penicillin-streptomycin (all reagents were supplied by Invitrogen; Auckland, New Zealand). Cells were cultured at 37°C in a humidified incubator with an atmosphere of 95% air and 5% carbon dioxide. For routine cultures the media were replenished every 2-3 days.

For each experiment, the initial cultures were established in T-75 flasks (Nunc, Denmark). One millilitre of frozen stock containing approximately 1 x 10^6 cells/ml was seeded to 12 ml of culture medium. After about 6-8 h, the cells adhered to the surface of the flasks. At this time the culture medium was replaced with fresh medium. All cultures were examined regularly to confirm the healthy status of the cells and the absence of contamination. This was done under a phase contrast inverted microscope (Leitz Diavert, Germany). Growth morphology and characteristics were also carefully noted using a 10x Phaco objective and 12.5x eyepieces. Where appropriate, images were captured digitally (1280 x 960 pixels) on a hand-held Fujifilm camera (FinePix 4700 zoom, Japan).

Cells were subcultured when reaching 80% confluency to improve cell growth. The culture medium was removed and the cells were washed with 2 ml phosphate-buffered saline (PBS) to remove traces of serum. This solution contained 0.13 M sodium chloride (NaCl), 14 mM di-Sodium hydrogen orthophosphate (Na_2HPO_4) and 3.5 mM sodium dihydrogen orthophosphate (NaH_2PO_4). The PBS was then discarded and the cells were treated for 2 min with 1 ml 0.25% (w/v) trypsin with 0.53 mM ethylenediaminetetra-acetic acid (EDTA) [Invitrogen; Auckland, New Zealand] to dissociate cells in the monolayer, and to detach the cells from the flask. Subsequently, 5 ml culture medium was added to the flask to re-suspend the cells. One millilitre aliquot of cell suspension was used to re-seed each T-75 flask. When cells were harvested for long term storage, the cells were resuspended in 10% dimethyl sulfoxide (DMSO) (Invitrogen; Auckland, New Zealand) containing DMEM and stored at -80^{o}C.

2.2.2. Single cell clone isolation

After subculturing, isolation of single cell clones was carried out according to the method of Freshney (2000). Conditioned medium was prepared to improve the plating efficiency of the cells. Firstly, the medium was harvested from cells of the late log phase. The medium was centrifuged for 5 min at room temperature and then the supernatant was diluted with 1 volume of fresh growth medium and stored at 4^{o}C before use (Fig. 2.1).

For single cell isolation (Fig. 2.2), a cell culture was trypsinised and the number of cells/ml was determined. To obtain a single cell for clone establishment, the culture was diluted serially to a final density of 3 cells/ml. One hundred µl of the diluted cell solution was then dispensed into each well in 96-well plates (Nunclon multidishes, Denmark). The plates were incubated until colonies formed. The clonal origin of the colony during its formation was confirmed by regular microscopic observation. When each single colony grew big enough to cover half of the area of the wells in the 96-well plates, they were treated with trypsin and transferred into a T-25

flask with 5 ml of conditioned. The cells were then subcultured as usual until they reached 80% confluency in the T-25 flask.

Supernatant was collected from 80% confluence monolayer cell culture.

Centrifuged at 3000 rpm for 10-15 min at room temperature. The pellet was discarded.

The supernatant was replenished with the same volume of fresh growth medium.

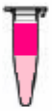

Figure 2.1. Preparation of conditioned medium. Collecting conditioned medium for single cell clone culture.

Exponentially grown MCF-7 cells were trypsinised.

Cell number was counted. The cell concentration was diluted with conditioned medium to < 3 cells/ml.

0.2 ml of the cell solution was seeded into each well of 96 well plates (about 0.7 cells/well).

Single colonies were noted. Wells with more than one colony were disregarded.

Figure 2.2. **Dilution cloning method.** Single cell clones were isolated from MCF-7 cells by dilution cloning.

2.2.3. Growth rate and doubling time

To determine growth rates, cells from each clone were seeded in 24-well plates (Nunclon multidishes, Denmark) at cell concentrations of 1 x 10^4 cells/ml/well. Cell morphology and growth characteristics were carefully noted under a phase contrast inverted microscope (Leitz Diavert, Germany). Cell counts were taken from three wells at time points. Cell growth rates were monitored over a range of time intervals until they reached the plateau phase, which was determined by at least three countings taken at three different time points that showed no increase in cell concentration. The culture media were changed every 2-3 days. The number of viable cells, as determined by trypan blue (Invitrogen; Auckland, New Zealand) exclusion, was counted daily using a hemocytometer and a Zeiss compound light microscope (Germany) at 125 x magnification. Mean values and standard deviations (SD) of the cell numbers were calculated. A semi-log growth curve was plotted and the lag time, population-doubling time (PDT), and plateau density were determined from the graph as described by Freshney (2000). The growth rates for all the clones were determined by separate growth experiments.

2.2.4. DNA extraction

To detect variation at genomic level, DNA extraction was carried out as described by Cao *et al*. (2003). DNA was isolated from exponentially growing cells of the three clones (B12, D4 and D9) showing the most variability in growth rate. DNA was extracted using a buffer containing 0.1 M Tris-HCl, pH 8, 20 mM EDTA, 1% sodium dodecyl sulphate (SDS) (Sigma-Aldrich; St. Louis, MO), 100 µg/ml proteinase K (Roche; Mannheim, Germany) and 10 mM 1,4-dithiothreitol (DTT) (Boehringer Mannheim; Mannheim, Germany) at 37^{o}C overnight. After overnight digestion, an equal volume of phenol and chloroform-isoamyl alcohol (25:24:1) was added to the digest and mixed well. DNA was then isolated by centrifugation at 10,000 x g for 10 min in an Eppendorf centrifuge (model 5417R) (Germany). The aqueous phase containing DNA was extracted with chloroform to remove residue phenol, followed by centrifugation as before. The purified DNA was precipitated out using 0.3 M sodium

acetate and ice cold 100% ethanol. Finally, purified DNA was solubilised in TE buffer (10 mM Tris-HCl, 1 mM EDTA, pH 8) and stored at 4^{o}C.

Quantitation of DNA was determined by a UV spectrophotometer (Ultraspec II 4050, LKB Biochrom Ltd; England). Absorbance wavelength was set at 260 nm and 280 nm. The A_{260}:A_{280} ratio was calculated to determine the purity of DNA. An A_{260}:A_{280} ratio of 1.8 is indicative of highly purified DNA. The DNA concentration was calculated using the Beer-Lambert law, where an A_{260} reading of 1.0 optical density (OD) unit is equivalent to 50 µg/ml double-stranded DNA (Sambrook *et al*., 1989).

Equation for calculating the DNA yield of the samples:

$$\text{DNA concentration} = A_{260} \times 50\ \mu g/ml \times \text{dilution factor}$$

The DNA was analysed by electrophoresis of 5 µl from each sample on a 1% agarose gel using 1x Tris-borate-EDTA (TBE) (0.9 M Tris base, 0.9 M boric acid, 12.5 mM EDTA, pH 8) buffer at 5V/cm. After electrophoresis, the gels were stained with ethidium bromide (0.5 µg/ml) and visualised on a UV transilluminator (UltraLum Sci Tech, New Zealand) at 300 nm wavelength. Molecular size marker was a mixture of Lambda DNA (λDNA) fragments digested with *Hind* III and *Eco* RI (λHE) [Invitrogen; Auckland, New Zealand] (see Appendix 3).

2.2.5. Polymerase chain reaction (PCR)

The entire mitochondrial genome was PCR amplified for clones B12, D4 and D9. These three clones showed distinctly different growth rates. Thirteen pairs of overlapping primer sets were designed to amplify the entire 16 569 bp mitochondrial genome (Table 2.1). Primers were based on the published human mitochondrial sequence from the Entrez database (accession number NC_001807) obtained from the National Centre for Biotechnology information (NCBI; http://www.ncbi.nlm.nih.gov.).

Table 2.1. **Primer pairs used for the PCR amplification of mtDNA.**

Pair	Primers	Nucleotide positions	Sequence (5' → 3')	Product size (bp)	Ta ^{o}C
A	12S F	628-647	ggctcacatcaccccataaa	2019	58
	16S R	2646-2627	tcgtggagccattcatacag		
B	16S F1	2335-2354	gcataagcctgcgtcagatc	2036	59
	ND1 R	4370-4351	ttttggattctcagggatgg		
C	ND1 F3	3930-3949	tctcaggcttcaacatcgaa	1637	58
	ND2 R	5566-5546	tgcaacttactgagggctttg		
D	ND2 F3	5199-5218	aattccatccaccctcctct	1560	59
	COI IR	6758-6738	aaccctaggaagccaattgat		
E	COI 2F	6611-6630	gatttttcggtcaccctgaa	990	59
	COI 2R	7600-7581	gctgcatgtgccattaagat		
F	T7 COII IF	7495-7514	T7-catggcctccatgacttttt	991	59
	T3 COII IR	8485-8466	T3-tttggtgagggaggtaggtg		
G	T7 ATPase6 F	8466-8485	T7- cacctacctccctcaccaaa	871	55
	T3 ATPase6 R	9336-9317	T3-gaggagcgttatggagtgga		
H	T7 COIII IF	9184-9203	T7- cctctacctgcacgacaaca	993	59
	T3 COIII IR	10176-10158	T3-gcactcgtaaggggtggat		
I	HMTL 1012 F	10124-10143	tttgactaccacaactcaac	2088	58
	HMTH12211 R	12211-12191	tctcggtaaataaggggtcgt		
J	ND5A F	12066-12085	ctcatgttcatacacctatc	1447	58
	ND5D R	13512-13492	ttggagtagaaacctgtgag		
K	ND5C F	12890-12909	gccttagcatgatttatcct	1262	57
	ND5B R	14151-14132	ggttatgtgattaggagtag		
L	ND6 F	14050-14069	ctccacctccatcatcacct	1957	59
	Cyt B R	16006-15986	agaatcttagctttgggtgct		
M	D-Loop F	15882-15901	tgggcctgtccttgtagtat	1400	59
	D-Loop R	710-692	ggggatgcttgcatgtgta		

F – forward primer, R – reverse primer, T7 – taatacgactcactataggg, T3 – attaaccctcactaaaggga, Ta – annealing temperature.

The primers were designed using a web based program, Primer3 (http://www.path.com.ac.uk/cgi.bin/primer3.cgi). For each primer pair design, the primer length, melting temperature (Tm), GC content and length of PCR product were taken into consideration. The compatibility of the primers was then checked to ensure that no primer dimers were formed using the FastPCR software (Kalendar 2004, http://www.biocenter.helsinki.fi/bi/programs/fastpcr.htm). The oligonucleotide primers were chemically synthesised by Invitrogen (Auckland, New Zealand). The generated

fragments were 800-2100 bp in length. The amplified fragments had at least 80 bp overlap at each end.

PCR amplification was carried out according to the manufacturer's instructions (Roche; Mannheim, Germany). Each 50 µl PCR reaction contained 1x PCR buffer containing 15 mM Mg^{2+} (Roche; Mannheim, Germany), 0.8 µM primers (Invitrogen; Auckland, New Zealand), 0.2 mM deoxyribonucleoside triphosphate (dNTPs) [Progen Biosciences; Queensland, Australia], 1.25 U Taq polymerase (Roche; Mannheim, Germany) and 100 ng DNA template. For each set of PCR, a negative control (without DNA template) and a positive control of a known DNA sequence were run in parallel to ensure that the PCR products were not due to contaminations in the PCR reagents, and that the PCR was amplifying specific DNA sequences. The cycle parameters were as followed: 94^{o}C for 2 min (initial denaturation); 30 cycles of 94^{o}C for 30 s (denaturation), 55^{o}C - 59^{o}C for 45 s (annealing) and 72^{o}C for 2 min (extension). The final extension proceeded for 7 min. The amplification was done on a PTC-225 Peltier Thermal Cycler (MJ Research, Germany). The size of the PCR fragments was estimated by comparison with λHE molecular markers after electrophoresis. The PCR products were stored at 4^{o}C until use.

2.2.6. Purification of PCR products

All PCR-amplified products were subsequently purified for sequencing using a GFX purification kit (Amersham Pharmacia Biotech; Freiburg, Germany). PCR products were also eluted from agarose gels using Matrix Gel Extraction Protocol (Life Technologies; Grand Island, NY). The bands of interest were excised with a sterile surgical scalpel and melted at 60^{o}C. These gel slices were then processed to obtain purified PCR products. The purified PCR products were stored in TE8 at 4^{o}C.

2.2.7. mtDNA sequencing and analysis

The purified PCR products were sequenced directly using an ABI PRISM BigDye Terminator v3.1 Cycle Sequencing kit (Applied Biosystems; Foster City, CA) on an ABI 377 automated DNA sequencer (Perkin-Elmer; Foster City, CA). Additional mtDNA primers for sequencing long fragments of PCR products were also designed (Table 2.2). The sequencing reactions contained 50 ng of purified PCR product, 0.5 µl BigDye Terminator (BDT) reaction mix, 1.75 µl 5x sequencing buffer (containing 350 mM Tris-HCl, pH 9.0 and 2.5 mM $MgCl_2$), 3.2 pmol primer and ddH_2O to a total volume of 10 µl. Thermocycling conditions were as followed: 96^oC x 10 s, 50^oC x 10 s, 60^oC x 1 min (25 cycles). Unincorporated primers and dye terminators were removed using DNA grade Sephadex-G50 (Amersham; Richmond, CA) gel filtration prior to sequencing.

Table 2.2. **Additional mtDNA primers used in ABI sequencing.**

Primers	Nucleotide positions	Sequence (5' → 3')
16S F	1591-1611	cacttggacgaaccagagtgt
12S R	1705-1686	gtaaggtggagtgggtttgg
ND1 F	3246-3265	cccggtaatcgcataaaact
16S R1	3366-3347	aggaatgccattgcgattag
ND2 F	4383-4402	cctatcacaccccatcctaa
ND2 R3	5309-5290	gtggggatgatgaggctatt
HMTL 9798 F	9798-9817	ttttgtagccacaggcttcc
HMTL 10688 F	10688-10708	tgggcctagccctactagtct
HMTH 10851 R	10851-10832	tgtgggtggttgtgttgatt
HMTH 1246 R	12461-12443	gatgcgacaatggattttac
Cyt B F	14621-14640	ccccacaaaccccattacta
ND6 R	14755-14736	ggggtcattggtgttcttgt

F – forward primer, R – reverse primer

All fragments were sequenced from both the forward and backward direction to assure sequence reading precision. The sequencing reactions were performed at least two times for confirmation. Sequences were edited to remove ambiguous portions from the 5' and 3' ends. The results of mtDNA sequence analysis

were then compared among clones with reference to the latest revised National Center for Biotechnology Information (NCBI) sequence viewer (accession number NC_001807, February 2006 version) using a DNA mutation analysis software (SEQUENCHER 4.5, USA).

2.2.8. Sensitivity of heteroplasmy detection

To establish the limits of detection of mtDNA heteroplasmy by sequencing, heteroplasmic sensitivity mixing experiments were carried out. DNA sample from a homoplasmic individual (D4) was mixed with the DNA sample from a heteroplasmic individual (B12) with a well-characterised heteroplasmic A2520T mutation within the 16S rRNA gene. The DNA mixture ratios were 50:50, 80:20, 90:10 and 95:5. The levels of heteroplasmy were resolved by calculating the total areas under the two overlapping peaks and expressed each as a percentage area of the total area (Harris *et al*., 2006).

2.2.9. Mutational analysis

(i) RNA secondary structure prediction

Secondary structures for the mutated human mitochondrial 16S rRNAs were generated using the RNAfold software from the Vienna RNA package (Hofacker 2003; http://rna.tbi.univie.ac.at/cgi-bin/RNAfold.cgi). RNAfold predicts RNA secondary structure based on free energy minimisation and pair probabilities.

(ii) Amino acid sequence analysis

Predictions of protein structure and function were performed using the tools found on the internet. Primary structural analysis to determine the hydropathicity

and polarity was carried out using the ProtScale software (http://www.expasy.org/tools/protscale.html), which implements the scale of Kyte and Doolittle (1982), and Grantham (1974), respectively. Functional analysis including protein secondary structure and transmembrane regions were predicted using nnPredict (http://www.cmpharm.ucsf.edu/~nomi/nnpredict.html) and TMpred (http://www.ch.embnet.org/software/TMPRED_form.html), respectively.

2.2.10. Isolation of mitochondria

Mitochondria were required to investigate the biogenetic activities in the cells of the three clones. Isolation of intact mitochondria was based on a modification of the method described by Madsen *et al*. (1996), where mitochondria were prepared by differential centrifugation. The entire process was performed at 4^{o}C. All glassware were first rinsed in sucrose-Hepes-EGTA (0.25 M sucrose, 10 mM Hepes-NaOH (pH 7.2), 2 mM EGTA) (SHE) buffer before use.

Exponentially growing cells of the three single clones (B12, D4 and D9) were collected by trypsinisation and re-suspensed in 50 µl PBS. The cell suspension was then incubated in 500 µl of ice-cold SHE buffer and treated with 0.01% digitonin (w/v) to remove the outer mitochondrial membrane. Fragments of inner membrane were obtained by osmotic rupture of the mitochondria, and enzymes, which were embedded in the inner mitochondrial membrane, were exposed. After 10 min of incubation on ice (4^{o}C), the cell suspension was homogenised using a glass-glass homogeniser by making at least 100 strokes to help breaking open the cell membrane completely.

The homogenate was then centrifuged at 700 x g for 10 min to pellet unbroken cells, nuclei and debris. The supernatant, which contained the mitochondria, was transferred to a new tube and the pellet was discarded. Mitochondria were sedimented from the supernatant by centrifugation at 12,000 x g for 15 min at 4^{o}C. The mitochondrial pellet had a brown core covered by a lighter fluffy layer. This pellet was carefully washed with 500 µl SHE buffer, followed by centrifugation at 700 x g for 5

min at 4°C. Subsequently, the washed pellet was re-suspend in 100 µl of SHE buffer and stored at -20°C until used for enzyme assays.

2.2.11. Quantitation of mitochondria (Bradford assay)

The mitochondrial protein concentration was determined according to the method of Bradford (1976) using dye reagent from Bio-Rad (Richmond, CA). The dye reagent consisted of Coomassie Blue G-250 which was dissolved in 95% ethanol and kept in the dark prior to the assay. The assay was carried out in triplicates; absorbance was determined at 595 nm using a UV-visible spectrophotometer (Shidmadzu UV-1601 PC, Japan). Protein concentrations were determined by colour changed (brown → blue) upon binding of protein to Coomassie Blue.

Dye reagent was prepared by diluting 1 part of Bio-Rad dye reagent concentrate with 4 parts of ddH_2O. A range of protein standards (0-1500 µg/ml) were made up from a stock solution of 2 mg/ml bovine serum albumin (BSA) (AppliChem; Darmstadt, Germany). These protein standards were prepared in SHE buffer, the same buffer as the mitochondrial samples to be assayed. Five µl of standard and 200 µl dye were added and made up to 1 ml with ddH_2O for each reading. The solution was mixed well and incubated at room temperature for 5 min before being assayed. A standard graph of absorbance against BSA concentration was plotted to provide a relative measurement of protein concentration.

2.2.12. Enzyme assays

To investigate whether a mutation in the mitochondrial genome correlated with any biochemical defect in the mitochondrial complex, enzymatic assays were carried out. Enzymatic measurements were performed in isolated mitochondria. All five oxidative phosphorylation (OXPHOS) enzymes were assayed using a UV-visible spectrophotometer (Shidmadzu UV-1601 PC, Japan) equipped with a temperature-controlled (Thermoltaake DC10, Germany) cuvette holder. Enzyme assays

were carried out in triplicates in a one ml reaction volume containing 25 µg/ml of mitochondria at 30°C. All enzyme activities were normalised with reference to the activity of the mitochondrial marker enzyme citrate synthase (CS) in each sample to discriminate very partial specific enzymatic OXPHOS defects (Barrientos 2002). All chemicals used for enzyme assays were obtained from Sigma-Aldrich (St. Louis, MO).

(i) Citrate synthase assay

CS activity was measured according to the method of Shepherd and Garland (1969). The reaction mixture contained 100 mM Tris-HCl (pH 8.0), 100 mM acetyl coenzyme A, 200 mM [5,5'-dithio-bis-(2-nitrobenzoic) acid] (DTNB), 0.1% (v/v) Triton X-100 . The assay was initiated by the addition of 200 µM oxaloacetate (OAA) after mitochondria were added for 3 min. CS coupled Coenzyme A to DTNB. The formation of 5-thio-2-nitrobenzoate was monitored at 412 nm. Control assays in which oxaloacetate was omitted, were also performed to quantify any transfer of the sulfhydryl groups to DTNB other than that caused by CS activity.

The millimolar extinction coefficient of DTNB is 13.6.

(ii) NADH-Ubiquinone oxidoreductase (Complex I) assay

The activity of rotenone-sensitive NADH:ubiquinone oxidoreductase was measured in 25 mM potassium phosphate buffer (pH 7.4) containing 5 mM magnesium chloride ($MgCl_2$), 2 mM potassium cyanide (KCN), 2.5 mg/ml albumin, 2 µg/ml antimycin A, 65 µM ubiquinone, 130 µM nicotinamide adenine dinucleotide (NADH) and the mitochondria sample at 340 nm according to Birch-Machin *et al*. (1994). Ubiquinone (CoQ_1) acted as an electron acceptor and was reduced to ubiquinol, showing a decrease in NADH absorbance. After 5 min, 2 µg/ml rotenone was added and the reaction was noted for a further 5 min. The rotenone-sensitive rate was then calculated by subtracting the rotenone-inhibited rates from the CoQ_1-stimulated rate.

The millimolar extinction coefficient of NADH is 6.81.

(iii) Succinate dehydrogenase (Complex II) assay

Mitochondrial complex II activity was measured based on a modification of the method described by Ackrell *et al*. (1978). This assay measured the reduction of ferricyanide at 420 nm. The assay was conducted in 100 mM potassium phosphate buffer (pH 7.4), 20 mM sodium succinate, 1 mg/ml BSA and mitochondria sample. This mixture was mixed well and placed in a 30^{o}C water bath for 10 min. After 10 min of incubation, 100 µM potassium ferricyanide ($K_3[Fe(CN)_6]$) was added and the reaction was registered for a further 3 min.

The millimolar extinction coefficient of ferricyanide is 1.0.

(iv) Ubiquinol -cytochrome c oxidoreductase (Complex III) assay

Mitochondrial complex III activity was measured according to the method of Birch-Machin *et al*. (1994). The reaction mixture contained 25 mM potassium phosphate buffer (pH 7.4), 5 mM $MgCl_2$, 2 mM KCN, 2.5 mg/ml BSA, 2 µg/ml rotenone, 15 µM cytochrome c (III) and the mitochondrial sample. The reaction was initiated by the addition of 35 µM ubiquinol which acted as a substrate. This enzyme donated electrons from ubiquinol to cytochrome c (III), and the reduction of cytochrome c was monitored by an increase in absorbance at a wavelength of 550 nm.

The millimolar extinction coefficient of cytochrome c (II) is 19.0.

The preparation of reduced ubiquinone (ubiquinol) was performed as described by Hatefi (1978). In a Falcon tube (BD Biosciences, Australia), 10-50 mg ubiquinone were dissolved in 3 ml of absolute ethanol, acidified to pH 2 with 6 M HCl. An equal volume of water was added. The quinine was then reduced with excess sodium borohydride ($NaBH_4$). The lid was closed after 2 ml of cyclohexane was added and the contents were vortexed briefly. After the cyclohexane was separated from the aqueous layer, it was extracted and evaporated to dryness under vacuum until reduced ubiquinone (ubiquinol) was collected in the tube as pale yellow oil. Absolute ethanol was added, followed by a small volume of 6 M HCl to retard oxidation. This solution

was then kept at -80^{o}C until use. Conversion to the oxidised quinone could be easily detected by the reappearance of the yellow colour of ubiquinone.

(v) Cytochrome C Oxidase (Complex IV) assay

The activity of complex IV was measured using a modified method of Birch-Machin *et al*. (1994). This assay measured the oxidation of cytochrome c (II) that led to a decrease in absorbance at 550 nm. The concentration of cytochrome c (II) was determined before each batch of assays. The assays were performed in a reaction mixture containing 10 mM potassium phosphate buffer (pH 7.4) and 15 µM cytochrome c (II). The reaction was initiated by the addition of mitochondrial sample and measured for 5 min. 100 mM ferricyanide was then added to fully oxidised cytochrome c (II).

The millimolar extinction coefficient of cytochrome c (III) is 19.1.

Cytochrome c (III) was dissolved in 10 mM potassium phosphate buffer (pH 7.4). The solution was reduced to cytochrome c (II) with a few crystals of sodium L-ascorbate and separated by Sephadex-G25 chromatography. A colour change was observed upon reduction of the solution. Reduced cytochrome c concentration was then determined using reduced-oxidised different extinction coefficient of $\Delta\varepsilon_{550\text{-}542}$ = 19.6 $mM^{-1}cm^{-1}$ prior to the assay. This was done by using a UV-visible spectrophotometer (Shimadzu UV-1601 PC, Japan) at wavelengths of 542 nm and 550 nm.

Equation for determining cytochrome c concentration:

$$[\text{Cytochrome c}]\ \text{mM} = \frac{A_{550\ (\text{reduced})} - A_{542\ (\text{reduced})} + A_{542\ \ (\text{oxidised})} - A_{550\ \ (\text{oxidised})}}{\Delta\varepsilon_{550-542\ (reduced-oxidised)}} \times Dilution$$

(vi) ATP synthase (Complex V) assay

The enzymatic activity of ATPase in the mitochondrial inner membrane was monitored at 340 nm, according to the method of Pullman *et al*. (1960). The millimolar extinction coefficient is 6.22. The reaction buffer contained 100 mM Tris buffer (pH 8.0), 200 μM NADH, 1 mM phosphoenol pyruvate (PEP) (pH 6.0), 2 U/ml L-lactic dehydrogenase (LDH), 4 U/ml pyruvate kinase (PK), 2.5 mM MgATP (pH 7.0) and observed for 3 min until the NADH level had stabilised. Mitochondrial samples were then added and the decrease in absorbance resulting from the consumption of hydrolysed ATP was measured. After 5 min, 0.1 mM oligomycin (ATP inhibitor) was added to measure the oligomycin insensitive rate.

2.2.13. Effect of extracellular adenosine 5'-triphosphate (ATP) on cell proliferation

Cell proliferation assay was carried out to evaluate the effect of extracellular ATP on cells growth. Exponentially growing B12 cells and D4 cells were seeded in 24-well plates (Nunclon multidishes, Denmark) at 1 x 10^4 cells/ml/well and cultured as described previously. The cells were left to attach to the flask for 24 h. After 24 h, B12 cells (slowest growth) were then treated with increasing ATP (Sigma-Aldrich; St. Louis, MO) concentrations (0 μM, 50 μM, 100 μM and 1 mM). D4, which was the fastest growing clone, was cultured without exogenous ATP as a reference for comparison. The culture medium was replaced daily by fresh medium containing the appropriate ATP concentrations to alleviate the concern about the degradation of ATP during incubation. Growth morphology and characteristics were carefully observed under a phase contrast inverted microscope (Leitz Diavert, Germany). The cell numbers from three wells were determined daily by trypan blue staining as described before. The growth rates were determined from triplicate experiments. Growth curves for each treatment were plotted.

2.2.14. RNA extraction from cell cultures

Total RNA was extracted from exponentially growing cells using TRI Reagent (Molecular Research Center, Inc, Cincinnati, OH) which contained phenol and guanidine thiocyanate in a procedure based on the method of Chomczynski and Sacchi (1987). Cells were first rinsed with PBS and subsequently lysed in TRI Reagent (1 ml per 5-10 x 10^6 cells) for 5 min at room temperature. RNA was separated from DNA and protein by extraction with chloroform. RNA was then precipitated with ½ volume of isopropanol and spun at 12,000 x g for 15 min at 4^{o}C. The RNA pellet was then washed with 75% ethanol, centrifuged at 7,500 x g for 5 min and vacuum dried for 5 min. RNA was then solubilised in 50-80 µl diethyl pyrocarbonate (DEPC)-treated water (Sigma-Aldrich; St. Louis, MO). The isolated RNA was subjected to RNase-free DNase I (Fermentas; Ontario, Canada) digestion for 30 min at 37^{o}C in the presence of Mg^{2+}. The reaction was arrested by 1 µl of 25 mM EDTA and incubated at 65^{o}C for 10 min. PCR was performed to check for potential DNA contamination by using purified RNA samples directly as the templates. Samples containing residual genomic DNA were redigested with RNase-free DNase I and assayed again for DNA contamination. The DNA-free RNA was then stored in 100% ethanol at -80^{o}C until use.

2.2.15. Quantitation and visualisation of RNA

The concentration of RNA was determined by using a fluorescence-based Quant-iT™ RNA Assay kit (Molecular Probes; Oregon, US) on a multiplex quantitative PCR system (MxPro-Mx3005P, Stratagene, US). The optical path of the sulfonated indocyanine dye Cy3 was assigned at excitation wavelength 635 nm and emission wavelength 665 nm. The quantity of RNA was determined by comparison with an *E.coli* rRNA standard curve (mass of RNA in ng vs. fluorescence). The purity of the isolated total RNA was assessed by UV spectrophotometry (Ultraspec II 4050, LKB Biochrom Ltd; England) by referring to absorbance ratios A_{260}:A_{280}. As RNA A_{260}:A_{280} ratio is dependent on both pH and ionic strength (Wilfinger *et al*., 1997), TE (pH 8) was used as a dilutant and a blank to assure accurate readings. The integrity of the total RNA was analysed by electrophoresis on a denatured 1% agarose-

formaldehyde gel using 1 x 3-(N-morpholino)-propanesulfonic acid (MOPS) buffer (Sigma-Aldrich; St. Louis, MO). The integrity of the total RNA was judged by the integrity of 28S and 18S rRNA.

2.2.16. Reverse transcription of RNA

Reverse transcription PCR analysis of mt-cDNA was carried out to investigate the expression of mutated 16S rRNA, ND1, ND4, ND6 and COX III genes involved in OXPHOS.

(i) cDNA synthesis

Two µg of DNase I-digested RNA template from each clone was copied into complementary DNA (cDNA) using GeneAmp Gold RNA PCR Core Kit (PE Biosystems; Foster City, CA). The total RNA was first incubated with 50 ng of hexamers and 1 mM of dNTP mix for 5 min at 65^{o}C and chilled on ice for another 5 min. A reaction mixture (40 units of RNase inhibitor, 4 µl of 5x RT buffer, 4 µl of 25 mM $MgCl_2$ and 2 µl of 0.1 M DTT) was added to the RNA/hexamers mixture mentioned above and incubated at 25^{o}C for 2 min. Briefly, 50 units of reverse transcriptase (RT) were added to each sample and incubated at 25^{o}C for 10 min followed by 42^{o}C for 50 min. This reaction was terminated by heating at 70^{o}C for 15 min and subsequently chilled on ice. Two units of RNase H was added to the synthesized cDNA and incubated for 20 min at 37^{o}C to digest any residual RNA. The cDNA was stored at -20^{o}C before proceeding to amplification of the target DNA.

To confirm the efficiency of the first-strand synthesis reaction, a positive control using 50 ng *in vitro* transcribed RNA from the chloramphenicol acetyltransferase (CAT) gene (Invitrogen; Auckland, New Zealand) was included. A negative control identical to the test assay but omitting the RT reaction was included for each gene tested to test for the presence of genomic DNA contamination.

(ii) Comparative RT-PCR

PCR was performed as mentioned before. Five genes were amplified: 16S rRNA, ND1, ND4, ND6 and COX III. Each primer pair (Table 2.3) annealed optimally at 59^{o}C, thereby permitting simultaneous amplification of the reactions (multiplex). The final reaction volume was 50 µl. Negative controls (using water instead of cDNA template) were included in each PCR run.

Table 2.3. **mtDNA primers used in RT-PCR.**

Primers	Nucleotide positions	Sequence (5' → 3')	Product size (bp)
16S F1	2335-2354	gcataagcctgcgtcagatc	1032
16S R1	3366-3347	aggaatgccattgcgattag	
ND1 F	3246-3265	cccggtaatcgcataaaact	1125
ND1 R	4370-4351	ttttggattctcagggatgg	
HMTL 1012 F	10124-10143	tttgactaccacaactcaac	2088
HMTH12211 R	12211-12191	tctcggtaaataaggggtcgt	
ND6 F	14050-14069	ctccacctccatcatcacct	706
ND6 R	14755-14736	ggggtcattggtgttcttgt	
T7 COIII IF	9184-9203	T7 - cctctacctgcacgacaaca	993
T3 COIII IR	10176-10158	T3 - gcactcgtaaggggtggat	

F – forward primer, R – reverse primer, T7 – taatacgactcactataggg, T3 – attaaccctcactaaaggga,

The internal reference was the amplification of 18S rRNA (Roche; Branchburg, NJ). The band intensity of 18S rRNA after electrophoresis and ethidium bromide staining was used as an internal reference. This provided an estimation of the relative amount of target RNA in the cell samples. Visualisation of gels was carried out on CHEMI GENIUS Bio Imaging System using GeneSnap version 6.05 (Syngene; England). Intensities of the PCR product bands were quantified by using GeneTools version 3.06 (SynGene; England).

2.2.17. Statistical analysis

All statistical analyses were performed using parametric methods. Data were expressed as means ± SD calculated from the number (*n*) of replicas. One-way analysis of variance (ANOVA) was used for statistical evaluation. Where appropriate, *post hoc* comparisons using the Tukey's Honestly Significant Different (HSD) test were carried out to determine which pairs of groups were statistically different. A *p*-value of < 0.05 was accepted as the level of statistical significance. Analyses were performed using GraphPad Prism Version 4.00 for Windows (GraphPad software, California; www.graphpad.com) or Microsoft® Windows® Excel 2003 software.

3.1. Morphology and characteristics of the clone cells

Six clones (B5, B12, D4, D9, E1 and E8) each derived from a single cell were isolated from MCF-7 stock. The images of cells growing in the centre of the culture flasks were captured digitally using a hand-held camera (Fig. 3.1A-F). These images represented cells after subculturing from the initial established single cell colonies. All cells showed a typical epithelial morphology and were regular in shape, with a clearly defined edge. As the cell density increased, most cells were arranged in clusters, and these clusters displayed a cobblestone appearance as they reached confluency. Unlike cells of other clones that tended to clump together in patches, clone B12 was more scattered (Fig. 3.1B). B12 cells also had poorer adhesion and required longer time to attach to the culture vessel after seeding.

At early confluency (3-day old), clones D4 and D9 had protruding structures growing from the membrane but disappeared when the cell density increased. However, the protruding structures were seen throughout the whole culture time particularly in E8 cells (Fig. 3.1F). E8 cells also had a granular look around the nucleus but cytoplasmic vacuolation was absent.

3.2. Growth curve and doubling time

Figure 3.2 shows cell counts plotted on a log scale against time. Cell number was calculated per well, per ml of culture medium (left y-axis), and per cm^2 of available growth surface in the well (right y-axis). The six single cell clones showed a characteristic growth pattern consisting of a lag phase, an exponential phase (log phase) and a stationary phase (plateau phase). In preliminary growth studies, the six clones revealed different growth rates (Fig. 3.2).

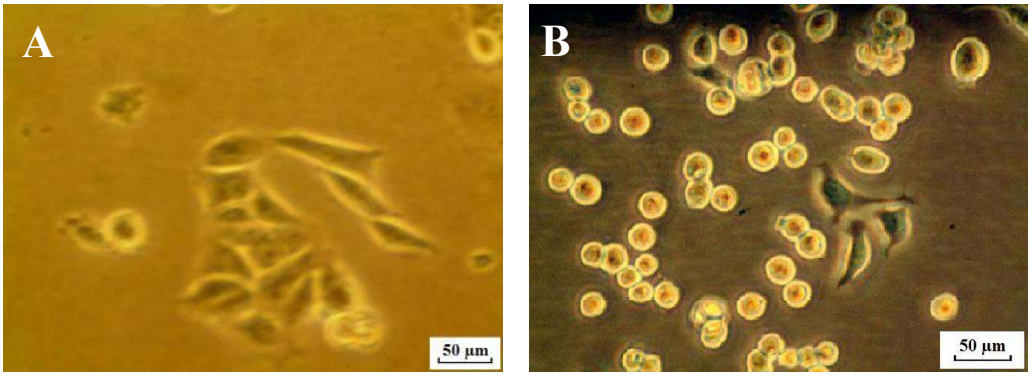

B5 – newly subcultured monolayer

B12 – contact inhibited and rounding up of the cells

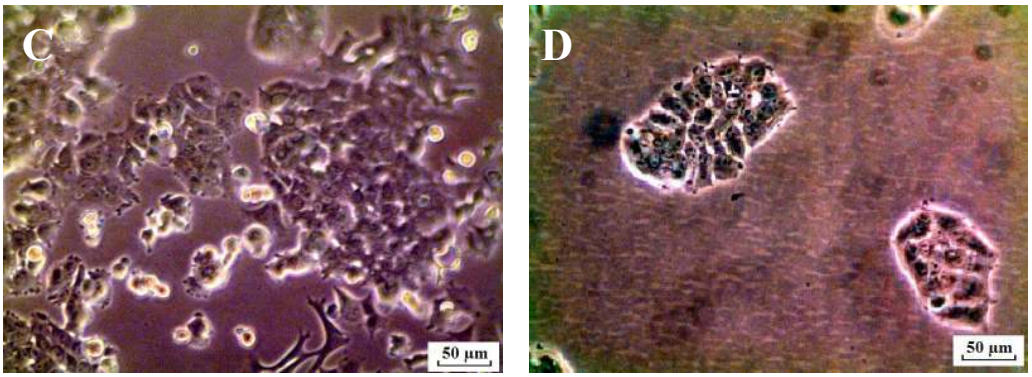

D4 – clusters at 60% confluency

D9 – discrete clusters

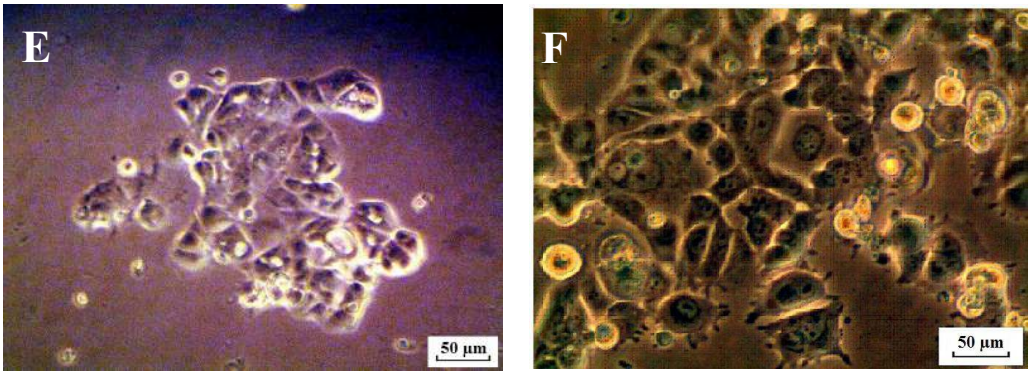

E1 – cells clumped together

E8 – protruding structure at 60% confluency

Figure 3.1. Growth morphology and characteristics of MCF-7 clones in culture. Six single cell clones of MCF-7 cells, cloned by dilution cloning. Epithelial morphology. Phase contrast. Scale bar 50 µm. A and B were taken at Day 1. D and E were taken at Day 2. C and F were taken at Day 4.

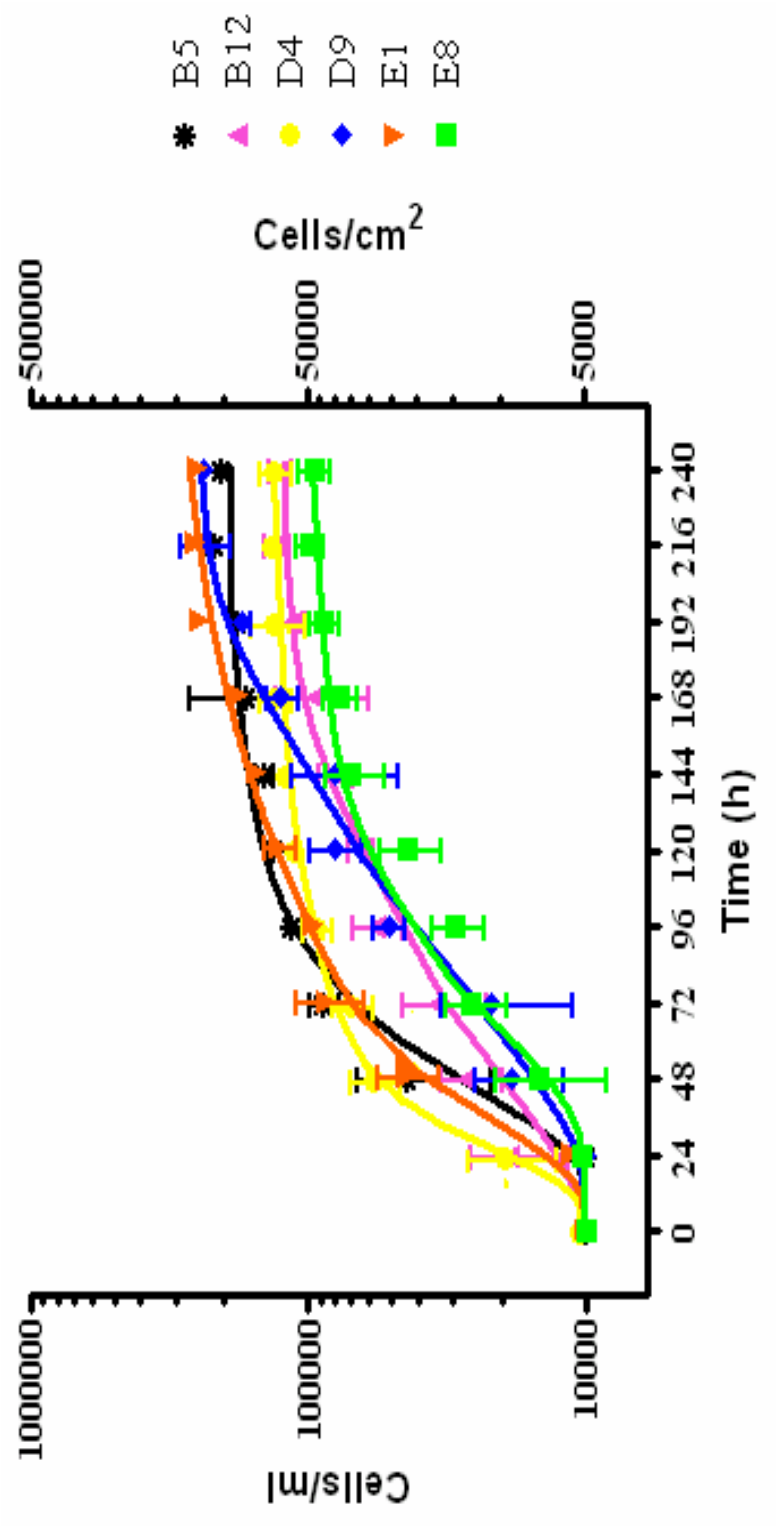

Figure 3.2. Growth curve of the six single cell clones. Semi log plot of the six clones after subculture that demonstrated variability in growth rate. Left axis represents the increase in cell concentration and right axis shows the cell density. Each time point was expressed as mean values ± SD of three independent experiments.

A one-way between-clones analysis of variance (ANOVA) was conducted to determine the significance of the observed variation in growth rates of the six clones. The mean doubling times of the clones are shown in Table 3.1. There was a statistically significant difference in growth rates among the different clones [$F(5,12) = 29.89$, $p < 0.0001$]. *Post hoc* comparisons using the Tukey's Honestly Significant Different (HSD) test and means grouping indicated that the mean doubling time of B12, D4 and D9 were significantly different from B5, E1 and E8 (see Appendix 2). Statistical significances were assessed by one-way analysis of variance (ANOVA). A summary of the *p*-values between clones is shown in Table 3.2.

Table 3.1. Doubling time of six cell clones. Values of the clones are shown as mean ± SD.

Cell clone	Mean doubling time (h)
B5	26.4 ± 0.5
B12	43.2 ± 4.8
D4	25.7 ± 1.9
D9	33.6 ± 0
E1	26.9 ± 0.5
E8	28.8 ± 0
MCF-7	29 *

* Doubling time supplied by the American Type Culture Collection (ATCC).

Table 3.2. Tukey HSD test of six single cell clones. Pairwise between-group comparisons showing *p*-values between clones. Statistical significance was set at *p*-value < 0.05. NS, not significant.

	B12	D4	D9	E1	E8
B5	< 0.001	NS	< 0.05	NS	NS
B12		< 0.001	< 0.01	< 0.001	< 0.001
D4			< 0.01	NS	NS
D9				< 0.05	NS
E1					NS

3.3. DNA extraction

In order to understand the role of mitochondrial function on the different growth rates observed in clones B12, D4 and D9, DNA was extracted from the exponentially growing cells of these three clones. Table 3.3 shows the purity and concentration of DNA obtained from the three clones. The A_{260}:A_{280} ratios of the three clones were greater than 1.8, indicating highly purified DNA. Figure 3.3 shows DNA analysed by electrophoresis. Subsequently, these DNA were used for PCR amplification of the entire mitochondrial genome and sequence analysis.

Table 3.3. The purity and concentration of DNA from three clones.

Clones	A_{260}:A_{280} ratio	Stock DNA concentration
B12	1.905	200 µg/ml
D4	1.853	315 µg/ml
D9	1.912	325 µg/ml

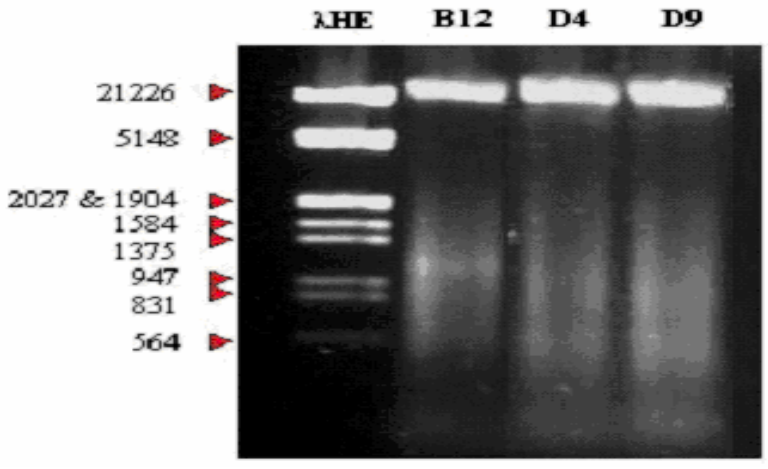

Figure 3.3. Analytical gel showing DNA extracted from the three clones of MCF-7 cells. Five microliters of DNA were separated by electrophoresis on 1% agarose gel, stained with ethidium bromide, and observed under ultraviolet illumination. Lane λHE: molecular weight marker; lanes B12, D4 and D9: DNA from single clones represented according to clone name.

3.4. PCR amplification and purification

Thirteen mitochondrial DNA fragments of the predicted sized were successfully amplified from each of the three clones using mtDNA specific primers (Table 2.1). The PCR products were size-fractionated on 1% agarose gels and each fragment was purified for later use as templates for sequencing. No visible PCR products were seen in the negative control (data not shown). Representative gels of the purified PCR products are depicted in Fig. 3.4-3.10. The purified PCR products were then stored at 4^{o}C until use for sequencing.

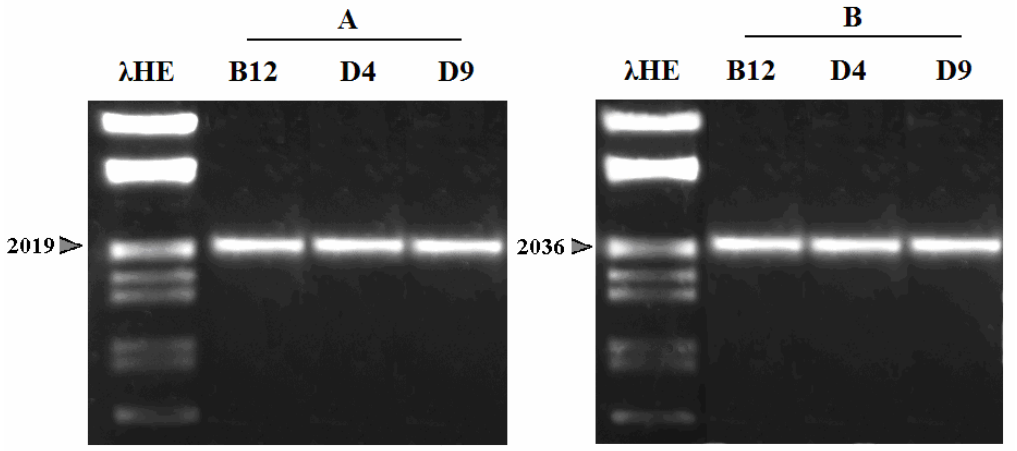

Figure 3.4. PCR amplification of mtDNA isolated from three single clones. 50 ng total DNA templates was amplified (50 µl PCR reaction) by primer pairs A and B (Table 2.1). The expected sizes of these products were 2019 bp and 2036 bp, respectively. Ten microlitres of PCR products were loaded per lane. Lane λHE: molecular weight marker; lanes B12, D4 and D9: DNA from single clones represented according to clone name.

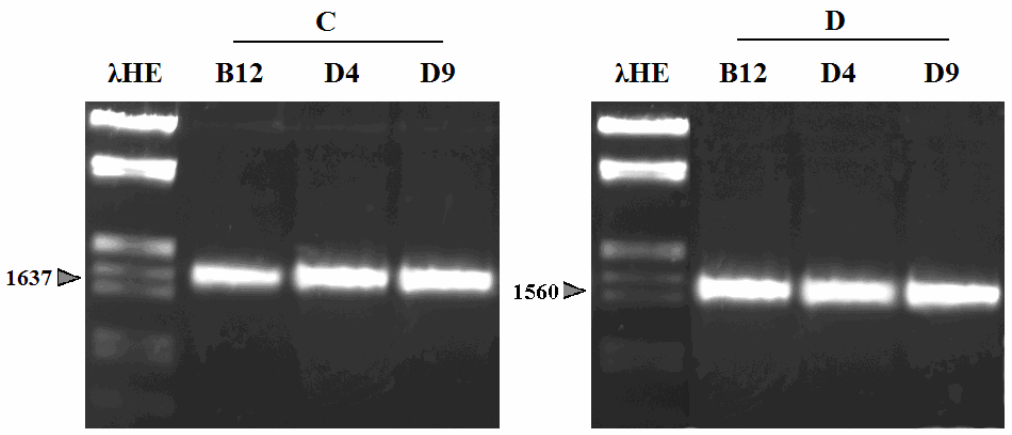

Figure 3.5. PCR amplification of mtDNA isolated from three single clones. 50 ng total DNA templates was amplified (50 µl PCR reaction) by primer pairs C and D (Table 2.1). The expected sizes of these products were 1637 bp and 1560 bp, respectively. Ten microlitres of PCR products were loaded per lane. Lane λHE: molecular weight marker; lanes B12, D4 and D9: DNA from single clones represented according to clone name.

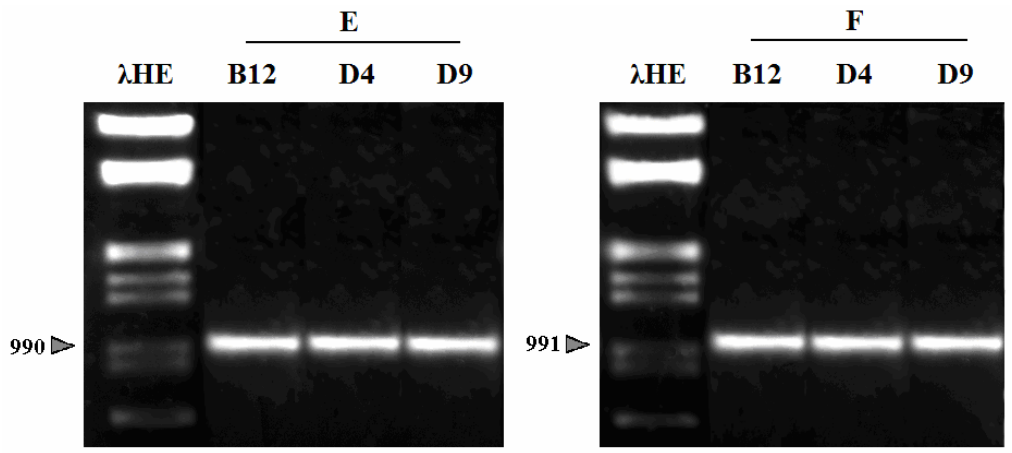

Figure 3.6. PCR amplification of mtDNA isolated from three single clones. 50 ng total DNA templates was amplified (50 µl PCR reaction) by primer pairs E and F (Table 2.1). The expected sizes of these products were 990 bp and 991 bp, respectively. Ten microlitres of PCR products were loaded per lane. Lane λHE: molecular weight marker; lanes B12, D4 and D9: DNA from single clones represented according to clone name.

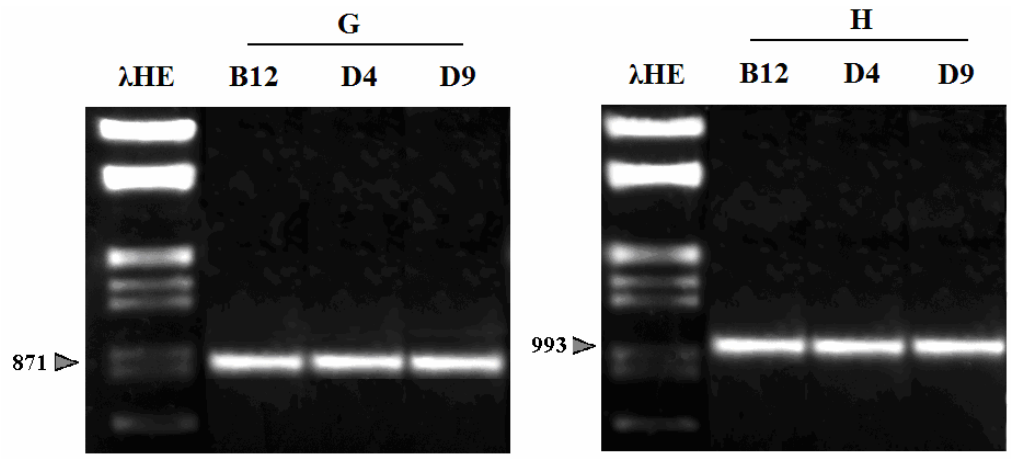

Figure 3.7. PCR amplification of mtDNA isolated from three single clones. 50 ng total DNA templates was amplified (50 µl PCR reaction) by primer pairs G and H (Table 2.1). The expected sizes of these products were 871 bp and 993 bp, respectively. Ten microlitres of PCR products were loaded per lane. Lane λHE: molecular weight marker; lanes B12, D4 and D9: DNA from single clones represented according to clone name.

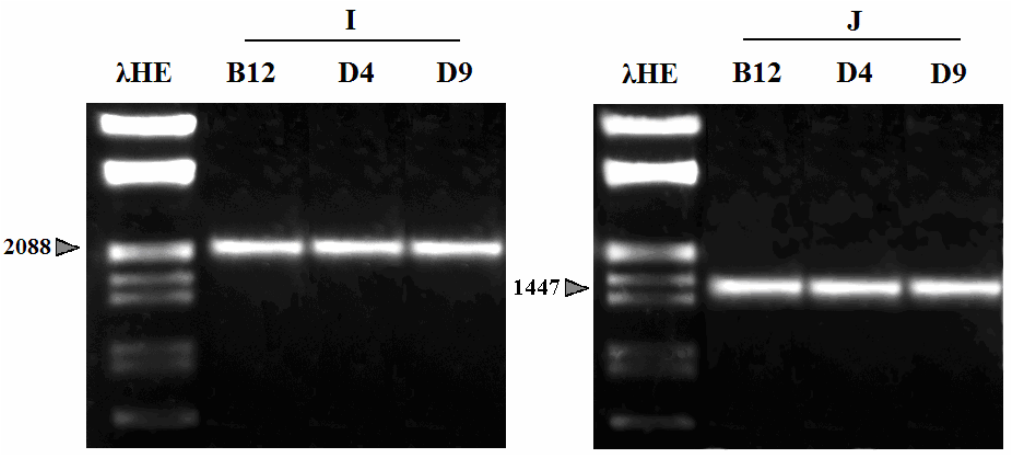

Figure 3.8. PCR amplification of mtDNA isolated from three single clones. 50 ng total DNA templates was amplified (50 µl PCR reaction) by primer pairs I and J (Table 2.1). The expected sizes of these products were 2088 bp and 1447 bp, respectively. Ten microlitres of PCR products were loaded per lane. Lane λHE: molecular weight marker; lanes B12, D4 and D9: DNA from single clones represented according to clone name.

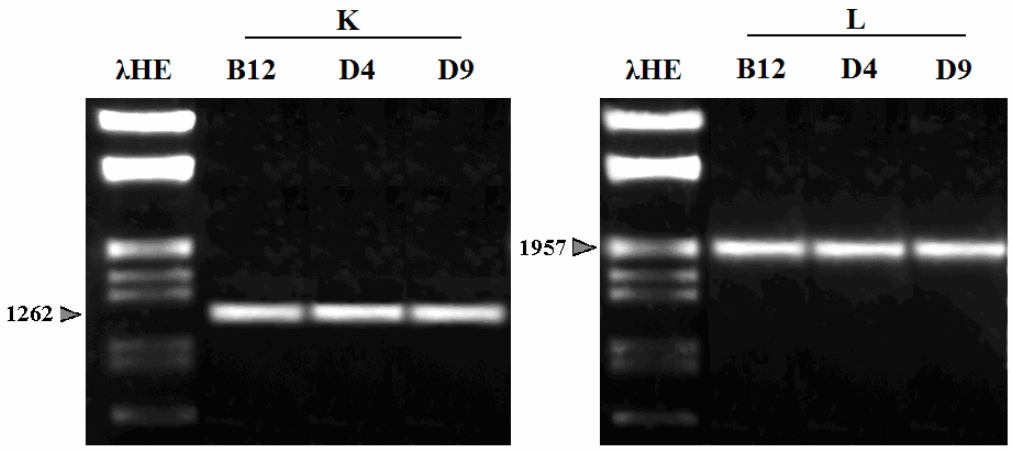

Figure 3.9. PCR amplification of mtDNA isolated from three single clones. 50 ng total DNA templates was amplified (50 µl PCR reaction) by primer pairs K and L (Table 2.1). The expected sizes of these products were 1262 bp and 1957 bp, respectively. Ten microlitres of PCR products were loaded per lane. Lane λHE: molecular weight marker; lanes B12, D4 and D9: DNA from single clones represented according to clone name.

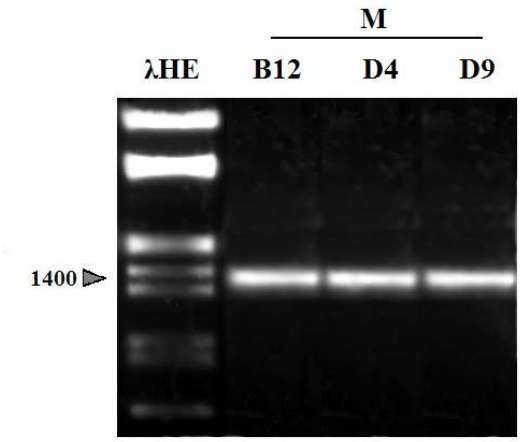

Figure 3.10. PCR amplification of mtDNA isolated from three single clones. 50 ng total DNA templates was amplified (50 µl PCR reaction) by primer pair M (Table 2.1). The expected sizes of these products were 1400 bp. Ten microlitres of PCR products were loaded per lane. Lane λHE: molecular weight marker; lanes B12, D4 and D9: DNA from single clones represented according to clone name.

3.5. mtDNA mutation analysis

Sequence analyses of the entire mitochondrial genome revealed 38 mutations common to all three clones (Table 3.4) and seven clone-specific mutations (Table 3.5) found in the clones. The common mutations consisted of transition, transversion, deletion and insertion. All base substitutions were homoplasmic. Of the 38 common mutations, 12 polymorphisms were in the hypervariable D loop region, 12 polymorphisms in the ND gene, 6 polymorphisms in the COX gene, 3 polymorphisms in the 16S rRNA, 2 polymorphisms in the Cyt b, 1 polymorphism each in the ATPase 6, $tRNA^{Thr}$ and the intergenic region, respectively. These mutations were different from the revised NCBI reference sequence (accession number NC_001807, version February 2006). As shown in Fig. 3.11 – 3.15, of the seven clone-specific mutations, one of these mutations was in a homoplasmic state (in ND4) and six displayed heteroplasmies (three in 16S rRNA, one each in ND1, ND6 and COX III). The results were confirmed by repeated amplification and sequencing with alternative primers.

Clone B12 harboured five transversion mutations at nucleotides (nts) 2480, 2513, 2520 (Fig. 3.11), 9527 (Fig. 3.12) and 14263 (Fig. 3.13). The mutations at 2480, 2513 and 2520 were found to be located at the 16S rRNA of mtDNA. Every mutation was heteroplasmic as indicated by the presence of double peaks at respective positions. The C9527T mutation resulted in an alanine → serine substitution at amino acid position 107 (A107S) in the COX III subunit. The C14263G mutation caused an aspartic acid → histidine substitution at amino acid position 138 (D138H) of the ND6 subunit. A heteroplasmic mutation was also found in clone D9, displaying both A and G nucleotides at nt 4137 (Fig. 3.14). This A4137C mutation resulted in a tyrosine → cysteine substitution at amino acid position 277 (Y277C) of the ND1 subunit. In clone D4, a C to T base substitution was detected at nt 11496 (Fig. 3.15). This C11496T mutation causes a leucine → phenylalanine substitution at amino acid 246 (L246F) of the ND4 subunit.

Table 3.4. **Common mutations in MCF-7 clones with respect to human mtDNA sequence**. (NCBI, version February 2006).

Nucleotide position	NCBI (21 Feb 2006)	MCF-7 clones	Gene	Amino acid change
73	G	A	D Loop	--
150	T	C	D Loop	--
195	C	T	D Loop	--
303	C	Deletion	D Loop	--
410	A	T	D Loop	--
2354	C	T	16S rRNA	--
2485	C	T	16S rRNA	--
2708	G	A	16S rRNA	--
5581	C	T	Intergenic	--
5896	C	Insertion	COX I	Frameshift
6777	T	C	COX I	Syn
7029	T	C	COX I	Syn
8702	G	A	ATPase 6	S → N
9378	G	A	COX III	Syn
9541	C	T	COX III	Syn
9967	G	A	COX III	V → I
10399	G	A	ND3	A → Y
10820	G	A	ND4	S → N
10874	C	T	ND4	P → L
11018	C	T	ND4	A → V
11720	A	G	ND4	D → G
11723	C	T	ND4	S → L
12706	T	C	ND5	F → L
12851	G	A	ND5	S → N
13261	T	C	ND5	S → P
14213	C	T	ND6	Syn
14320	T	C	ND6	N→D
14581	G	A	ND6	Syn
14767	T	C	Cyt b	Syn
14906	A	G	Cyt b	Y → C
15933	C	T	$tRNA^{Thr}$	--
16149	C	T	D Loop	--
16173	C	T	D Loop	--
16184	C	Deletion	D Loop	--
16185	C	A	D Loop	--
16191	C	T	D Loop	--
16225	T	C	D Loop	--
16322	T	C	D Loop	--

NCBI = National Center for Biotechnology Information. rRNA, ribosomal RNA; COX, cytochrome c oxidase; ATPase, ATP synthase; ND, NADH dehydrogenase; cyt b, cytochrome b; tRNA, transfer RNA; Syn, synonymous mutation; n/a, not applicable.

Table 3.5. Summary of the single nucleotide polymorphisms (SNPs) detected in three clones.

Clone	Mutation	Gene	Amino acid change	Heteroplasmy
B12	G2480T	*h*16S rRNA	n/a	29.2%
B12	C2513G	*h*16S rRNA	n/a	42.9%
B12	A2520T	*h*16S rRNA	n/a	55.1%
B12	C14263G	*h*ND6	D138H	35%
B12	C9527T	*h*COX III	A107S	15.8%
D4	C11496T	ND4	L246F	-
D9	A4137G	*h*ND1	Y277C	50%

h, heteroplasmy; n/a, not applicable. rRNA, ribosomal RNA; ND, NADH dehydrogenase. The number in between the base refers to the nucleotide position. The number in between the amino acid abbreviation refers to the residue position. Heteroplasmy refers to the amount of mutant DNA in percentage.

Fig. 3.11-3.14 show chromatograms of well-resolved peaks. The peaks were well-defined with nice even spacing between them. These peaks were consistent and reproducibly obtained in every sequence analysis. In addition, there was little background noise present at the peak baselines. However, these noise peaks were not reproducible and consistent. They frequently showed indistinct crests and troughs and did not interfere with the proper base calling. The secondary peaks running above, under or overlapped the main peaks indicated heteroplasmies. These peaks were reproducible and were denoted by repeatedly distinct crest at the same point every sequencing. They were further confirmed by repeated sequencing from both forward and reverse directions to ensure reading accuracy.

Fig. 3.15 showed a chromatogram of fairly far along the sequence, where the peaks were no longer sharp but have begun to broaden and more rounded in shape. Similar chromatogram pattern was also found by Zhu *et al*. (2005) which showed a homoplasmic mtDNA mutation in breast cancer tissue at A16293G.

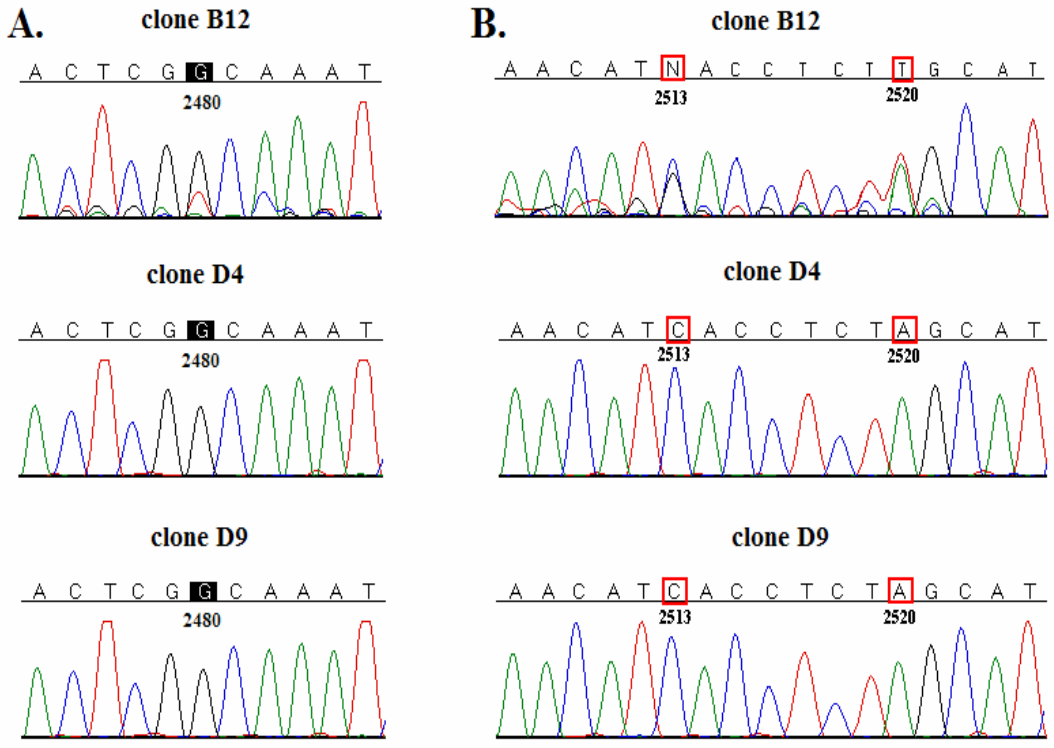

Figure 3.11. Sequencing patterns of the mutation sites in mitochondrial 16S rRNA gene from the three clones. There is a G to T transversion at nt 2480 (A), a C to G transversion at nt 2513 (B), and an A to T transversion at nt 2520 (B). The presence of two peaks in B12 indicates heteroplasmic mutation.

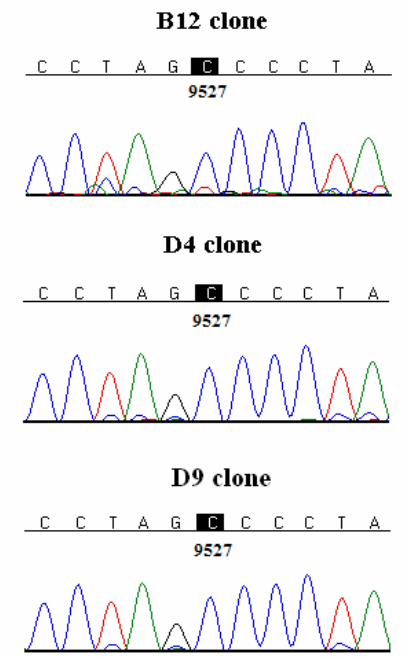

Figure 3.12. Identification of C9527T mutation in the mitochondrial COX III gene.

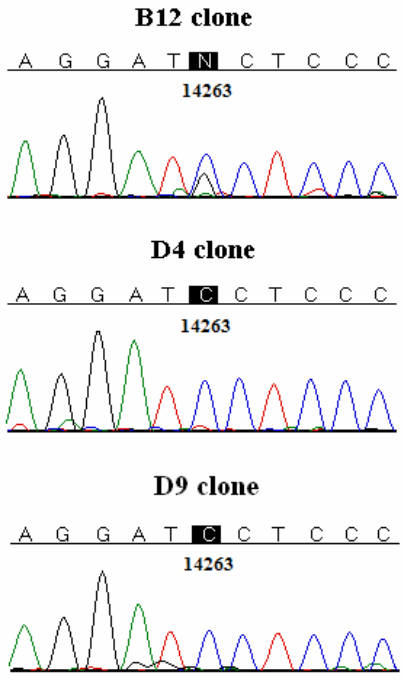

Figure 3.13. Identification of C14263G mutation in the mitochondrial ND6 gene.

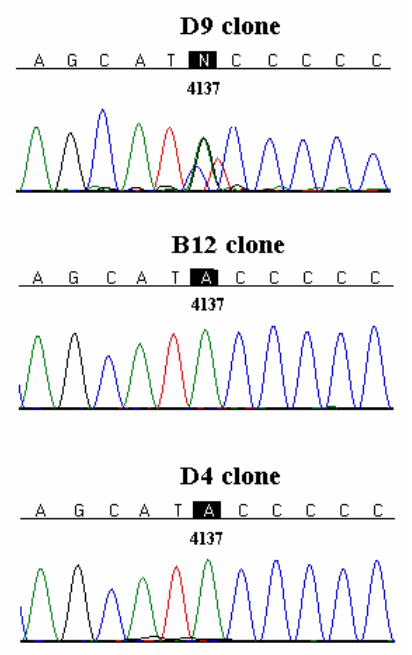

Figure 3.14. Identification of A4137G mutation in the mitochondrial ND1 gene.

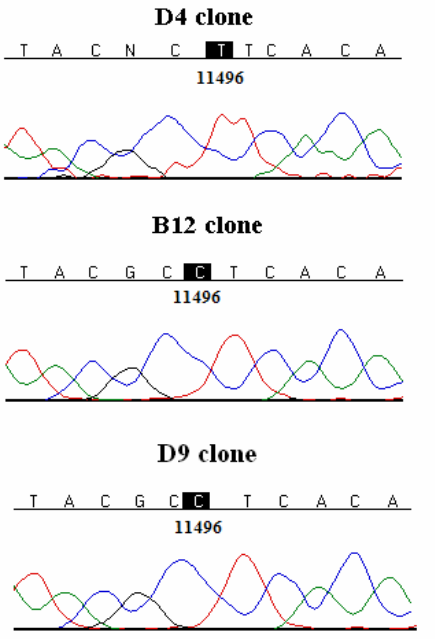

Figure 3.15. Identification of C11496T mutation in the mitochondrial ND4 gene.

3.6. Sensitivity of heteroplasmy detection

DNA of D4, a homoplasmic individual was mixed with the DNA sample from a heteroplasmic individual B12 possessing a heteroplasmic A2520T mutation within the 16S rRNA gene (Fig. 3.16). The mixing experiments revealed that effective proportion of the DNA mixture were 69 : 31, 77.6 : 12.4, 93.8 : 6.2 and 97 : 3. These observations suggested that heteroplasmic mtDNA variants representing as low as 12% can be detected by ABI sequencing method (Harris *et al*., 2006).

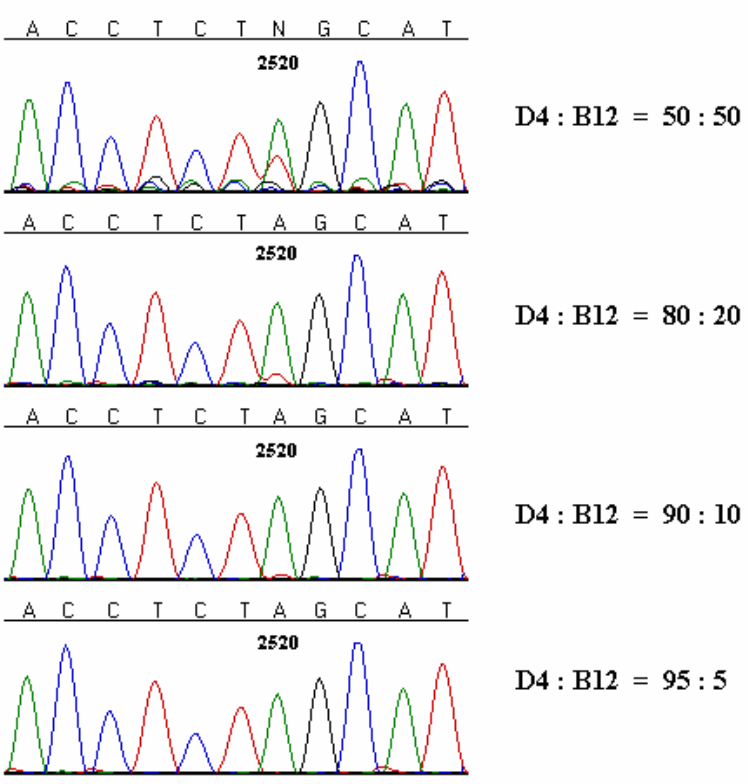

Figure 3.16. Detection of A2520T mtDNA heteroplasmy. Chromatogram showed the heteroplasmic sensitivity of the mixing experiments. The ratios of the mixing experiments are shown on the right.

3.7. RNA secondary structure prediction

To investigate the possible functional effect of the mutations found in 16S rRNA gene, prediction of their minimum free energy (MFE) secondary structures was performed using the RNAfold software (Hofacker 2003). Full secondary structure modelings were performed by inputting the entire 16S rRNA sequences. The secondary structure of 16S rRNA is largely determined by internal base pairing. D4 and D9 showed concordance by presenting the same 16S rRNA secondary structure (Fig. 3.17A). Clones D4 and D9 also share identical structure with normal human 16S rRNA (data not shown). However, the three substitutions (G2480T, C2513G and A2520T) found in B12 resulted in a dramatic change of the folding (Fig. 3.17B). The predicted secondary structure of B12 16S rRNA had more extended helical segments than the common secondary structure of D4-D9 16S rRNA. These heteroplasmic mutations are predicted to alter the secondary structure of the 16S rRNA molecule. The predicted initial free energies (dG) are -362.20 and -360.61 kcal/mole for D4-D9 and B12, respectively.

3.8. Amino acid sequence analysis

The Kyte-Doolittle scale (Kyte and Doolittle 1982) was used for delineating hydrophobic character of the amino acids by referring to the physicochemical properties of amino acid side chains. The polypeptide secondary structure was predicted using nnPredict software on the internet (http://www.cmpharm.ucsf.edu/~nomi/nnpredict.html). The results were noted in three classes of secondary structure: α-helix, β-strand and 'no prediction'. The predicted secondary structure type for each residue is the type with the highest propensity or probability.

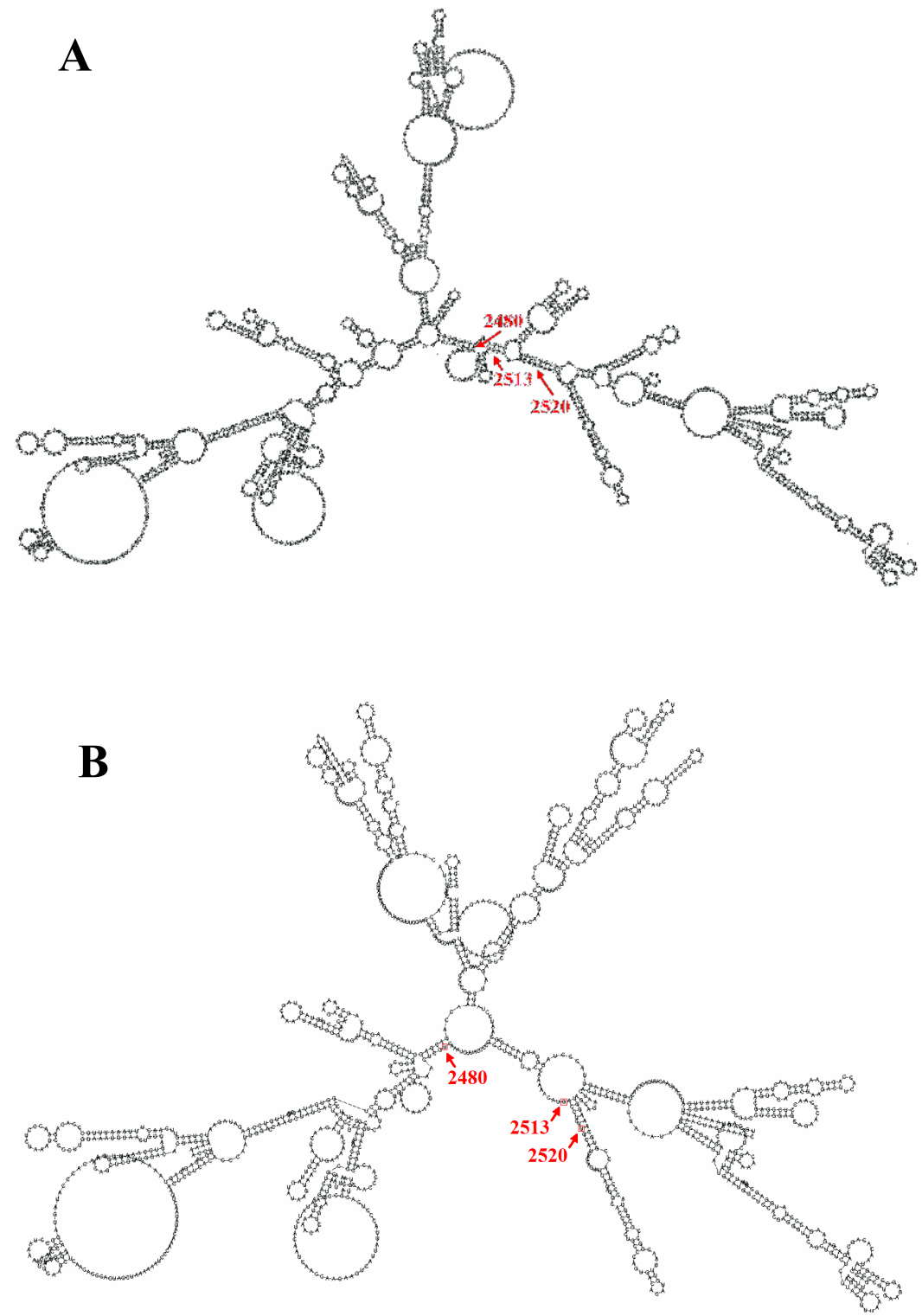

Figure. 3.17. Secondary structures prediction of 16S rRNA by the RNAfold software. Arrows indicate the location of heteroplasmic nucleotides. A, common secondary structure of D4 and D9 16S rRNA. B, secondary structure of B12 16S rRNA.

3.8.1. A4137G heteroplasmic mutation in D9

The A4137G mutation found in clone D9 changed the hydrophobicity and volume, replacing the large, hydrophilic tyrosine with the small and less hydrophilic cysteine. This substitution was predicted to alter the Kyte-Doolittle hydropathy profile for ND1 (Table 3.6). There was also a slight change in the polarity. However, no change was observed in the amino acid secondary structure (Fig. 3.18).

Table 3.6. Hydropathicity and polarity analysis of amino acid residue 277 of ND1.

Amino acid property	Tyrosine to Cysteine change at residue 277	
	B12 and D4	D9
Hydropathicity[a]	-1.143	-0.600
Polarity[b]	8.157	8.057

[a]Hydropathicity was analysed by averaging over a window size of 7. The different properties of the amino acid were compared between the clones. Regions with values above 0 are hydrophobic in character and less likely to interact with water (Kyte and Doolittle 1982).

[b]The polarity reading denotes the charge of the amino acid. The amino acid is likely to be basic or acidic when the reading reaches above 10. The reading 5-7 indicates that the amino acid is likely to be nonpolar (Grantham 1974).

	267										277										287
Normal	T	S	L	F	L	W	I	R	T	A	Y	P	R	F	R	Y	D	Q	L	M	H
B12 and D4	T	S	L	F	L	W	I	R	T	A	Y	P	R	F	R	Y	D	Q	L	M	H
D9	T	S	L	F	L	W	I	R	T	A	C	P	R	F	R	Y	D	Q	L	M	H
B12 and D4	H	H	H	H	H	E	E	H	-	-	-	-	-	-	-	-	-	H	H	H	H
D9	H	H	H	H	H	E	E	H	-	-	-	-	-	-	-	-	-	H	H	H	H

Figure 3.18. nnpredict secondary structure prediction for ND1 at amino acid residue 277.
H = α-helix, E = β-strand, - = no prediction.

3.8.2. C9527T heteroplasmic mutation in B12

The C9527T mutation found in clone B12 changed the hydrophobicity and polarity, replacing the small, nonpolar hydrophobic alanine with the polar and uncharged, hydrophilic serine. This substitution was predicted to alter the Kyte-Doolittle hydropathy profile for COX III (Table 3.7). The amino acid secondary structure was predicted as shown in Fig. 3.19. The result shows that the new serine amino acid shortens an α-helix and lengthens a β-strand.

Table 3.7. Hydropathicity and polarity analysis of amino acid residue 107 of COX III.

Amino acid property	Alanine to Serine change at residue 107	
	D4 and D9	B12
Hydropathicity[a]	0.014	-0.357
Polarity	8.000	8.157

[a]Hydropathicity was analysed by averaging over a window size of 7. The different properties of the amino acid were compared between the clones. Regions with values above 0 are hydrophobic in character and less likely to interact with water (Kyte and Doolittle 1982).

[b]The polarity reading denotes the charge of the amino acid. The amino acid is likely to be basic or acidic when the reading reaches above 10. The reading 5-7 indicates that the amino acid is likely to be nonpolar (Grantham 1974).

	97										107										117
Normal	F	F	W	A	F	Y	H	S	S	L	A	P	T	P	Q	L	G	G	H	W	P
D4 and D9	F	F	W	A	F	Y	H	S	S	L	A	P	T	P	Q	L	G	G	H	W	P
B12	F	F	W	A	F	Y	H	S	S	L	S	P	T	P	Q	L	G	G	H	W	P
D4 and D9	H	H	E	H	H	E	-	-	-	-	-	-	-	-	-	-	-	-	-	-	-
B12	H	H	E	H	E	E	-	-	-	-	-	-	-	-	-	-	-	-	-	-	-

Figure 3.19. nnpredict secondary structure prediction for COX III at amino acid residue 107. H = α-helix, E = β-strand, - = no prediction.

3.8.3. C11496T homoplasmic mutation in D4

The C11496T mutation found in clone D4 causes slight changed in the hydrophobicity and polarity (Table 3.8). The amino acid secondary structure was predicted as shown in Fig. 3.20. The result shows that the new phenylalanine amino acid replaces three α-helices with β-strands.

Table 3.8. Hydropathicity and polarity analysis of amino acid residue 246 of ND4.

Amino acid property	Leucine to Phenylalanine change at residue 246	
	B12 and D9	D4
Hydropathicity[a]	1.529	1.386
Polarity	6.500	6.543

[a]Hydropathicity was analysed by averaging over a window size of 7. The different properties of the amino acid were compared between the clones. Regions with values above 0 are hydrophobic in character and less likely to interact with water (Kyte and Doolittle 1982).

[b]The polarity reading denotes the charge of the amino acid. The amino acid is likely to be basic or acidic when the reading reaches above 10. The reading 5-7 indicates that the amino acid is likely to be nonpolar (Grantham 1974).

	236										246									256
Normal	L	K	L	G	G	Y	G	M	M	R	L	T	L	I	L	N	P	L	T	K	H
B12 and D9	L	K	L	G	G	Y	G	M	M	R	L	T	L	I	L	N	P	L	T	K	H
D4	L	K	L	G	G	Y	G	M	M	R	F	T	L	I	L	N	P	L	T	K	H
B12 and D9	H	H	H	-	-	-	-	H	H	E	E	E	E	H	-	-	-	H	-	-	-
D4	H	H	H	-	-	-	-	E	E	E	E	E	E	E	-	-	-	H	-	-	-

Figure 3.20. nnpredict secondary structure prediction for ND4 at amino acid residue 246.
H = α-helix, E = β-strand, - = no prediction.

3.8.4. C14263G heteroplasmic mutation in B12

The C14263G mutation found in clone B12 changed the hydrophobicity, polarity, volume and acidity. The polar, acidic aspartate was replaced by the bigger, polar, basic histidine. This substitution was predicted to alter the Kyte-Doolittle hydropathy profile for ND6 (Table 3.9). The amino acid secondary structure was predicted as shown in Fig. 3.21. The predicted change in the ND6 subunit shows that the new histidine amino acid extends an additional β-strand.

Table 3.9. Hydropathicity and polarity analysis of amino acid residue 138 of ND6.

Amino acid property	Aspartate to Histidine change at residue 138	
	D4 and D9	B12
Hydropathicity[a]	-0.643	-0.600
Polarity	9.029	8.657

[a]Hydropathicity was analysed by averaging over a window size of 7. The different properties of the amino acid were compared between the clones. Regions with values above 0 are hydrophobic in character and less likely to interact with water (Kyte and Doolittle 1982).

[b]The polarity reading denotes the charge of the amino acid. The amino acid is likely to be basic or acidic when the reading reaches above 10. The reading 5-7 indicates that the amino acid is likely to be nonpolar (Grantham 1974).

	128										138									148
Normal	E	G	E	G	S	G	L	I	R	E	D	P	I	G	A	G	A	L	Y	D	Y
D4 and D9	E	G	E	G	S	G	L	I	R	E	D	P	I	G	A	G	A	L	Y	D	Y
B12	E	G	E	G	S	G	L	I	R	E	H	P	I	G	A	G	A	L	Y	D	Y
D4 and D9	E	-	-	-	-	-	-	E	E	-	-	-	-	-	-	-	-	E	H	H	H
B12	E	-	-	-	-	-	-	E	E	E	-	-	-	-	-	-	-	E	H	H	H

Figure 3.21. nnpredict secondary structure prediction for ND6 at amino acid residue 138.
H = α-helix, E = β-strand, - = no prediction.

3.9. Enzyme assays

Enzyme biochemical studies were carried out to determine the impact of those mtDNA mutations on respiratory enzyme activities. The mitochondria concentrations of cell extracts from B12, D4 and D9 cells were determined using Bradford assay (see Appendix 3). Calculations of enzyme activity were based on the linear portions of the reaction rates. Figure 3.23 shows the mean values of the mitochondrial marker citrate synthase (CS) activity. There was a significant decrease (4-fold) in citrate synthase activity of clone B12 compared to clone D4. Table 3.10 summarises the mitochondrial OXPHOS enzyme-specific activities of the three clones. The result showed that defective OXPHOS was associated with specific mutation of mtDNA in individual clones. Nevertheless, respiratory complex activities directly reflect the electron transfer capacity. The enzymatic activities of all the enzyme assays were standardised with reference to CS, which was generally accepted as an indicator for the number and/or volume of mitochondria in a mitochondrial preparation (DiDonato *et al*., 1993). Hence, the ratio of respiratory complex/CS activities would indicate whether the change in enzyme activity was directly related to the specific mtDNA mutation, or was due to impairment in electron transfer chain activities (Ruiz-Pesini *et al*., 1998).

As shown in Figure 3.23, there was variation in the mean values of the five respiratory chain complexes upon normalisation to CS activity. One-way ANOVA and *post hoc* Tukey's HSD test were used to determine the statistical significance of the difference in the electron transport activities of respiratory enzymes in mitochondria among the three clones (Table 3.11). A p-value < 0.05 was accepted as the level of statistical significance. After correction for CS, there were statistically significant differences in all enzymes activities between clones B12 and D4. An increase in complex I and decreases in complex II, III, IV and V of clone B12 were observed compared to D4. However, no statistically significant differences were observed between clones B12 and D9 in citrate synthase, complex II, III and IV enzymes activities. Although statistically insignificant, the overall results obtained showed that the activities of respiratory chain complexes were diminished with respect to mtDNA mutation in the clones.

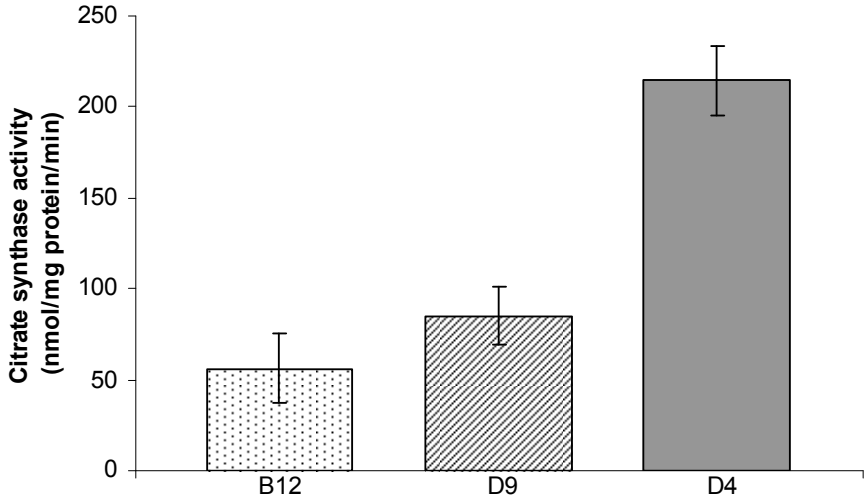

Figure 3.22. Citrate synthase activity in clones B12, D9 and D4. Citrate synthase activity was determined by the method of Shepherd and Garland (1969), and represented as nmol/mg protein/min. The data represents as mean ± SD of three different measurements.

Table 3.10. Mitochondrial OXPHOS enzyme-specific activities in MCF-7 clones. Results are expressed as nmol/min/mg protein. The data are shown as mean value ± SD (n=3).

	Complex I	Complex II	Complex III	Complex IV	Complex V
B12	691.9 ± 74.5	947.1 ± 225.9	207.7± 43.7	88.8 ± 16.1	186.7 ± 39.5
D9	301.4 ± 62.0	1389.4 ± 329.9	354.7 ± 40.9	186.1 ± 24.3	351.1 ± 63.9
D4	569.7 ± 37.1	10345.6 ± 873.9	1064.6 ± 79.6	612.8 ± 34.1	1751.7 ± 430.3

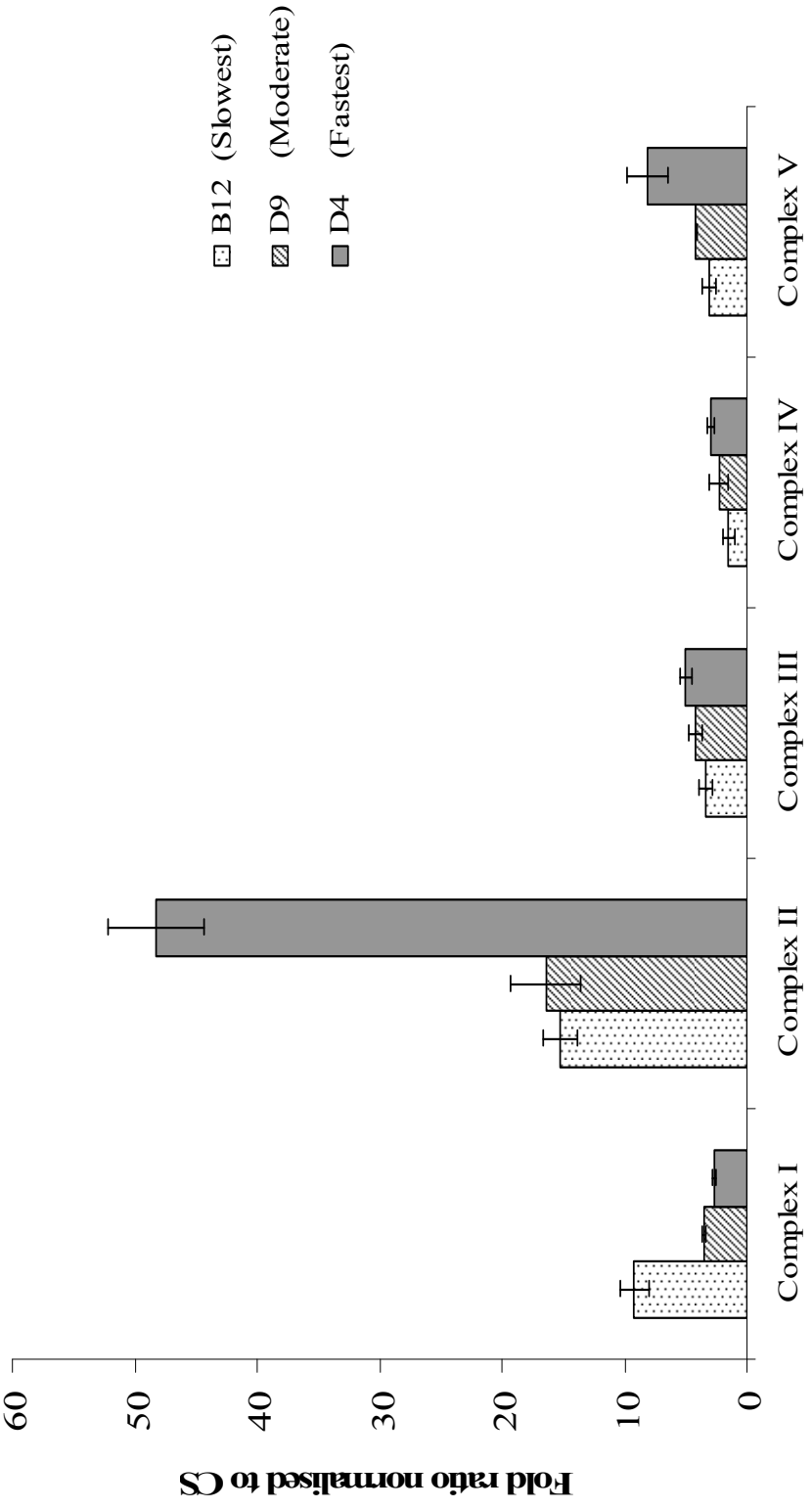

Figure 3.23. Respiratory chain biochemistry in MCF-7 clones. The respiratory enzyme complexes were assayed as described in 'Materials and Methods'. Values of enzymatic activities of the respiratory chain complexes were normalised to CS. The data represents as mean ± SD of three different measurements.

Table 3.11. Statistical significance analysis of citrate synthase (CS) and the normalised mitochondrial respiratory enzyme activities in B12, D4 and D9 clones. Pairwise between-group comparisons showing *p*-values between clones.

Respiratory enzyme	Clone	D4	D9
Citrate synthase (CS)	**B12**	$p < 0.001$	NS
	D4		$p < 0.001$
Complex I/CS	**B12**	$p < 0.01$	$p < 0.01$
	D4		$p < 0.01$
Complex II/CS	**B12**	$p < 0.001$	NS
	D4		$p < 0.01$
Complex III/CS	**B12**	$p < 0.05$	NS
	D4		NS
Complex IV/CS	**B12**	$p < 0.05$	NS
	D4		NS
Complex V/CS	**B12**	$p < 0.01$	$p < 0.05$
	D4		$p < 0.05$

I, complex I (NADH-ubiquinone oxidoreductase); II, complex II (succinate dehydrogenase); III, complex III (ubiquinol-cytochrome c oxidoreductase); IV, complex IV (cytochrome c oxidase); V, complex V (ATP synthase). Statistical significances were assessed by one-way ANOVA and Tukey's HSD test. Statistical significance was set at *p*-value < 0.05. NS, not significant.

3.10. Effect of extracellular ATP on cell proliferation

In order to determine whether the slow growth rate observed in clone B12 was due to low ATP production by these cells, B12 cells were cultured in the presence of exogenous ATP at different concentrations (0 μM, 50 μM, 100 μM and 1 mM). D4 (fastest growth) was cultured without exogenous ATP as a reference for comparison. Phase contrast micrographs showing morphology of the cells were taken 48 h after seeding (Fig. 3.24). The cell density increased with increasing ATP concentrations. The cell population doubling times were determined by daily cell number estimation. Figure 3.25 shows the growth curve for each treatment. Table 3.12 summarises the mean doubling time of the cells growth under different conditions. A one-way ANOVA was used as a parametric approach to assess the effect of extracellular ATP on the cells. There was a statistically significant difference in growth rates when different ATP concentration was supplemented to the culture media [$F(4,10) = 80.55$, $p < 0.0001$]. *Post-hoc* comparisons using the Tukey HSD test was carried out to determine the significance of the differences between pairs in the five groups (see Appendix 3). Statistical significance was assessed by one-way analysis of variance (ANOVA). Table 3.13 shows the *p*-values for different comparisons. No significant effect on the growth rate was observed when the cells were cultured in the presence of 50 μM ATP. However, a clear and reproducible effect on the growth rate was observed at 100 μM, while a maximal response was observed at 1 mM.

Table 3.12. Doubling time of B12 (at different ATP concentration) and D4 (without ATP).

Cell	Mean doubling time (h)
D4	21.6 ± 1.4
B12 (no ATP)	40.8 ± 2.4
B12 – 50 μM ATP	36 ± 2.4
B12 – 100 μM ATP	26.4 ± 2.4
B12 – 1 mM ATP	19.2 ± 1.4

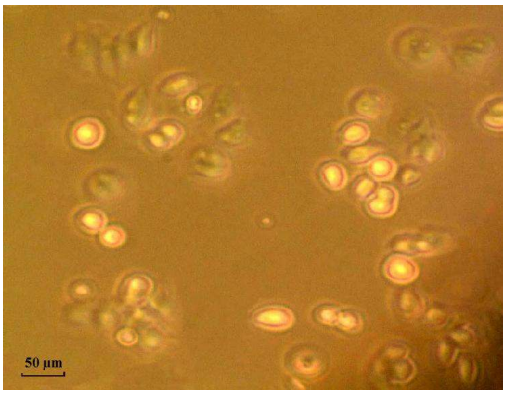

B12 – no ATP

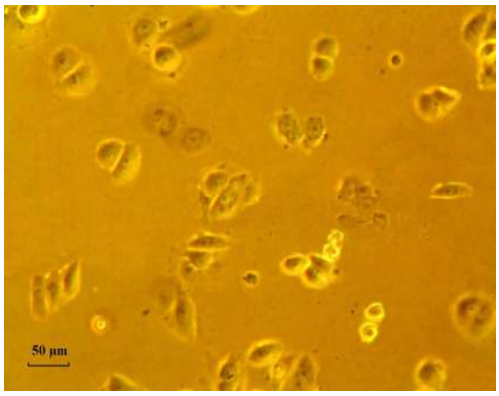

B12 treated with 50 µM ATP

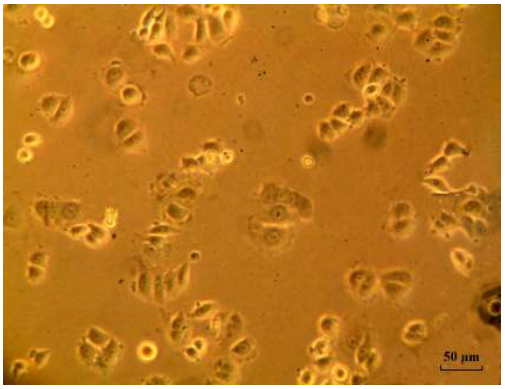

B12 treated with 100 µM ATP

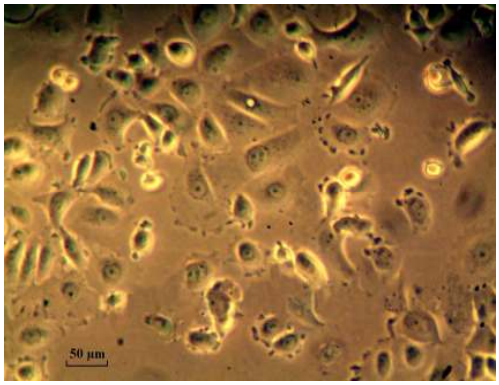

B12 treated with 1 mM ATP

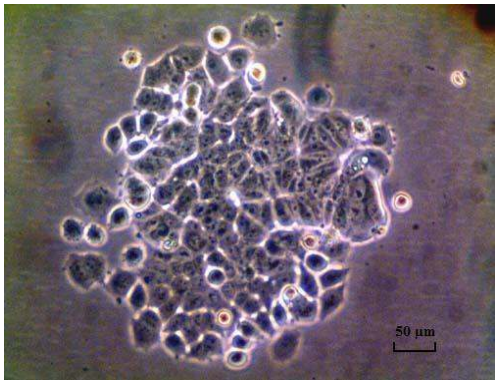

D4 – no ATP

Figure 3.24. Growth morphology and characteristic showing the effect of extracellular ATP on cultured cells. 48 h after seeding at 1 x 10^4 cells/ml/well. The cell proliferation increased with the concentration of extracellular ATP. Phase contrast. Scale bar 50 µm.

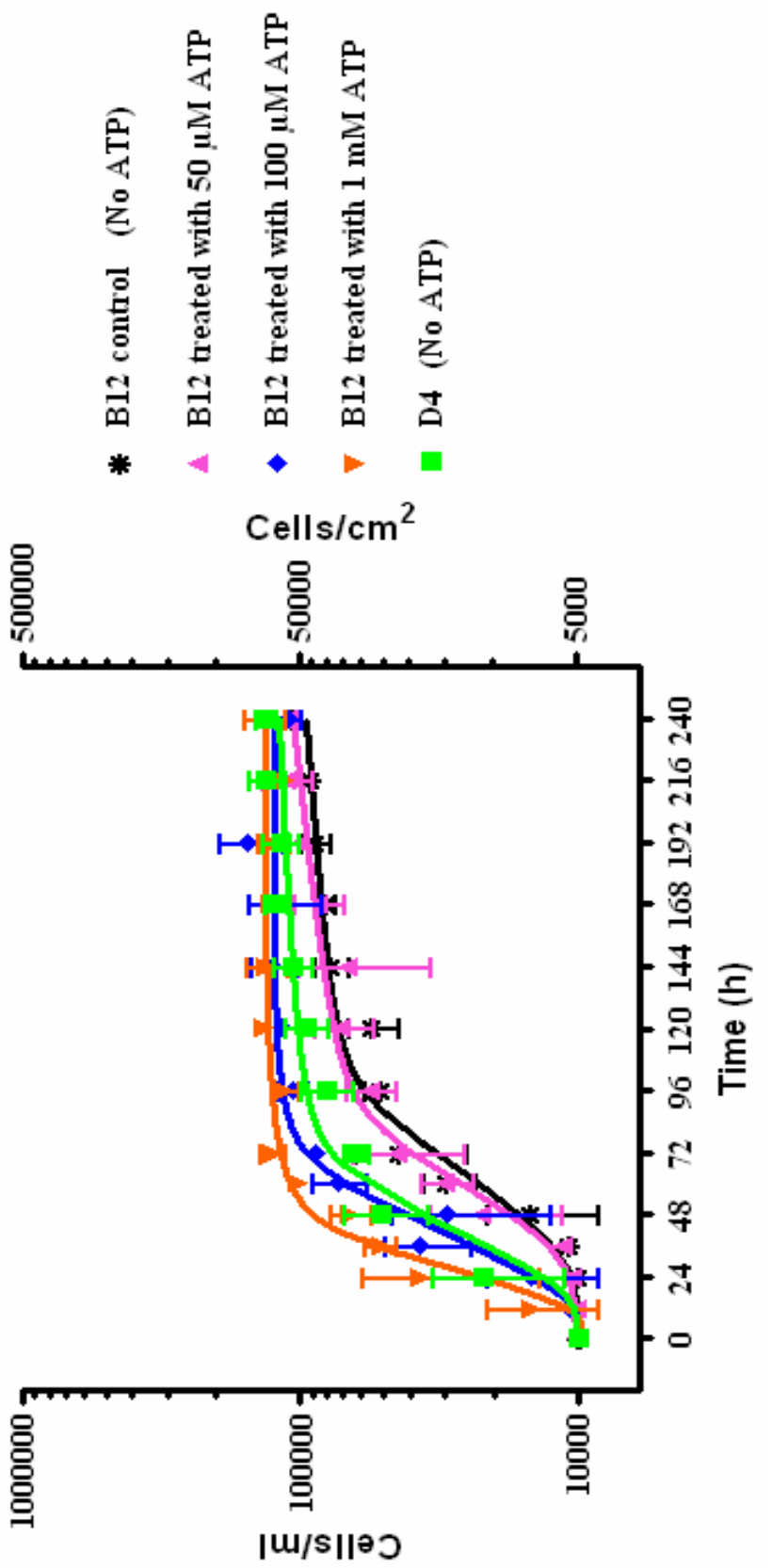

Fig 3.25. Effect of extracellular ATP on growth. Cells were plated in 24-well dishes. The viable cells were counted at the indicated times. The data for each clone are expressed as mean ± S.D. of three separate experiments. Results show a significant increase in the growth rate of B12 cells as the concentration of extracellular ATP increased.

Table 3.13. Tukey HSD test of B12 (at different ATP concentration) and D4 (without ATP). Pairwise between-group comparisons showing *p*-values between clones. Statistical significance was set at *p*-value < 0.05. NS, not significant.

	B12 (50 µM ATP)	B12 (100 µM ATP)	B12 (1mM ATP)	D4 (no ATP)
B12 (no ATP)	NS	< 0.001	< 0.001	< 0.001
B12 (50 µM ATP)		< 0.001	< 0.001	< 0.001
B12 (100 µM ATP)			< 0.05	NS
B12 (1mM ATP)				< 0.01

3.11. RNA extraction from cell cultures

In order to investigate the effect of exogenous ATP on cellular function, RNA was extracted from clone B12 grown in different ATP concentrations, clone D4 and D9. The RNA was then separated and analysed on a denatured gel. Figure 3.26 shows 28S and 18S rRNA bands. The total RNA samples were then tested for genomic DNA contamination by direct PCR using the RNA preparation as templates before the RNA was used for cDNA synthesis (data not shown).

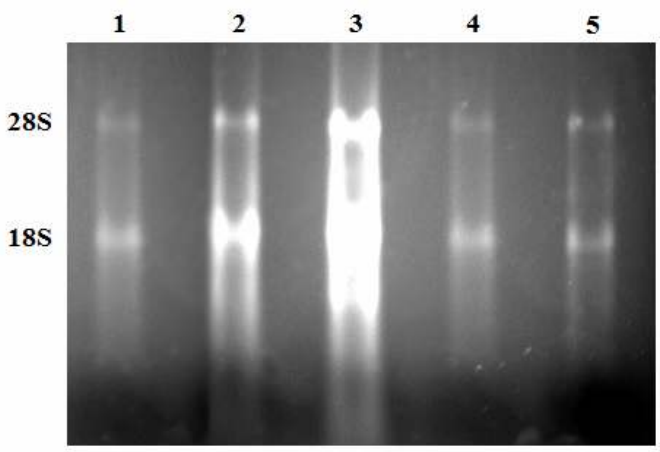

Figure 3.26. Representative gel image of total RNA. Total RNA were separated by gel electrophoresis on denatured 1% agarose-formaldehyde gel. Bright 28S and 18S rRNA bands; and an even mRNA smear were present. Lane 1: B12. Lane 2: B12 treated with 100 µM ATP. Lane 3: B12 treated with 1 mM ATP. Lane 4: D4. Lane 5: D9.

3.12. Comparative reverse-transcription PCR (RT-PCR)

Normalisation based on 18S rRNA was used to correct for differences arising from variation in the quality and quantity of starting RNA in each assay. 18S rRNA was chosen over β-actin and glyceraldehydes-3-phosphate dehydrogenase (GAPDH) because expression of 18S rRNA under different experimental conditions was not found to be affected by exogenous ATP concentration in the culture media (Finnegan 1993; Yamada 1997). Expression of the selected genes was expressed relative to 18S rRNA. Figure 3.27 shows the RT-PCR products of four selected genes. The band intensities of the RT-PCR products were found to be increased with increasing amount of ATP added to the culture medium. D4, which was the fastest growing clone showed the lowest band intensity as compared to D9, the moderately fast growing clone. The levels of expression of the genes relative to 18S rRNA were further determined by using GeneTools as described in 'Materials and methods'. Figure 3.28 shows a consistent correlation between the ATP concentration and B12 gene expression. To rule out the contamination by genomic DNA, total RNA samples without RT reaction were subjected to PCR amplification. However, no DNA fragment was detected (data not shown).

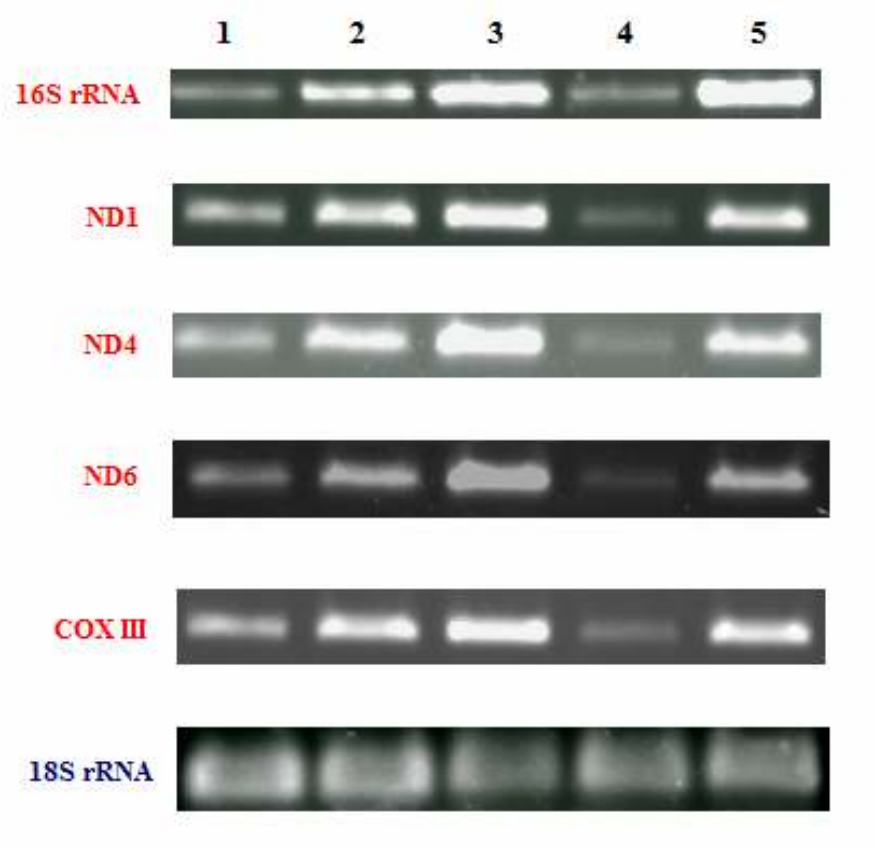

Figure 3.27. Representative results of RT-PCR analysis. RT-PCR gel image analysis of MCF-7 clone cells cultured with or without extracellular ATP treatment. Approximately 2 µg of each treated RNA was used in the RT-PCR reaction for the amplification of 16S rRNA, ND1, ND4, ND6 and COX III. All PCR amplifications were performed three times. The relative level of mRNA of each gene was analysed as described in "Materials and Methods". One-tenth of each RT-PCR reaction was assessed on a 1% agarose gel and stained with ethidium bromide. The mRNA level of housekeeping gene, 18S rRNA, was used as an internal standard for sample normalisation. Lane 1: B12. Lane 2: B12 treated with 100 µM ATP. Lane 3: B12 treated with 1 mM ATP. Lane 4: D4. Lane 5: D9.

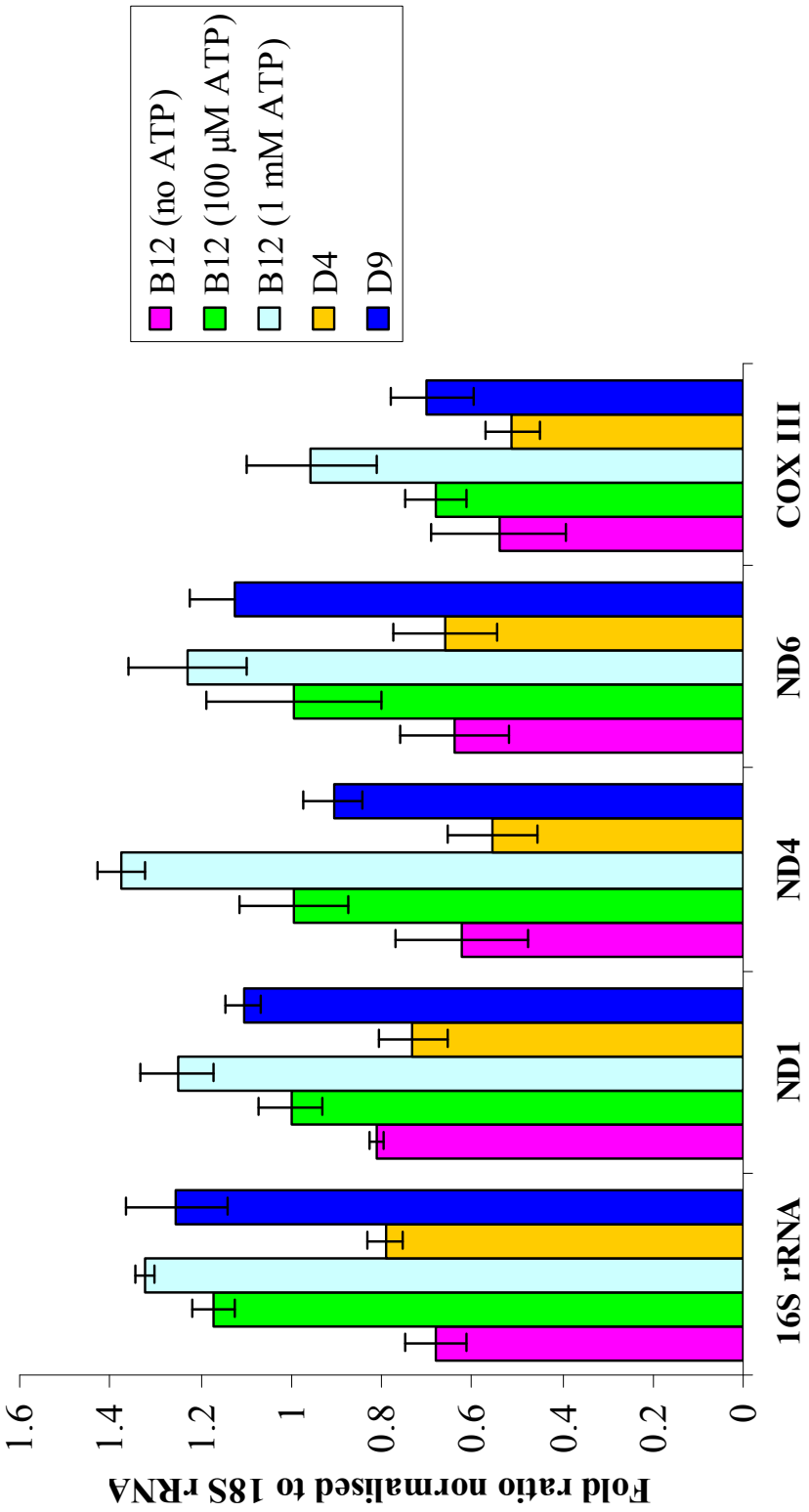

Figure 3.28. Graphical representation of the comparative RT-PCR. Results were expressed as ratios of the gene-specific signal to the internal control (16S rRNA) signal. The average data points of the triplicates were plotted with standard deviation as error bars.

4.1. Cell morphology and growth characteristics

MCF-7 cell line was established from the pleural effusion of a patient who was diagnosed with adenocarcinoma of the breast (Soule *et al.* 1973). This cell line has been shown by Resnicoff *et al*. (1987) to be highly heterogeneous with the ability to generate clonal variation. Resnicoff and coworkers demonstrated that MCF-7 cells could be fractionated in Percoll gradients to yield several subpopulations with different characteristics: variability in growth rate; DNA synthesis; expression of *ras* oncogene-encoded protein p21, estrogen receptors, and carcinoembryonic antigen (CEA). Interestingly, one of the minor fractions appeared to contain the stem cells. In addition to the phenotypic variability, these findings suggested that this cell line may be also prone to genetic heterogeneity. This is likely due to spontaneous mutation *in vitro*, which could be associated with the higher rate of cell proliferation (cited in Freshney, 2000).

In the present study, six clones (B5, B12, D4, D9, E1 and E8) were isolated and established from single cells obtained by serial dilution of a MCF-7 stock culture. When the six isolated clones were grown individually, the clones demonstrated variance in cell morphology and growth characteristics. Most cells clumped together and formed discrete clusters before reaching confluency (Fig. 3.1A, C, D, E, F). This is a typical morphology of cancer cells. In contrast, clone B12 was more scattered and it was likely due to contact inhibition (Fig. 3.1B). As for doubling time, clone D4 was the fastest growing and clone B12 was the slowest; the others attained intermediate rates (Table 3.1). These results supported the findings of Resnicoff *et al.* (1987). However, Resnicoff and coworkers did not investigate the cells at the genomic level to account for the observed differences, although it is likely that the growth variability is influenced by different genomic background.

Cells may take longer to recover when reseeded if they are withdrawn from the cycle due to delayed subculture (Freshney, 2000). Hence, the cells were subcultured as soon as they reach 80% confluency. When the clones were subcultured, they showed a consistent growth rate characteristic of a specific clone and did not

change over different passages. It is, therefore, hypothesized that these clones with different growth characteristics may represent different sublines, although they coexisted in the stock culture. The observed variations in growth characteristics in different clones may be resulted from mutational changes in nuclear and/or mitochondrial genes. The present study focused on mutational analyses of the mitochondrial genome because mitochondria are the powerhouse of a cell. They provide energy for all the cellular functions including growth and cell division. Due to time constraint, the nuclear genome was not included in this study. When a mutation in the mtDNA was identified, the effect of the mutation was determined by investigating the oxidative phosphorylation activites of the clones.

4.2. Mutational analysis

In the present study, comparison of the clones B12, D4 and D9 has revealed a total of seven mutations by direct DNA sequencing: three within 16S rRNA gene and one each within the amino acid coding regions of ND1, COX III, ND4 and ND6 genes, respectively (Table 3.5). These results suggested that the clones were genetically different in the mitochondrial genome. Six out of the seven mutations were in a heteroplasmic state within the sensitivity of the method (Harris *et al*., 2006). Heteroplasmy, the presence of a mixture of normal and mutant mtDNA, may be a phase in the establishment of a pathogenic mutation. This phenomenon is of particular significance if it results in a change of a highly conserved nucleotide base or amino acid residue (Riordan-Eva and Harding, 1995; Chinnery and Schon, 2003).

4.2.1. Amino acid change in ND1

Homology studies revealed that Tyr^{277} (A4137, ND1) is highly conserved in eukaryotes (Table 4.1). Tyrosine is a polar, hydrophilic amino acid with a large benzene ring side chain. It is less strictly segregated from water due to the possession of a polar -OH group. Cysteine is a small, polar molecule which is less

hydrophilic than tyrosine. The replacement of tyrosine (with a large side chain) by cysteine (with a small side chain) is very likely to destabilise the protein fold conformation. Hydropathicity and polarity analysis showed that there is a slight change in the parameters (Table 3.6). Residue 277 in clone D9 becomes less hydrophilic in comparison with clones B12 and D4. However, there is no significant alteration in the secondary structure in ND1 subunit as a result of Cys^{277} (Fig. 3.18). As the conserved nature of Tyr^{277} suggests that this mutation may influence the function of complex I in most eukaryotes, variant amino acids are, nevertheless, also found in Drosophila yakuba and Pichia canadensis. Hence, further studies would be required to investigate the effect of this mutation.

Table 4.1. Amino acid homology showing comparison of residue 277 between species. Homology analysis was done by using the Basic Local Alignment Search Tool (BLAST) at the National Center for Biotechnology Information (NCBI) website (http://www.ncbi.nlm.nih.gov/blast). Residues 277 in the species are in bold.

Species	Amino acid sequence									NCBI reference (accession number)
					277					
Clone D9	I	R	T	A	**C**	P	R	F	R	this study
Clones B12 and D4	I	R	T	A	**Y**	P	R	F	R	this study
Human	I	R	T	A	**Y**	P	R	F	R	NP_536843
Chimpanzee	I	R	T	A	**Y**	P	R	F	R	NP_008186
Iguana	V	R	A	S	**Y**	P	R	F	R	NP_115836
Xenopus laevis	V	R	A	S	**Y**	P	R	F	R	NP_008134
Chicken	I	R	A	S	**Y**	P	R	F	R	NP_006915
Bovine	I	R	A	S	**Y**	P	R	F	R	YP_209205
Mouse	I	R	A	S	**Y**	P	R	F	R	NP_904328
Zebrafish	M	R	A	S	**Y**	P	R	F	R	NP_059331
Drosophila yakuba	A	R	G	T	**L**	P	R	F	R	NP_006914
Pichia canadensis	V	R	A	S	**F**	P	R	L	R	NP_038213

4.2.2. Amino acid change in COX III

Homology studies showed that Ala^{107} (C9527T, COX III) in clone B12 is highly conserved in vertebrates although serine is also found in two lower organisms (Table 4.2). Nevertheless, this invariant Ala^{107} residue is believed to be residing in the conserved region and formed part of the putative membrane-spanning segment III of the COX III polypeptide in eukaryotes (Haltia *et al*., 1991). Site-directed mutagenesis study of Haltia *et al*. (1991) demonstrated that this region is important for COX III to serve in the biosynthesis of functional proton-translocating cytochrome c oxidase complex. Hence, a substitution at this position with a different amino acid is likely to disrupt its biological function.

Alanine is a non-polar, hydrophobic amino acid. It is less strictly segregated from water due to its smaller size. Serine is an uncharged, hydrophilic amino acid with a polar –OH group. As the nature of the amino acid side chains has significant influence on the topography of the protein, these changes in chemical properties of residue 107 would be expected to significantly alter the hydropathicity and polarity of the COX III polypeptide. Analyses of these parameters revealed that this region does become more hydrophilic and there is an increased in polarity (Table 3.7). Secondary structure analysis predicted a decrease in the length of transmembrane α-helix and an increase in the peripheral β-strand (Fig. 3.19).

In membranous polypeptides, α-helices and β- strands pack by stacking their amino acid side chains. α-helices act as the polypeptides structural support, providing rigidity within the membrane, whereas β-strands allow the polypeptide to be flexible in one direction (Fersht, 1985). Hence, the polypeptide with increased flexibility is likely to obstruct the function of COX III.

Table 4.2. Amino acid homology showing comparison of residue 107 between species. Homology analysis was done by using the Basic Local Alignment Search Tool (BLAST) at the National Center for Biotechnology Information (NCBI) website (http://www.ncbi.nlm.nih.gov/blast). Residues 107 in the species are in bold.

Species	Amino acid sequence									NCBI reference (accession number)
					107					
Clone B12	H	S	S	L	**S**	P	T	P	Q	this study
Clones D4 and D9	H	S	S	L	**A**	P	T	P	Q	this study
Human	H	S	S	L	**A**	P	T	P	Q	NP_536849
Chimpanzee	H	S	S	L	**A**	P	T	P	Q	NP_008192
Chicken	H	S	S	L	**A**	P	T	P	E	NP_006921
Zebrafish	H	S	S	L	**A**	P	T	P	E	NP_059337
Bovine	H	S	S	L	**A**	P	T	P	E	YP_209211
Iguana	H	S	S	L	**A**	P	T	P	E	CAC37089
Xenopus laevis	N	S	S	L	**A**	P	T	Y	E	NP_008140
Mouse	H	S	S	L	**V**	P	T	H	D	NP_904334
Drosophila yakuba	H	S	S	L	**S**	P	A	I	E	NP_006907
Pichia canadensis	H	S	A	M	**S**	P	A	I	E	NP_038214

4.2.3. Amino acid change in ND4

Homology studies showed that Leu^{246} (C11496T, ND4) in clone D4 is poorly conserved within eukaryotes (Table 4.3). The limited conservation of Leu^{246} suggests that it may have little functional significance in the ND4 polypeptide. Both leucine and phenylalanine are non-polar hydrophobic amino acids. However, phenylalanine contains a benzene ring and has larger side chain than leucine. The stability of proteins mainly arises from the formation of intramolecular hydrogen bonds and the reduction in the surface area accessible to solvent that occurs upon folding (Garrett and Grisham, 2005). Hence, the replacement of a small side chain by a larger side chain may be unfavourable to the fold conformation of ND4 polypeptide. This

change in chemical properties between the amino acids is reflected in the hydropathicity analysis, as residue 246 becomes less hydrophobic in clone D4 compared to clones B12 and D9 (Table 3.8). Polarity of the residue 107 is, however, not significantly altered by the leucine to phenylalanine change.

Secondary structure analysis predicted that Phe^{246} altered the secondary structure of ND4 polypeptide by replacing three transmembrane α-helices with three peripheral β-strands (Fig. 3.20). Hence, an increase in the peripheral β-strands may result in a more flexible polypeptide, which in turn may have an effect on the function of complex I. The effect of this mutation on the function of complex I remains to be elucidated.

Table 4.3. Amino acid homology showing comparison of residue 246 between species. Homology analysis was done by using the Basic Local Alignment Search Tool (BLAST) at the National Center for Biotechnology Information (NCBI) website (http://www.ncbi.nlm.nih.gov/blast). Residues 246 in the species are in bold.

Species	Amino acid sequence									NCBI reference (accession number)
					246					
Clone D4	G	M	M	R	**F**	T	L	I	L	this study
Clones B12 and D9	G	M	M	R	**L**	T	L	I	L	this study
Human	G	M	M	R	**L**	T	L	I	L	NP_536852
Chimpanzee	G	M	M	R	**L**	T	L	I	L	NP_008195
Pichia canadensis	A	I	I	R	**L**	I	L	I	N	NP_038220
Bovine	G	M	L	R	**I**	T	L	I	L	YP_209214
Mouse	G	M	I	R	**I**	S	I	I	L	NP_904337
Iguana	G	I	I	R	**I**	T	L	T	L	NP_115845
Xenopus laevis	G	I	I	R	**I**	S	I	T	L	NP_008143
Chicken	G	I	M	R	**V**	T	L	L	M	NP_006924
Drosophila yakuba	G	L	L	R	**V**	I	N	F	L	NP_006910
Zebrafish	G	M	M	R	**M**	M	V	M	L	NP_059340

4.2.4. Amino acid change in ND6

Homology studies showed that Asp^{138} (C14263G, ND6) in clone B12 is well conserved in vertebrates (Table 4.4). Both aspartate and histidine are characterised by being polar and hydrophilic amino acids, with histidine being larger in size, less hydrophilic and polar than aspartate (Table 3.9). Secondary structure analysis predicted the extension of β-strand in clone B12 (Fig. 3.21), which is likely to increase the flexibility of ND6 polypeptide. Aspartate is believed to play several important roles in nucleotide biosynthesis. Nitrogen atom derived from $–NH_2$ group of aspartate is used to form ribonucleotides (purine and pyrimidine rings), precursors to DNA and RNA (Garrett and Grisham, 2005). In addition, aspartate interacts with the metal ions from the incoming nucleotide added during the elongation of a polynucleotide chain by DNA polymerase (Doublie *et al*., 1998; Kiefer *et al*., 1998). Hence, the alteration of aspartate to histidine at residue 138 is very likely to affect the function of complex I.

Table 4.4. Amino acid homology showing comparison of residue 138 between species. Homology analysis was done by using the Basic Local Alignment Search Tool (BLAST) at the National Center for Biotechnology Information (NCBI) website (http://www.ncbi.nlm.nih.gov/blast). Residues 138 in the species are in bold.

Species	Amino acid sequence									NCBI reference (accession number)
					138					
Clone B12	L	I	R	E	**H**	P	I	G	A	this study
Clones D4 and D9	L	I	R	E	**D**	P	I	G	A	this study
Human	L	I	R	E	**D**	P	I	G	A	NP_536854
Chimpanzee	L	I	R	E	**D**	P	I	G	A	NP_008197
Chicken	F	A	R	L	**D**	F	S	G	V	NP_006927
Zebrafish	V	I	R	A	**D**	V	S	G	V	NP_059342
Xenopus laevis	V	M	R	G	**D**	W	V	G	V	NP_008145
Iguana	V	S	R	S	**D**	F	G	G	V	NP_115847
Bovine	F	F	S	E	**E**	A	M	G	I	YP_209216
Mouse	V	M	L	E	**G**	G	I	G	V	NP_904339

4.2.5. RNA secondary structure prediction

The prediction using RNA fold software showed modelling structure of B12 appeared to be completely different from the common structure of D4 and D9 (Fig. 3.17). Seemingly, the combined effect of mutations at G2480T, C2513G and A2520T had introduced significant changes in the secondary structure of the 16S rRNA molecule of clone B12. The predicted initial free energies (dG) are -362.20 and -360.61 kcal/mole for D4-D9 and B12, respectively. This suggests that clone B12 is likely to have a lesser stable 16S rRNA secondary structure. These findings shed light on the possible functional effects of clone B12.

Mitochondrial 16S rRNA is an essential component of the ribosomal large subunit, which are responsible for protein synthesis in all living cells. The 16S rRNAs adopt an evolutionarily conserved secondary structure with four domains that appear to fold independently, and are closed by long-range base-pairing interactions (Klug and Cummings, 2000). Conformational conservation of rRNA is essential in maintaining ribosome function. Biological activity of rRNA is dependent on its structural conformation (Burk *et al*., 2002). Previous study showed that 16S rRNA plays a role in protein folding activity (Sulijoadikusumo *et al*., 2001). The secondary structure of the rRNA molecule is potentially the most important determinant of its protein folding activity. Hence, any mutations that affect the secondary structure of 16S rRNA is likely to disrupt its function.

Tan *et al*. (2002) pointed out that transcription of the mitochondrial genome generates two polycistronic primary transcripts that are subsequently processed to produce mature mRNA, rRNA and tRNA. Hence, mtDNA mutations affecting the folding of secondary structure of the RNA precursors could be deleterious to the maturation of RNA. In addition, as ribosomes are essential for translation, rRNA mutations may also cause major assembly defects or interfere with tRNA protection activity (Noller, 1991). Therefore, it is very likely that the translation of the 13 mtDNA-encoded polypeptides will be affected, resulting in generalised OXPHOS deficiencies. Further molecular studies of RNA processing may be needed to elucidate the biological effect of these sequence variations.

4.3. Enzyme assays

Oxidative phosphorylation (OXPHOS) is the final step of the energy-producing pathway. It is mediated by mitochondrial membrane-bound enzyme complexes that transport electrons from NADH and $FADH_2$ to oxygen, generating a proton gradient that ultimately leads to the production of ATP (Smeitink *et al*., 2001). Defects in complexes III and IV in clone B12 is likely to disrupt respiration and decrease the mitochondrial proton electrochemical potential gradient across the mitochondrial inner membrane (Fig. 4.1). As proton electrochemical potential gradient is the driving force for ATP synthesis, decreasing it may eventually hinder ATP production, as evidenced by the low activity of complex V in clone B12. In addition, mitochondria also affect cytoplasmic Ca^{2+} metabolism in two ways: indirectly via Ca^{2+}-dependent ATPases to pump excess Ca^{2+} from the cytoplasm to the extracellular environment or intracellular Ca^{2+} depots; and directly through the mitochondrial membrane potential which drives the uptake of Ca^{2+} into mitochondria through a Ca^{2+}-uniporter (James and Murphy, 2002). Hence, a defective mitochondrial ATP synthesis may inhibit Ca^{2+} uptake, leading to a decrease in dehydrogenase activity and substrate supply. The diminished substrate supply will further affect the generation of proton electrochemical potential gradient, hence worsening the condition.

Interestingly, these observations correlated with the results obtained from mutation screening and secondary structure modelling, which suggested that the structural changes due to heteroplasmic mutations in 16S rRNA of clone B12 at G2480T, C2513G and A2520T are very likely to disrupt the mitochondrial OXPHOS function due to aberrant gene products, in which the complexes involved in the respiratory chain. These findings indicate that the secondary structure of 16S rRNA is most likely a determinant of the changes in OXPHOS activity. Nevertheless, the exact mechanism of interaction remains unclear.

Furthermore, COX III has a distinct role in the assembly of the functional oxidase and acts as a structural stabilizer of the mature oxidase complex IV (Haltia *et al*., 1991). The C9527T mutation found in clone B12, causing COX III more prone to structural perturbation and may result in poorly assembled cytochrome c oxidase complex. The conformational change of the complex is likely to cause a lower

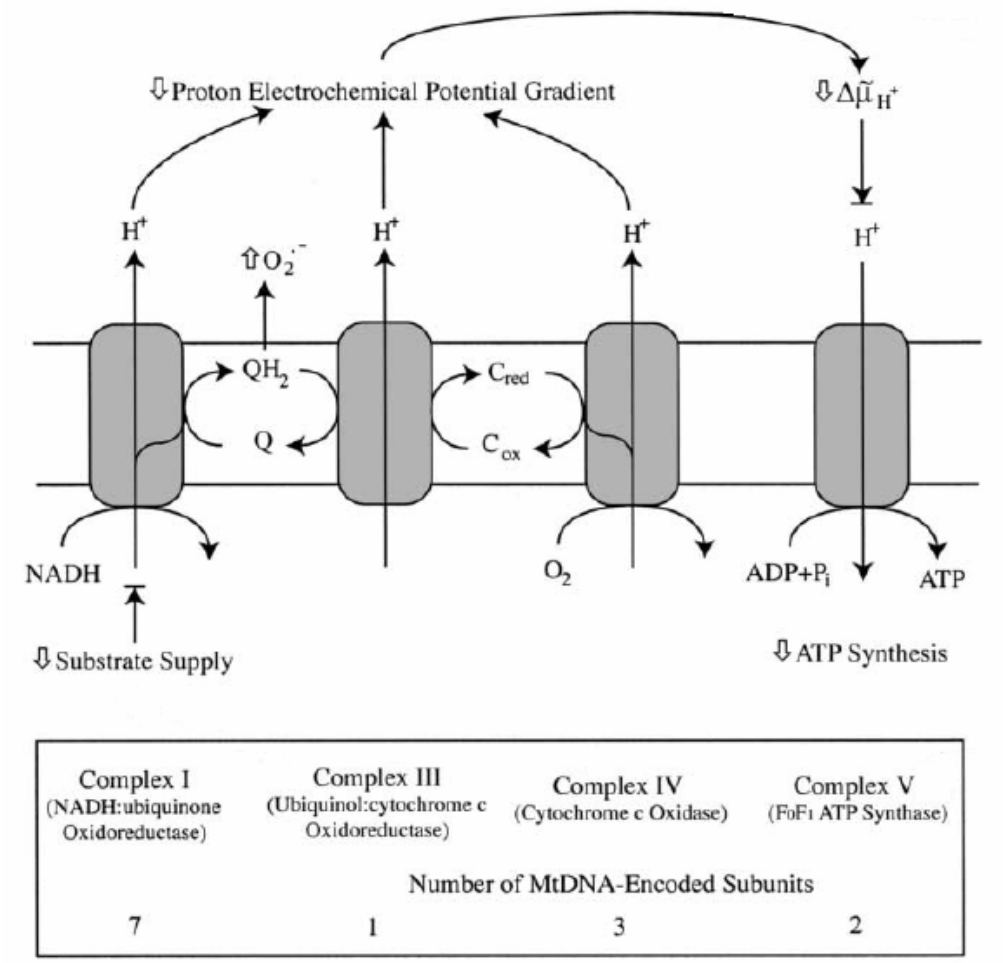

Figure 4.1. The effect of mtDNA mutations on oxidative phosphorylation. The respiratory chain transfers electrons from reduced substrates to oxygen and uses the difference in redox potential to pump protons across the inner membrane to establish a proton electrochemical potential gradient which is then used to drive ATP synthesis by ATP synthase (complex V). Inhibition of complex I would oxidise the respiratory chain, while disruption of complexes III, IV or V would lead to a complete or partially reduced respiratory chain. The point at which electron transport is blocked will affect the redox state of electron carriers, such as ubiquinone and cytochrome c. The accumulation of NADH from inhibition of the respiratory chain will also affect cell redox balance. Additionally, a disruption of ATP supply would inhibits Ca^{2+} uptake, leading to a decrease in dehydrogenase activity and substrate supply, thus worsen the whole chain reaction. O_2 = Superoxide; Q = ubiquinone; QH_2 = ubiquinol; C_{ox} = ferricytochrome *c;* C_{red} = ferrocytochrome *c;* $\Delta\mu_{H+}$ = proton motive force; $\Delta\psi_m$ = mitochondrial membrane potential; Pi = phosphate. Adapted from James and Murphy (2002).

affinity of cytochrome for substrate ubiquinol. As a result, there is a decrease in complex III activity in clone B12. This may lead to an impaired proton translocation and a deficit in electrochemical gradient, which ultimately may hinder proper ATP production. mtDNA mutations leads to a deficiency in mitochondrial enzyme activities and a decrease in ATP synthesis have also been reported previously (Heddi *et al*., 1999; James *et al*., 1999; Hsieh *et al*., 2001). Based on these findings, it is tempting to conclude that the presence of mtDNA mutations is associated with reduction in OXPHOS activity and ATP production. The deficiency in mitochondrial ATP synthesis may account for the slow growth in clone B12. The heteroplasmic mtDNA mutations found in clone B12 could be deleterious.

The inability to assemble correctly functioning mitochondrial proteins may cause an upregulation of the production of many mitochondrial polypeptides or stimulate the biogenesis of the whole organelle, in an attempt to compensate for an energy deficit (James and Murphy, 2002). This was shown by a significant decrease in the activity of nuclear-encoded mitochondrial enzyme citrate synthase (CS) in clone B12 compared to clones D4 and D9 (Fig. 3.22). These could probably reflect a compensatory mechanism for responding to a reduced energy metabolism in these cells as a consequence of mutations in 16S rRNA gene found in clone B12. Similar result was also observed by Bhat (2002), demonstrating a decrease in CS activity in estrogen-induced hamster kidney tumours compared to untreated controls.

Nonetheless, clone D4 and D9 exhibited 3-fold decrease in complex I activity compared to clone B12 (Fig. 3.23). These findings suggest that the mutations C11496T in ND4 and A4137T in ND1, in clone D4 and D9, respectively, are likely to affect the respiratory function of complex I. The exact function of the mitochondrially encoded complex I subunits is unclear, but it is likely that they are involved in proton translocation and contribute to the quinone binding site (Friedrich *et al.,* 1990). However, despite this diminished complex I activity, the ultimate ATP production as reflected in complex V activity of both D4 and D9 are relatively higher than clone B12. This suggests that the lower complex I activity is not sufficient to compromise ATP production. The mutations in clone D4 and D9 are likely to fall within their mutation tolerance levels (threshold effect), at which point they could compensate for the effect of the mutations. Hence, an active ATPase in the absence of functioning complex I may

still form a membrane potential by acting as an H^+ pump and consuming glycolytically generated ATP (James and Murphy, 2002). This could probably explain why cell growth of clone D4 (fastest growth) and D9 (moderate growth) were not compromised compared to clone B12 (slowest growth).

Furthermore, the OXPHOS system is under the control of two separate genetic systems, which involves interplay between the mitochondrial and the nuclear genomes (Smeitink *et al*., 2001). Hence, an alternative explanation to this observation may be that there is a cooperative interaction of nuclear genes in clone D4 and D9 with complex II. It is known that many nuclear proteins are required for mtDNA replication, transcription and translation (Brown and Wallace, 1994). Thus, many aspects of mitochondrial disease may be related to the structure, variation, and regulation of nuclear genes involved in OXPHOS. This conjecture is supported by the findings showing relatively higher nuclear encoded complex II activity in clone D4 and D9. The low complex II activity in clone B12 may suggest the presence of mutations in the nuclear genome, since complex II is solely encoded by nuclear genome. Seemingly, mutations in nuclear genes can exert their phenotypic effects by indirectly inactivating OXPHOS or destabilizing the mtDNA. The specific nuclear and mitochondrial roles and their possible relationships, however, have yet to be established.

4.4. Effect of extracellular ATP on cell proliferation

In the present study, mutational and enzymatic analyses suggest that energy production in B12 may be compromised. If this is true, would supplementing the culture medium with extracellular ATP enhance the growth rate of the slow growth clone? In the present study, extracellular ATP was found to stimulate proliferation significantly in the slowest growing clone B12 as compared to untreated cells when ATP concentration was greater than 100 μM ATP (Fig. 3.25, Table 3.12). At 1 mM ATP, clone B12 had a faster growth rate than the fastest clone D4 without ATP supplement. This observation is consistent with the findings of Dixon *et al*. (1997) who reported that ATP induced cell proliferation in MCF-7 breast cancer cells *in vitro*. Dixon *et al*. also demonstrated that ATP acted on its mitogenic effect through

interaction with cell surface receptors known as P2-purinoceptors. It is believed that activation of these designated purigenic P2 receptors by ATP leads to the release of intracellular Ca^{2+} and hence inducing cell growth.

Several investigators have also observed stimulation of proliferation by purinergic receptor agonists in other cell types *in vitro*, including renal epithelial cells (Paller *et al*., 1998), human ovarian cancer cell line OVCAR-3 (Popper and Batra, 1993), aortic smooth muscle cells (Wang *et al*., 1992), brain astrocytes (Hindley *et al*., 1994), mesangial cells (Schulze-Lohoff *et al*., 1992, 1995, 1996; Huwiler and Pfeilschifter, 1994), and human melanomas (White *et al*., 2005). In addition, *in vitro* studies of isolated proximal tubule segments suggested that exogenous ATP is sequentially degraded to ADP, AMP and finally adenosine by ectonucleotidases before restoring intracellular ATP levels (Mandel *et al*., 1988).

In contrast to the observations in the present study, extracellular ATP was found to inhibit cell proliferation. The anti-cancer activity of adenine nucleotides was first described by Rapaport (1983). It is reported that low levels of extracellular ATP significantly inhibit the growth of human tumour cells *in vitro* (CAPAN-1, a pancreatic adenocarcinoma; HT29, a colon adenocarcinoma) and subsequently yield substantial cell killing by initiating arrest in the S phase of the cell cycle. Furthermore, the role of extracellular ATP in attenuation of cell growth via G-protein-coupled $P2Y_2$ receptors were also reported in endometrial cancer cells (Katzur *et al.,* 1999) and human ovarian cancer cells, EFO-21 and EFO-27 (Schultze-Mosgau *et al*., 2000).

In addition, Rapaport (1983) postulated that the antiproliferation induced tumor cell killing action is attributed to the permeabilisation of tumor cell membrane by extracellular ATP. Similar finding was also observed by Schulze-Lohoff *et al*. (1998) who found that the inhibition of cell proliferation through the activation of P2Z/P2X receptors could lead to apoptosis and necrosis of mesangial cells. Interestingly, pore formation was found in the plasma membrane of the mesangial cells. Schulze-Lohoff *et al*. (1998)'s observation suggested that the porous membrane is associated with the P2Z/P2X receptors. However, whether the pore formation is involved in the mechanism of cell death remains uncertain.

Previously, Saribas *et al*. (1993) had demonstrated that ATP reversibly increases the plasma membrane permeability of transformed 376 mouse fibroblasts to macromolecules as large as 20 kDa. Presumably, ATP may cause the generation of a growing hole in the plasma membrane. This finding could probably account for the morphological change in B12 cells treated with 1 mM ATP, where the cells appeared to be larger in size (Fig. 3.24). The possibility is that the exogenous ATP alters the membrane permeability through the interaction with P2Z receptors. This postulation may suggest the possible occurrence of osmosis where solvent molecules move across the more permeable membrane from extracellular space into the cells, causing them to swell. However, it is not clear how the pore is formed. Whether it is due to membrane damage or the formation of a protein-pore complex remains to be elucidated.

In the present study, extracellular ATP has probably induced cell proliferation in clone B12 via the P2 receptors. Millimolar concentrations of ATP may also have induced the pore formation via other P2 receptors. In line with the observations from this present study, Batra and Fadeel (1994) and Schulze-Lohoff *et al*. (1998) had presented evidences that different P2 receptors may become functional at different concentrations of ATP. These findings were of particular interest, in that their studies suggested that the extracellular actions of ATP are likely to be cell-specific, and depend on the expression of P2 receptor types, as well as the amount of nucleotides in the extracellular space. Further investigation is required to confirm the mechanism of action of the specific P2 purinoceptors on these cells, and to determine whether the variability in cell growth can be related solely to ATP, or if other factors are also involved.

4.5. Comparative RT-PCR analysis

Given the extensive effect of extracellular ATP may have on the cells, it is important to determine whether extracellular ATP affects gene expression. Reverse transcription-PCR analysis indicated the expression of the respiratory chain complexes containing mutations, i.e. 16S rRNA, ND1, ND4, ND6 and COX III genes. The mRNA expression profile of the extracellular ATP-treated B12 cells is clearly different from

that of the untreated B12 cells. The PCR products of mtDNA 16S rRNA, ND1, ND4, ND6, COX III in clone B12 were increased substantially with ATP supplement in the culture medium (Fig. 3.27). This increase in transcript levels may suggest increased transcription rates or transcript stability. Extracellular ATP, thus, is likely to have an upregulating effect on the gene expression. Heddi *et al*. (1999) had observed an increased gene expression in tissues of mitochondrial disease patients. These researchers had delineated that high levels of mutant mtDNAs were associated with a high induction of the mtDNA and nuclear OXPHOS genes. Hence, it is likely that the mutated cells and/or tissues induce mitochondrial biogenesis to compensate for the metabolic deficiency due to OXPHOS impairment associated with mtDNA mutations. However, the effect of nuclear genes on mitochondrial function is still an open question. It is not clear whether other genes whose products interact with OXPHOS are also involved. It is also not known whether extracellular ATP alone accounts for the differences in gene expression between the clones. Another important question that arises is whether there is a causative relationship between the severity of mutations and level of induction. The mechanism for the compensatory induction, however, has not been fully characterised.

4.6. Future directions

The relevance of these findings to the role of mtDNA mutations in cell growth remains anticipating, as it highlights the potential importance of ATP in mitochondrial disease and carcinogenesis. Further studies are required to extend the observations from this study and address the mechanisms underlying the proliferative response to extracellular nucleotides in vitro. Also, the study of mitochondrial gene expression by analysing mtRNA processing and translational protein products in cell cultures in response to OXPHOS defects may shed light on the pathogenic role of a novel mtDNA mutation. Other important areas for future research include studies of intergenomic signaling pathways in carcinogenesis and the potential role of mitochondria and mtDNA mutations in the immunological surveillance of tumour cells.

4.7. Conclusions

It is hypothesised that any mutation that alters a functional gene in mtDNA is likely to compromise cell functions by affecting OXPHOS and ATP production, which ultimately affect cell proliferation. In the present study, the important role of mitochondria in energy metabolism was determined by comparing the effect of mtDNA mutations on growth patterns and OXPHOS enzyme activities; as well as the effect of ATP supplement to culture using five different MCF-7 cell line derived clones. The isolated clones had shown distinct growth pattern and morphology. The difference in proliferation rates among the clones was ascertained by the doubling times. The clone's slow growth rate was likely the result of mitochondrial mutations in the 16S rRNA gene, ND1, ND4, ND6 and COX III. The five heteroplasmic mutations found in clone B12 appeared to be deleterious to the cell by disrupting mitochondrial OXPHOS activities and reducing energy output.

From molecular screening and secondary structure modelling, it was evident that the three mutations in 16S rRNA found in clone B12 were sufficient to disrupt normal ribosomal function and could contribute to lowering the efficiency of OXPHOS. The observed variation in enzyme activities among clones may be related to mutations in the mtDNA, and mtDNA mutations appeared to compromise ATP production. This conclusion was further supported by the observation that the slow growth rate of clone B12 could be restored by supplementing the culture with ATP. In addition, the severity of the OXPHOS activities was roughly correlated with the number of mutations in the affected clone.

In conclusion, the results obtained from this study strongly suggest that cell growth largely depends on the ATP production originating in the mitochondrial compartment. Specific mitochondrial dysfunctions could be the underlying cause of growth retardation. In short, the variability in functional manifestations of mtDNA of clone B12 stems from a number of factors, including the nature of the mutation, number of mutation (mutation load) and the gene specifically affected.

ACKNOWLEDGEMENTS

First of all, I would like to express my sincere gratitude and appreciation to Assoc. Prof. Frank Sin, for accepting me as an MSc student in his laboratory, allowing me to embark on a new path of my medical career. His enlightening guidance and support during the whole period as my thesis supervisor helped me to extend my understanding in research. This project has been a meaningful and pleasant experience with excitements and joys of discoveries, which I will always remember. He has also spent lots of time correcting and suggesting improvements to my thesis. Without his help, this thesis would not have been completed.

I wish to express my gratitude to my co-supervisors Dr. Drusilla Mason and Dr. Steven Gieseg for giving me their valuable insights and direction in improving my thesis. I would also like to thank Dr. Ellen Podivinsky and Dr. Barbara Thomson for their kindly suggesting ideas to make certain areas more coherent. The knowledge I gained from all of them had helped me a lot in every part of this thesis.

Moreover, I would like to thank Linda Morris and Joanne Burke who helped me with the coordination and the use of the facilities in the lab, Craig Galilee for his assistance in sequencing and Matt Walters for colour printing. Also, thanks to the staff in the School of Biological Sciences for helping me in one way or another.

I would also like to extend my thanks to my labmates (Selina, Lucy, Claudia, Sadia, Jacquie and Jennifer) for their generous assistance and continual encouragement during the years of my MSc study. Also, thanks to members from other labs (Melanie, Jonci, Thorsten, Iris, Margee, Sandra, Bruce, Antoine, Kak Zunika, Tina, Sandi, Ermin, Nick, Iain, Noraini, Suhaimi) who gave me valuable advice and sharing their experience with me. Thank you all for the lovely farewell party which touched my heart deeply.

I am truly privileged and grateful to New Zealand's International Aid & Development Agency (NZAID) for offering me a scholarship in supporting me in my academic pursuits and helping me to fulfill my dream. Also, special appreciation to all the staff in International Student Support (ISS), namely Eunice McKessar, Maree

Thomas, Jonie Chang, Bex Gilchrist, Sarah Beaven; former ISS advisors Gareth Morgan and John Pickering for their unwavering patience, encouragement and support all the way. Also, thanks to Walter Raymond for his guidance on academic writing and Geraldine Murphy for proofreading.

Not to forget a bunch of lovely people (Mel, Priscilla, Etienne, Nima, Edmund, Maureen, Angie, Amy, Pooy, Sanitta, Sue, Chen Lei, Phuong, Satoe, Heintze, Nelson, Nilanka, Alma, Greg, Baby NZ, Bing, Rex, Joshua, Lawrence, Thomas, Yangden, Kathyrn, Fiona, Wendy, Tim, Nixon, Fred, Kolo, the staff in Ilam Village …… and many more) whom I have met during my stay in New Zealand. Thanks for your friendship and companionship, making my staying in NZ pleasant and memorable. It has been a wonderful and rewarding experience having you guys around! Special thanks to Mel, Priscilla, Etienne and Nima for being such good friends. Thanks for your thoughtfulness and care. You guys are always there when I need help or someone to talk to. I will always remember the countless food and baking sessions, birthday celebration, and all the fun we had together, making my stay in Christchurch so unforgettable and fulfilling! As I head back to my part of the world, I will surely miss you all so dearly.

Last but not least, I would like to thank my family for their life-long love, inspiration and faith in me over the years. Their incredible support lifts me up from time to time. To my fiancé, MY, thank you for everything you have done for me and all the love and support you have shown me over the past years. You are my guardian angel!

Without all of you, this work could not have been completed. Wishing everybody all the best in your future endeavours! Take care … till we meet again someday! Miss you all …

'Syabas, harap jumpa lagi!'

The Best Is Yet To Be ……

REFERENCES

Abbracchio, M.P., Burnstock, G. (1994) Purinoceptors: are there families of P2X and P2Y purinoceptors? *Pharmacol. Ther*. **64(3):** 445-475.

Ackrell, B.A.C., Kearney, E.B., Singer, T.P. (1978) Mammalian succinate dehydrogenase. *Methods Enzymol*. **53**: 466-483.

Anderson, S., Bankier, A.T., Barrell, B.G., de Bruijn, M.H.L., Coulson, A.R., Drouin, J., Eperon, I.C., Nierlich, D.P., Roe, B.A., Sanger, F., Schreier, P.H., Smith, A.J.H., Staden, R., Young, I.G. (1981) Sequence and organization of the human mitochondrial genome. *Nature.* **290:** 457-465.

Baggetto, L.G. (1993) Role of mitochondria in carcinogenesis. *Eur. J. Cancer*. **29A(1):** 156-159.

Barnard, E.A., Burnstock, G., Webb, T.E. (1994) G protein-coupled receptors for ATP and other nucleotides: a new receptor family. *Trends Pharmacol. Sci*. **15(3):** 67-70.

Barrientos, A. (2002) In vivo and in organelle assessment of OXPHOS activities. *Methods* 26: 307-316.

Batra, S. and Fadeel, I. (1994) Release of intracellular calcium and stimulation of cell growth by ATP and histamine in human ovarian cancer cells (SKOV-3). *Cancer Lett*. **77(1):** 57-63.

Beal, M.F. (2005) Mitochondria take center stage in aging and neurodegeneration. *Ann. Neurol.* **58:** 495-505.

Bean, B.P. (1992) Pharmacology and electrophysiology of ATP-activated ion channels.*Trends Pharmacol. Sci*. **13(3):** 87-90.

Bhat, H.K. (2002) Depletion of mitochondrial DNA and enzyme in estrogen-induced hamster kidney tumors: a rodent model of hormonal carcinogenesis. *J. Biochem. Mol. Toxicol.* **16(1)**: 1-9.

Birch-Machin, M.A., Briggs, H.L., Saborido, A.A., Bindoff, L.A., Turnbull, D.M. (1994) An evaluation of the measurement of the activities of complexes I-IV in the respiratory chain of human skeletal muscle mitochondria. *Biochem Med Metab Biol*. **51(1)**: 35-42.

Bradford, M. (1976) A rapid and sensitive method for the quantitation of microgram quantities of protein utilizing the principle of protein-dye binding. *Anal Biochem*. **72(7)**:248-254.

Brini, M., Pinton, P., King, M.P., Davidson, M., Schon, E.A., Rizzuto, R. (1999) A calcium signaling defect in the pathogenesis of a mitochondrial DNA inherited oxidative phosphorylation deficiency. Nature Med. **5:** 951–954.

Brown, M.D. and Wallace, D.C. (1994) Molecular basis of mitochondrial DNA disease. *J. Bioenerg. Biomembr.* **26(3):** 273-89.

Burk, A., Douzery, E.J.P., Springer, M.S. (2002) The secondary structure of mammalian mitochondrial 16S rRNA molecules: refinements based on a comparative phylogenetic approach. *J. Mammal. Evol*. **9(3)**: 225-252.

Campbell, N.A. and Reece, J.B. (2002) *Biology*. 6th ed. Benjamin Cummings. San Francisco.

Cao, W., Hashibe, M., Rao, J-Y., Morgenstern, H., Zhang, Z-F. (2003) Comparison of methods of DNA extraction from paraffin-embedded tissues and buccal cells. *Cancer Detect. Prev*. **27(5)**: 397-404.

Cavalli, L.R. and Liang, B.C. (1998) Mutagenesis, tumorigenicity, and apoptosis: are the mitochondria involved? *Mutat Res*. **398(1-2):**19-26.

Chance, B., Sies, H., Boveris, A. (1979) Hydroperoxide metabolism in mammalian organs. *Physiol. Rev*. **59(3):** 527-605.

Chinnery, P.F., Howell, N., Lightowlers, R.N., Turnbull, D.M. (1997) Molecular pathology of MELAS and MERRF. The relationship between mutation load and clinical phenotypes. *Brain.* **120 (Pt 10):** 1713-1721.

Chinnery, P.F., Johnson, M.A., Wardell, T.M., Singh-Kler, R., Hayes, C., Brown, D.T., Taylor, R.W., Bindoff, L.A., Turnbull, D.M. (2000a) The epidemiology of pathogenic mitochondrial DNA mutations. *Ann. Neurol.* **48(2):** 188-193.

Chinnery, P.F. and Schon, E.A. (2003) Mitochondria. *J. Neurol. Neurosurg. Psychiatry.* **74:** 1188-1199.

Chomczynski, P. and Sacchi, N. (1987) Single step method of RNA isolation by acid guanidinium thiocyanate-phenol-chloroform extraction. *Anal. Biochem*. **162**: 156-159.

Coutinho-Silva, R., Stahl L., Cheung, K.K., de Campos, N.E., de Oliveira Souza, C., Ojcius, D.M., Burnstock, G. (2005) P2X and P2Y purinergic receptors on human intestinal epithelial carcinoma cells: effects of extracellular nucleotides on apoptosis and cell proliferation. *Am. J. Physiol. Gastrointest. Liver Physiol.* **288(5):** G1024-G1035.

Cusack, N. J. (1993) P2 receptor: subclassification and structure-activity relationships. *Drug Dev. Res.* **28:** 244-252.

DiDonato, S., Zeviani, M., Giovannini, P., Savarese, N., Rimoldi, M., Mariotti, C., Girotti, F., Caraceni, T. (1993) Respiratory chain and mitochondrial DNA in muscle and brain in Parkinson's disease patients. *Neurology.* **43(11):** 2262-2268.

Díez-Sánchez, C., Ruiz-Pesini, E., Lapeña, A.C., Montoya, J., Pérez-Martos, A., Enríquez, J.A., López-Pérez, M.J. (2003) Mitochondrial DNA content of human spermatozoa. *Biol. Reprod*. **68(1):** 180-185.

DiMauro, S. and Schon, E.A. (2001) Mitochondrial DNA mutations in human disease. *Am. J. Med. Genet.* **106(1):** 18-26.

Dixon, C.J., Bowler, W.B., Fleetwood, P., Ginty, A.F., Gallagher, J.A., Carron, J.A. (1997) Extracellular nucleotides stimulate proliferation in MCF-7 breast cancer cells via P2-purinoceptors. *Br. J. Cancer.* **75(1):** 34-39.

Doublie, S., Tabor, S., Long, A.M., Richardson, C.C., Ellenberger, T. (1998) Crystal structure of a bacteriophage T7 DNA replication complex at 2.2 A resolution. *Nature.* **391(6664):** 251-258.

Falzoni, S., Munerati, M., Ferrari, D., Spisani, S., Moretti, S., Di Virgilio, F. (1995) The purinergic P2Z receptor of human macrophage cells. *J. Clin. Invest*. **95:** 1207–1216.

Fersht, A. (1985) *Enzyme structure and mechanism.* 2nd Edition, W.H. Freeman and Company, New York.

Finnegan, M., Goepel, J., Hancock, B. and Goyns, M. (1993) Investigation of the Expression of Housekeeping Genes in Non-Hodgkin's Lymphoma. *Leuk. Lymphoma* **10**: 387-393.

Floyd, R.A. and Carney, J.M. (1992) Free radical damage to protein and DNA: Mechanisms involved and relevant observations on brain undergoing oxidative stress. *Ann. Neurol.* **32(S1):** S22-S27.

Floyd, R.A. (1999) Antioxidants, oxidative stress, and degenerative neurological disorders. *Proc. Soc. Exp. Biol. Med.* **222:** 236 –245.

Foresta, C., Rossato, M., Di Virgilio, F. (1992) Extracellular ATP is a trigger for the acrosome reaction in human spermatozoa. *J. Biol. Chem.* **267(27):** 19443-19447.

Foresta, C., Rossato, M., Chiozzi, P., Di Virgilio, F. (1996c) Mechanism of human sperm activation by extracellular ATP. *Am. J. Physiol*. **270(6):** C1709-C1714.

Frank, S.A. and Hurst, L.D. (1996) Mitochondria and male disease. *Nature*. **383(6597)**: 224.

Freshney, R.I. (2000) *Culture of animal cells: A manual of basic technique*. 4th ed. Wiley-Liss Inc. New York.

Friedrich, T., Strohdeicher, M., Hofhaus, G., Preis, D., Sahm, H., Weiss, H. (1990) The same domain motif for ubiquinone reduction in mitochondrial or chloroplast NADH dehydrogenase and bacterial glucose dehydrogenase. *FEBS Lett.* **265(1-2):** 37-40.

Garrett, R.H. and Grisham, C.M. (2005) *Biochemistry*. 3rd ed. Thomson Brooks/Cole. California.

Gordon, J.L. (1986) Extracellular ATP: effects, sources and fate. *Biochem J*. **233(2)**: 309-319.

Grantham, R. (1974) Amino acid difference formula to help explain protein evolution. S*cience*. **185(4154)**: 862-864.

Gray, M.W., Burger, G., Lang, B.F. (1999) Mitochondrial evolution. *Science.* **283(5407):** 1476-1481.

Hanna, M.G. and Nelson, I.P. (1999) Genetics and molecular pathogenesis of mitochondrial respiratory chain diseases. *Cell. Mol. Life Sci*. **55:** 691-706.

Harris, T.P., Gomas, K.P., Weir, F., Holyoake, A.J., McHugh, P., Wu, M., Sin, Y., Sin, I.L., Sin, F.Y. (2006) Molecular analysis of polymerase gamma gene and mitochondrial polymorphism in fertile and subfertile men. *Int J Androl.* 29(3): 421-433.

Haltia, T., Saraste, M., Wikstrom, M. (1991) Subunit III of cytochrome c oxidase is not involved in proton translocation: a site-directed mutagenesis study. *EMBO J*. **10(8):** 2015-2021.

Hatefi, Y. (1978) Preparation and properties of dihydroubiquinone: Cytochrome c oxidoreductase (Complex III). *Methods Enzymol*. **53**: 35-40.

Hatefi, Y. (1985) The mitochondrial electron transport and oxidative phosphorylation system. *Annu. Rev. Biochem.* **54:** 1015–1069.

Heddi, A., Stepien, G., Benke, P.J., Wallace, D.C. (1999) Coordinate induction of energy gene expression in tissues of mitochondrial disease patients. *J. Biol. Chem*. **274(33):** 22968-22976.

Hindley, S., Herman, M.A., Rathbone, M.P. (1994) Stimulation of reactive astrogliosis in vivo by extracellular adenosine diphosphate or an adenosine A2 receptor agonist. *J. Neurosci. Res*. **38(4):** 399-406.

Hofacker, I.L. (2003) Vienna RNA secondary structure server. *Nucl. Acids Res*. **31**: 3429-3431.

Holyoake, A.J., Sin, I.L., Benny, P.S., Sin, F.Y.T. (1999) Association of a novel human mtDNA ATPase6 mutation with immature sperm cells. *Androl*. **31**: 339-345.

Holyoake, A.J., McHugh, P., Wu, M., O'Carroll, S., Benny, P., Sin, I.L., Sin, F.Y.T. (2001) High incidence of single nucleotide substitutions in the mitochondrial genome is associated with semen parameters in men. *Int. J. Androl*. **24**: 175-182.

Hsieh, R-H., Li, J-Y., Pang, C-Y., Wei, Y-H. (2001) A novel mutation in the mitochondrial 16S rRNA gene in a patient with MELAS syndrome, diabetes mellitus, hyperthyroidism and cardiomyopathy. *J. Biomed. Sci*. **8**: 328-335.

Huang, N.N, Wang, D.J., Heppel, L.A. (1989) Extracellular ATP is a mitogen for 3T3, 3T6, and A431 cells and acts synergistically with other growth factors. *Proc. Natl. Acad. Sci. USA*. **86(20):** 7904-7908.

Humphreys, B.D., Rice, J., Kertesy, S.B., Dubyak, G.R. (2000) Stress-activated protein kinase/JNK activation and apoptotic induction by the macrophage P2X7 nucleotide receptor. *J. Biol. Chem*. **275(35):** 26792-26798.

Huwiler, A. and Pfeilschifter, J. (1994) Stimulation by extracellular ATP and UTP of the mitogen-activated protein kinase cascade and proliferation of rat renal mesangial cells. *Br. J. Pharmacol*. **113**: 1455–1463.

James, A.M., Wei, Y.H., Pang, C.Y., Murphy, M.P. (1996) Altered mitochondrial function in fibroblasts containing MELAS and MERRF mitochondrial DNA mutations. *Biochem. J*. **318:** 401–407.

James, A.M., Sheard, P.W., Wei, Y.H., Murphy, M.P. (1999) Decreased ATP synthesis is phenotypically expressed during increased energy demand in fibroblasts containing mitochondrial tRNA mutations. *Eur. J. Biochem*. **259:** 462–469.

James, A.M. and Murphy, M.P. (2002) How mitochondrial damage affects cell function. *J. Biomed. Sci.* **9:** 475-487.

Kalendar, R. (2004) FastPCR, PCR primer design, DNA and protein tools, repeats and own database searches program. (http://www.biocenter.helsinki.fi/bi/bare-1_html/fastpcr.htm).

Kao, S.H., Chao, H.T., Wei, Y.H. (1995) Mitochondrial deoxyribonucleic acid 4977-bp deletion is associated with diminished fertility and motility of human sperm. *Biol. Reprod*. **52**: 729-736.

Kao, S.H., Chao, H.T., Wei, Y.H. (1998) Multiple deletions of mitochondrial DNA are associated with the decline of motility and fertility of human spermatozoa. *Mol. Hum. Reprod.* **4(7)**: 657-666.

Katzur, A.C., Koshimizu, T., Tomic, M., Schultze-Mosgau, A., Ortmann, O., Stojilkovic, S.S. (1999) Expression and responsiveness of P2Y2 receptors in human endometrial cancer cell lines. *J. Clin. Endocrinol. Metab*. **84(11):** 4085-4091.

Kiefer, J.R., Mao, C., Braman, J.C., Beese, L.S. (1998) Visualizing DNA replication in a catalytically active Bacillus DNA polymerase crystal. *Nature*. **391(6664):** 304-307.

Klug, W.S. and Cummings, M.R. (2000) *Concepts of genetics*. 6th ed. Prentice Hall. New Jersey.

Kyte, J. and Doolittle, R. (1982) A Simple Method for Displaying the Hydropathic Character of a Protein, *J. Mol Biol*. **157**: 105-132.

Longley, M.J., Nguyen, D., Kunkel, T.A., Copeland, W.C. (2001) The fidelity of human DNA polymerase gamma with and without exonucleolytic proofreading and the p55 accessory subunit. *J. Biol. Chem.* **276(42)**: 38555-38562.

Luo, X., Pitkänen, S., Kassovska-Bratinova, S., Robinson, B.H., Lehotay, D.C. (1997) Excessive formation of hydroxyl radicals and aldehydic lipid peroxidation products in cultured skin fibroblasts from patients with complex I deficiency. *J. Clin. Invest*. **99:** 2877–2888.

Madsen, K., Ertbjerg, P., Pedersen, P.K. (1996) Calcium content and respiratory control index of isolated skeletal muscle mitochondria: Effects of different isolation media. *Anal. Biochem*. **237**: 37-41.

Mandel, L.J., Takano, T., Soltoff, S.P., Murdaugh, S. (1988) Mechanisms whereby exogenous adenine nucleotides improve rabbit renal proximal function during and after anoxia. *J. Clin. Invest.* **81(4):** 1255-64.

Mecocci, P., MacGarvey, U., Kaufman, A.E., Koontz, D., Shoffner, J.M., Wallace, D.C., Beal, M.F. (1993) Oxidative damage to mitochondrial DNA shows marked age-dependent increases in human brain. *Ann. Neurol*. **34**: 609-616.

Noller, H.F. (1991) Ribosomal RNA and translation. *Annu. Rev. Biochem.* **60:** 191-227.

Ojala, D., Montoya, J., Attardi, G. (1981) tRNA punctuation model of RNA processing in human mitochondria. *Nature.* **290(5806):** 470-474.

Paller, M.S., Schnaith, E.J., Rosenberg, M.E. (1998) Purinergic receptors mediate cell proliferation and enhanced recovery from renal ischemia by adenosine triphosphate. *J. Lab. Clin. Med.* **131(2):** 174-183.

Penta, J.S., Johnson, F.M., Wachsman, J.T., Copeland, W.C. (2001) Mitochondrial DNA in human malignancy. *Mutat. Res.* **488:** 119-133.

Pizzo, P., Murgia, M., Zambon, A., Zanovello, P., Bronte, V., Pietrobon, D. and Di Virgilio, F. (1993) Role of P2z purinergic receptors in ATP-mediated killing of tumor necrosis factor (TNF)-sensitive and TNF-resistant L929 fibroblasts. *J. Immun.* **109:** 3372-3378.

Popper, L.D. and Batra, S.C. (1993) Release of intracellular calcium by prenylamine in human ovarian tumour cells. *Cancer Lett.* **71(1-3):**5-10.

Poulsen, H.E., Prieme, H., Loft, S. (1998) Role of oxidative DNA damage in cancer initiation and promotion. *Eur. J. Cancer Prev.* 7: 9–16.

Praticò, D., Uryu, K., Leight, S., Trojanoswki, J.Q., Lee V.M.Y. (2001) Increased lipid peroxidation precedes amyloid plaque formation in an animal model of Alzheimer amyloidosis. *J. Neurosci*. **21:** 4183-4187.

Pulkes, T., Hanna, M.G. (2001) Human mitochondrial DNA diseases. *Adv. Drug Deliv. Rev*. **49(1-2)**: 27-43

Pullman, M.E., Penefsky, H.S., Datta, A., Racker, E. (1960) Partial resolution of the enzymes catalyzing oxidative phosphorylation. I. Purification and properties of soluble dinitrophenol-stimulated adenosine triphosphatase. *J Biol Chem*. **235**: 3322-3329.

Purves, W.K., Orians, G.H., Heller, H.C. (1994) *Life: The Science of Biology*. 4th ed. Sinauer Associates. Massachusetts.

Rapaport, E. (1983) Treatment of human tumor cells with ADP or ATP yields arrest of growth in the S phase of the cell cycle. *J. Cell. Physio*. **114:** 279-283.

Rathbone, M.P., Deforge, S., Deluca, B., Gabel, B., Laurenssen, C., Middlemiss, P., Parkinson S. (1992) Purinergic stimulation of cell division and differentiation: mechanisms and pharmacological implications. *Med. Hypotheses*. **37(4):** 213-219.

Resnicoff, M., Medrano, E.E., Podhajcer, O.L., Bravo, A.I., Bover, L., Mordoh, J. (1987) Subpopulations of MCF7 cells separated by Percoll gradient centrifugation: a model to analyze the heterogeneity of human breast cancer. *Proc. Natl. Acad. Sci. USA*. **84:** 7295-7299.

Riordan-Eva, P. and Harding, A.E. (1995) Leber's hereditary optic neuropathy: the clinical relevance of different mitochondrial DNA mutations. *J. Med. Genet*. **32(2):** 81-87.

Ropp, P.A. and Copeland, W.C. (1996) Cloning and characterization of the human mitochondrial DNA polymerase, DNA polymerase gamma. *Genomics*. **36(3)**: 449-458.

Rossato, M., La Sala, G.B., Balasini, M., Taricco, F., Galeazzi, C., Ferlin, A., Foresta, C. (1999) Sperm treatment with extracellular ATP increases fertilisation rates in in-vitro fertilisation for male factor infertility. *Hum. Reprod.* **14(3):** 694-697.

Rossignol, R., Faustin, B., Rocher, C., Malgat, M., Mazat, J.P., Letellier, T. (2003) Mitochondrial threshold effects. *Biochem. J*. **370(Pt 3):** 751-762.

Ruiz-Pesini E., Díez-Sánchez C., Lapeña A.C., Pérez-Martos A., Montoya J., Alvarez E., Arenas J., López-Pérez M.J. (1998) Correlation of sperm motility with mitochondrial enzymatic activities. *Clin. Chem*. **44(8)**: 1616–1620.

Ruiz-Pesini E., Lapeña A-C., Díez-Sánchez C., Pérez-Martos A., Montoya J., Alvarez E., Díaz M., Urriés A., Montoro L., López-Pérez M.J., Enríquez J.A. (2000) Human mtDNA haplogroups associated with high or reduced spermatozoa motility. *Am. J. Hum. Genet*. **67**: 682-696.

Sambrook, J., Fritsh, E.F. and Maniatis, T. (1989) *Molecular Cloning: A Laboratory Manual*, 2nd ed, **Vol.1**, Cold Spring Harbor Laboratory Press, Cold Spring Harbor.

Sanchez-Cespedes, M., Parrella, P., Nomoto, S., Cohen, D., Xiao, Y., Esteller, M., Jeronimo, C, Jordan, R.C.K., Nicol, T., Koch, W.M., Schoenberg, M., Mazzarelli, P., Fazio, V.M., Sidransky, D. (2001) Identification of a Mononucleotide Repeat as a Major Target for Mitochondrial DNA Alterations in Human Tumors. *Cancer Res*. **61:** 7015-7019.

Saribas, A.S., Lustig, K.D., Zhang, X., Weisman, G.A. (1993) Extracellular ATP reversibly increases the plasma membrane permeability of transformed mouse fibroblasts to large macromolecules. *Anal. Biochem*. **209(1):** 45-52.

Sawyer, D.E. and Van Houten, B. (1999) Repair of DNA damage in mitochondria. *Mutat. Res.* **434:** 161-176.

Schon, E.A., Bonilla, E., DiMauro, S. (1997) Mitochondrial DNA mutations and pathogenesis. *J. Bioenerg. Biomembr*. **29**: 131-149.
Schon, E.A. (2000) Mitochondrial genetics and disease. *Trends Biochem. Sci.* **25(Nov)**: 555-560.

Schulze-Lohoff, E., Zanner, S., Ogilvie, A., Sterzel, R.B. (1992) Extracellular ATP stimulates proliferation of cultured mesangial cells via P2-purinergic receptors. *Am. J. Physiol.* **263(3 Pt 2**): F374-F383.

Schulze-Lohoff, E., Schagerl, S., Ogilvie, A., Sterzel, R.B. (1995) Extracellular ATP augments mesangial cell growth induced by multiple growth factors. *Nephrol. Dial. Transplant.* **10(11):** 2027-2034.

Schulze-Lohoff, E., Ogilvie, A., Sterzel, R.B. (1996) Extracellular nucleotides as signalling molecules for renal mesangial cells. *J. Auton. Pharmacol.* **16(6):** 381-384.

Schulze-Lohoff, E., Hugo, C., Rost, S., Arnold, S., Gruber, A., Brune, B., Sterzel, R.B. (1998) Extracellular ATP causes apoptosis and necrosis of cultured mesangial cells via P2Z/P2X7 receptors. *Am. J. Physiol*. **275(6 Pt 2)**: F962-F971.

Schultze-Mosgau, A., Katzur, A.C., Arora, K.K., Stojilkovic, S.S., Diedrich, K., Ortmann, O. (2000) Characterization of calcium-mobilizing, purinergic P2Y(2) receptors in human ovarian cancer cells. *Mol. Hum. Reprod*. **6(5):** 435-442.

Shuster, R.C., Rubenstein, A.J., Wallace, D.C. (1988) Mitochondrial DNA in anucleate human blood cells. *Biochem. Biophys. Res. Commun.* **155(3):** 1360-1365.

Selak, M.A., Armour, S.M., MacKenzie, E.D., Boulahbel, H., Watson, D.G., Mansfield, K.D., Pan, Y., Simon, C., Thompson, C.B., Gottlieb, E. (2005) Succinate links TCA cycle dysfunction to oncogenesis by inhibiting HIF-α prolyl hydroxylase. *Cancer Cell.* **7(1):** 77–85.

Shay, J.W. and Werbin, H. (1987) Are mitochondrial DNA mutations involved in the carcinogenic process? *Mutat. Res.* **186:** 149-160.

Shepherd, J.A. and Garland, P.B. *Citrate synthase from rat liver*, in Methods in Enzymology. New York: Academic Press. Vol. XIII (Lowenstein J.M., ed), 1969: 11-19.

Smeitink, J.A., van den Heuvel, L., DiMauro, S. (2001) The genetics and pathology of oxidative phosphorylation. *Nat. Rev. Genet*. **2:** 342-352.

Smeitink, J.A., Zeviani, M., Turnbull, D.M., Jacobs, H.T. (2006) Mitochondrial medicine: A metabolic perspective on the pathology of oxidative phosphorylation disorders. *Cell Metab*. **3:** 9-13.

Snustad, D.P. and Simmons, M.J. (2003) *Principles of genetics*. 3rd ed. John Wiley & Sons. New York.

Soltoff, S.P., Avraham, H., Avraham, S., Cantley, L.C. (1998) Activation of P2Y2 receptors by UTP and ATP stimulates mitogen-activated kinase activity through a pathway that involves related adhesion focal tyrosine kinase and protein kinase C. *J. Biol. Chem*. **273(5):** 2653-2660.

Soule, H.D., Vazguez, J., Long, A., Albert, S., Brennan, M. (1973) A human cell line from a pleural effusion derived from a breast carcinoma. *J. Natl. Cancer Inst.* **51(5):** 1409-1416.

St John, J.C., Sakkas, D., Barratt, C.L.R. (2000) A role for mitochondrial DNA and sperm survival. J. *Androl*. **21(2)**: 189-199.

Sulijoadikusumo, I., Horikoshi, N., Usheva, A. (2001) Another function for the mitochondrial ribosomal RNA: protein folding. *Biochem*. **40**: 11559-11564.

Taira, T., Saito, Y., Niki, T., Iguchi-Ariga, S.M.M., Takahashi, K., Ariga, H. (2004) DJ-1 has a role in antioxidative stress to prevent cell death. *EMBO Rep.* **5(2):** 213–218.

Tan, D-J., Bai, R-K., Wong, L-J.C. (2002) Comprehensive scanning of somatic mitochondrial DNA mutations in breast cancer. *Cancer Res*. **62**: 972-976.

Taylor, R.W. and Turnbull, D.M. (2005) Mitochondrial DNA mutations in human disease. *Nat. Rev. Genet.* **6:** 389-402.

Wagstaff, S.C., Bowler, W.B., Gallagher, J.A., Hipskind, R.A. (2000) Extracellular ATP activates multiple signalling pathways and potentiates growth factor-induced c-fos gene expression in MCF-7 breast cancer cells. *Carcinogenesis.* **21(12):** 2175-2181.

Wallace, D.C. (1999) Mitochondrial diseases in man and mouse. *Science.* **283:** 1482-1487.

Wallace, D.C. (2000) Mitochondrial defects in cardiomyopathy and neuromuscular disease. *Am. Heart J.* **139(2):** S70-S85.

Wang, D.J., Huang, N.N., Heppel, L.A. (1992) Extracellular ATP and ADP stimulate proliferation of porcine aortic smooth muscle cells. *J. Cell Physiol.* **153(2):** 221-233.

White, N., Ryten, M., Clayton, E., Butler, P., Burnstock, G. (2005) P2Y purinergic receptors regulate the growth of human melanomas. *Cancer Lett.* **224(1):** 81-91.

White, N. and Burnstock, G. (2006) P2 receptors and cancer. *Trends Pharmacol. Sci*. **27(4):** 211-217.

Wilfinger, W.W., Mackey, K., and Chomczynski, P. (1997) Effect of pH and ionic strength on the spectrophotometric assessment of nucleic acid purity. *Biotechniques*. **22(3)**: 474-6, 478-81.

Wong, L-J.C, Lueth, M., Li, X-N., Lau, C.C., Vogel, H. (2003) Detection of Mitochondrial DNA Mutations in the Tumor and Cerebrospinal Fluid of Medulloblastoma Patients. *Cancer Res*. **63:** 3866-3871.

Yamada, H., Chen, D., Monstein, H. and Hakanson, R. (1997) Effects of Fasting on the Expression of Gatrin, Cholecystokinin, and Somatostatin Genes and Various Housekeeping Genes in the Pancreas and Upper Digestive Tract of Rats. *Biochem. Biophys. Res. Commun.* **231**: 835-838.

Zeviani, M. and Di Donato, S. (2004) Mitochondrial disorders. *Brain*. **127:** 2153-2172.

Zhu, W., Qin, W., Bradley, P., Wessel, A., Puckett, C.L., Sauter, E.R. (2005) Mitochondrial DNA mutations in breast cancer tissue and in matched nipple aspirate fluid. *Carcinogenesis.* **26(1):** 145-152.

Zienolddiny, S., Ryberg, D., Haugen, A. (2000) Induction of microsatellite mutations by oxidative agents in human lung cancer cell lines. *Carcinogenesis.* **21(8):** 1521-1526

Appendix 1: Abbreviations

A	adenine or adenosine; one letter code for alanine
A_{260}	absorbance at wavelength of 260 nm
A_{280}	absorbance at wavelength of 280 nm
bp	base pair
C	cytosine or cytidine; one letter code for cysteine
kDa	kilo Dalton
DNA	deoxyribonucleic acid
G	guanine or guanosine; one letter code for glycine
g	gravity
h	hours
M	molar
min	minutes
nt	nucleotide
RNA	ribonucleic acid
rpm	revolutions per minute
s	seconds
T	thymine or thymidine; one letter code for threonine
U	unit
UV	ultraviolet
V	volts
v/v %	volume per volume percent
w/v %	weight per volume percent

Units

g	grams	l	litres
m	metres		

Prefixes

m	milli (1 x 10^{-3})	n	nano (1 x 10^{-9})
µ	micro (1 x 10^{-6})	p	pico (1 x 10^{-12})

Appendix 2: Recipes

1x PBS

NaCl	7.6 g
Na_2HPO_4	3.8 g
NaH_2PO_4	0.42 g
ddH_2O to 1 l	

Sterilise by autoclave (wet run at 121°C, at 100 kPa pressure).

10x TBE electrophoresis buffer

Tris base	218 g
Boric acid	110 g
EDTA	9.3 g
ddH_2O to 2 l	

Adjust pH to ≈ 8 using NaOH. Autoclave (wet run at 121°C, at 100 kPa pressure).

λHE marker

Eco RI buffer	10 µl
λDNA	22.42 µl
Hind III	0.67 µl
Eco RI	0.83 µl
ddH_2O	66.08 µl

Incubate overnight at 37^{o}C. Store in fridge at 4^{o}C.

1% Agarose gel

Agarose	0.35 g
1x TBE	35 ml

Dissolve in microwave until clear solution. Swirl gently.

Allow the gel to set ≥ 30 min at room temperature.

TE 8 buffer

Tris-HCl	1.211 g
EDTA	0.372 g
ddH_2O to 1 l.	

Adjust pH to ≈ 8 using NaOH. Autoclave (wet run at 121°C, at 100 kPa pressure).

SHE buffer

Sucrose	8.558 g
Hepes	2.383 g
EGTA	0.094 g
ddH_2O to 100 ml.	

Adjust pH to ≈ 7.2 using NaOH. Store at 4°C.

0.1% DEPC-treated water

1. Add 1 ml of DEPC to 1000 ml ddH_2O.
2. Mix well and incubate overnight at room temperature.
3. Autoclave (wet run at 121°C, at 100 kPa pressure) to inactivate the remaining DEPC.
4. Store at room temperature.

5x MOPS running buffer

MOPS	20.39 g
Sodium acetate	3.281 g
EDTA	1.861 g
0.1% DEPC-treated water to 1 l.	

Adjust pH to ≈ 7 using NaOH.

Sterilise the solution by filtration through a 0.2 micron Millipore filter.

Store in the dark and discard if it turns yellow.

Do not autoclave.

RNA sample buffer

Deionised Formamide	10 ml
37% Formaldehyde	3.5 ml
5x MOPS	2 ml

Divide into 500 µl aliquots and store at -20°C.

Use 2 parts sample buffer for each part of RNA.

Denatured 1% agarose-formaldehyde gel

Agarose	0.35 g

0.1% DEPC-treated water	:	5x MOPS	:	37% Formaldehyde
Ratio	3.5	:	1.1	: 1

Cast the gel in the fumehood. Allow the gel to set at room temperature.

Appendix 3: Raw data of results

Cell count of six clones

B5-P4

Time (h)				Mean	SD
0	10000	10000	10000	10000	0
24	10000	10000	10000	10000	0
48	22000	44000	66000	44000	22000
72	88000	77000	99000	88000	11000
96	110000	110000	121000	113667	6350.853
120	132000	132000	132000	132000	0
144	143000	132000	154000	143000	11000
168	165000	264000	66000	165000	99000
192	187000	176000	176000	179667	6350.853
216	220000	209000	220000	216333	6350.853
240	198000	209000	209000	205333	6350.853

B12-P4

Time (h)				Mean	SD
0	10000	10000	10000	10000	0
24	10000	22000	22000	18000	6928.203
48	22000	22000	33000	25666.67	6350.853
72	44000	33000	22000	33000	11000
96	55000	66000	44000	55000	11000
120	66000	66000	55000	62333.33	6350.853
144	88000	66000	77000	77000	11000
168	99000	121000	55000	91666.67	33605.56
192	121000	99000	110000	110000	11000
216	110000	132000	132000	124666.7	12701.71
240	132000	110000	121000	121000	11000

D4-P4

Time (h)				Mean	SD
0	10000	10000	10000	10000	0
24	22000	11000	22000	18333	6350.853
48	55000	44000	66000	55000	11000
72	66000	77000	55000	66000	11000
96	88000	99000	77000	88000	11000
120	99000	110000	110000	106333	6350.853
144	110000	110000	121000	113667	6350.853
168	121000	143000	110000	124667	16802.78
192	121000	99000	154000	124667	27682.73
216	132000	121000	132000	128333	6350.853
240	121000	110000	143000	124667	16802.78

D9-P4

Time (h)				Mean	SD
0	10000	10000	10000	10000	0
24	10000	10000	10000	10000	0
48	22000	11000	22000	18333	6350.853
72	22000	11000	33000	22000	11000
96	55000	55000	44000	51333.33	6350.853
120	66000	77000	99000	80666.67	16802.78
144	88000	44000	110000	80666.67	33605.56
168	110000	143000	121000	124666.7	16802.78
192	165000	154000	165000	161333.3	6350.853
216	242000	187000	286000	238333.3	49601.75
240	242000	220000	253000	238333.3	16802.78

E1-P4

Time (h)				Mean	SD
0	10000	10000	10000	10000	0
24	11000	11000	11000	11000	0
48	33000	44000	55000	44000	11000
72	110000	66000	77000	84333	22898.33
96	88000	99000	99000	95333	6350.853
120	110000	143000	121000	124667	16802.78
144	154000	143000	154000	150333	14620.76
168	176000	176000	176000	176000	0
192	242000	253000	231000	242000	11000
216	253000	264000	242000	253000	11000
240	253000	253000	242000	249333	6350.853

E8-P4

Time (h)				Mean	SD
0	10000	10000	10000	10000	0
24	10000	11000	10000	10333	577.3503
48	11000	22000	11000	14667	6350.853
72	22000	33000	22000	25667	6350.853
96	33000	22000	33000	29333	6350.853
120	44000	33000	55000	44000	11000
144	66000	88000	55000	69667	16802.78
168	77000	88000	66000	77000	11000
192	88000	99000	77000	88000	11000
216	88000	110000	99000	99000	11000
240	88000	110000	88000	95333	12701.71

Statistical analysis: Doubling time of the six clones

	B5	B12	D4	D9	E1	E8
Number of values	3	3	3	3	3	3
Minimum	25.9	38.4	24	33.6	26.4	28.8
Median	26.4	43.2	25.4	33.6	26.9	28.8
Maximum	26.9	48	27.8	33.6	27.36	28.8
Mean	26.4	43.2	25.73	33.6	26.89	28.8
Std. Deviation	0.5	4.8	1.922	0	0.4801	0
Std. Error	0.2887	2.771	1.11	0	0.2772	0
Lower 95% CI	25.16	31.28	20.96	33.6	25.69	28.8
Upper 95% CI	27.64	55.12	30.51	33.6	28.08	28.8

One-way analysis of variance	**(ANOVA)**
P value	P<0.0001
Are means signif. different? (P < 0.05)	Yes
Number of groups	6
F	29.89
R squared	0.9257

ANOVA Table	**SS**	**df**	**MS**
Treatment (between columns)	677.8	5	135.6
Residual (within columns)	54.43	12	4.536
Total	732.2	17	

Tukey's Multiple Comparison Test	**Mean Diff.**	**q**	**P value**	**95% CI of diff**
B5 vs B12	-16.8	13.66	P < 0.001	-22.64 to -10.96
B5 vs D4	0.6667	0.5422	P > 0.05	-5.175 to 6.508
B5 vs D9	-7.2	5.856	P < 0.05	-13.04 to -1.358
B5 vs E1	-0.4867	0.3958	P > 0.05	-6.328 to 5.355
B5 vs E8	-2.4	1.952	P > 0.05	-8.242 to 3.442
B12 vs D4	17.47	14.21	P < 0.001	11.62 to 23.31
B12 vs D9	9.6	7.808	P < 0.01	3.758 to 15.44
B12 vs E1	16.31	13.27	P < 0.001	10.47 to 22.16
B12 vs E8	14.4	11.71	P < 0.001	8.558 to 20.24
D4 vs D9	-7.867	6.398	P < 0.01	-13.71 to -2.025
D4 vs E1	-1.153	0.938	P > 0.05	-6.995 to 4.688
D4 vs E8	-3.067	2.494	P > 0.05	-8.908 to 2.775
D9 vs E1	6.713	5.46	P < 0.05	0.8716 to 12.56
D9 vs E8	4.8	3.904	P > 0.05	-1.042 to 10.64
E1 vs E8	-1.913	1.556	P > 0.05	-7.755 to 3.928

Mean grouping test

Clone	Mean	Tukey grouping
D4	25.40	A
B5	26.40	A
E1	26.89	A
E8	28.80	AB
D9	33.60	B
B12	43.30	C

Note:

A ranked list of means (ascending order) and letter codes were used to illustrate groupings of the variation in Tukey's test. Means with the same single letter code are not significantly different. Where two letter codes overlap, the means are not significantly different. In this case, B12 clone can be distinguished as significantly different from other clones.

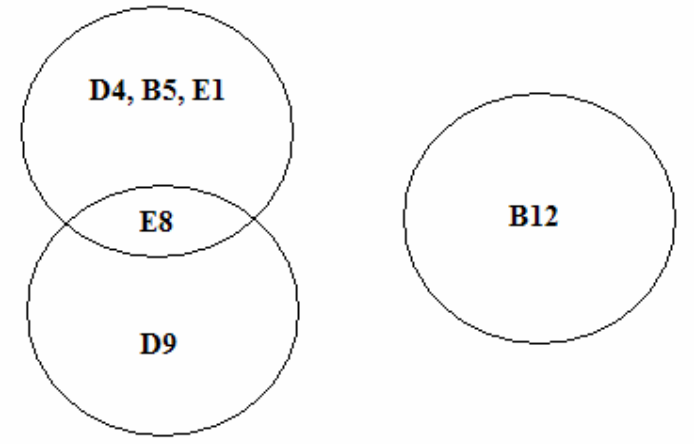

Cell count of clones treated with or without extracellular ATP

B12 control (no ATP)

Time (h)				Mean	SD
0	10000	10000	10000	10000	0
12	10000	10000	10000	10000	0
24	10000	10000	10000	10000	0
36	11000	10000	11000	10666.67	577.3503
48	22000	11000	11000	14666.67	6350.853
60	33000	22000	33000	29333.33	6350.853
72	55000	55000	22000	44000	19052.56
96	55000	44000	55000	51333.33	6350.853
120	66000	55000	44000	55000	11000
144	66000	77000	88000	77000	11000
168	88000	77000	77000	80666.67	6350.853
192	99000	88000	77000	88000	11000
216	88000	99000	88000	91666.67	6350.853
240	110000	99000	110000	106333.3	6350.853

B12 treated with 50 µM ATP

Time (h)				Mean	SD
0	10000	10000	10000	10000	0
12	10000	10000	10000	10000	0
24	10000	10000	11000	10333.33	577.3503
36	11000	11000	11000	11000	0
48	11000	22000	33000	22000	11000
60	33000	22000	33000	29333.33	6350.853
72	33000	66000	33000	44000	19052.56
96	66000	55000	44000	55000	11000
120	55000	88000	66000	69666.67	16802.78
144	99000	66000	33000	66000	33000
168	88000	99000	66000	84333.33	16802.78
192	99000	99000	99000	99000	0
216	110000	88000	132000	110000	22000
240	110000	99000	121000	110000	11000

B12 treated with 100 μM ATP

Time (h)				Mean	SD
0	10000	10000	10000	10000	0
12	11000	11000	10000	10666.67	577.3503
24	11000	22000	11000	14666.67	6350.853
36	44000	22000	44000	36666.67	12701.71
48	33000	11000	44000	29333.33	16802.78
60	55000	77000	88000	73333.33	16802.78
72	88000	88000	88000	88000	0
96	121000	99000	99000	106333.3	12701.71
120	121000	121000	110000	117333.3	6350.853
144	99000	132000	143000	124666.7	22898.33
168	110000	154000	88000	117333.3	33605.56
192	110000	165000	187000	154000	39661.06
216	121000	121000	132000	124666.7	6350.853
240	110000	99000	121000	110000	11000

B12 treated with 1 mM ATP

Time (h)				Mean	SD
0	10000	10000	10000	10000	0
12	11000	22000	11000	14666.67	6350.853
24	11000	55000	44000	36666.67	22898.33
36	44000	55000	55000	51333.33	6350.853
48	55000	77000	66000	66000	11000
60	110000	99000	99000	102666.7	6350.853
72	110000	132000	132000	124666.7	12701.71
96	121000	99000	121000	113666.7	12701.71
120	143000	132000	132000	135666.7	6350.853
144	154000	132000	110000	132000	22000
168	121000	132000	132000	128333.3	6350.853
192	110000	121000	143000	124666.7	16802.78
216	110000	110000	121000	113666.7	6350.853
240	143000	154000	110000	135666.7	22898.33

D4

Time (h)				Mean	SD
0	10000	10000	10000	10000	0
24	33000	22000	11000	22000	11000
48	33000	55000	66000	51333.33	16802.78
72	66000	55000	66000	62333.33	6350.853
96	77000	66000	99000	80666.67	16802.78
120	77000	99000	110000	95333.33	16802.78
144	88000	110000	121000	106333.3	16802.78
168	110000	132000	121000	121000	11000
192	121000	132000	99000	117333.3	16802.78
216	110000	143000	143000	132000	19052.56
240	132000	121000	143000	132000	11000

Statistical analysis: Doubling time of the clones

	B12 (no ATP)	B12 (50 µM ATP)	B12 (100 µM ATP)	B12 (1 mM ATP)	D4
Number of values	3	3	3	3	3
Minimum	38.4	33.6	19.2	14.4	21.6
Median	40.8	36	21.6	14.4	24
Maximum	43.2	38.4	24	16.8	24
Mean	40.8	36	21.6	15.2	23.2
Std. Deviation	2.4	2.4	2.4	1.386	1.386
Std. Error	1.386	1.386	1.386	0.8	0.8
Lower 95% CI	34.84	30.04	15.64	11.76	19.76
Upper 95% CI	46.76	41.96	27.56	18.64	26.64

One-way analysis of variance	**(ANOVA)**
P value	P<0.0001
Are means signif. different? (P < 0.05)	Yes
Number of groups	5
F	80.55
R squared	0.9699

ANOVA Table	**SS**	**df**	**MS**
Treatment (between columns)	1361	4	340.2
Residual (within columns)	42.24	10	4.224
Total	1403	14	

Tukey's Multiple Comparison Test	**Mean Diff.**	**q**	**P value**	**95% CI of diff**
B12 no ATP vs B12 - 50µM ATP	4.8	4.045	P > 0.05	-0.7224 to 10.32
B12 no ATP vs B12 - 100µM ATP	19.2	16.18	P < 0.001	13.68 to 24.72
B12 no ATP vs B12 - 1mM ATP	25.6	21.57	P < 0.001	20.08 to 31.12
B12 no ATP vs D4	17.6	14.83	P < 0.001	12.08 to 23.12
B12 - 50µM ATP vs B12 - 100µM ATP	14.4	12.14	P < 0.001	8.878 to 19.92
B12 - 50µM ATP vs B12 - 1mM ATP	20.8	17.53	P < 0.001	15.28 to 26.32
B12 - 50µM ATP vs D4	12.8	10.79	P < 0.001	7.278 to 18.32
B12 - 100µM ATP vs B12 - 1mM ATP	6.4	5.394	P < 0.05	0.8776 to 11.92
B12 - 100µM ATP vs D4	-1.6	1.348	P > 0.05	-7.122 to 3.922
B12 - 1mM ATP vs D4	-8	6.742	P < 0.01	-13.52 to -2.478

Mean grouping test

Clone	Mean	Tukey grouping
B12 with 1 mM ATP	15.20	A
B12 with 100 µM ATP	21.60	B
D4 (no ATP)	23.20	B
B12 with 50 µM ATP	36.00	C
B12 (no ATP)	40.80	C

Note:

A ranked list of means (ascending order) and letter codes were used to illustrate groupings of the variation in Tukey's test. Means with the same single letter code are not significantly different. Where two letter codes overlap, the means are not significantly different. In this case, B12 clone treated with 1 mM ATP can be distinguished as significantly different from other clones.

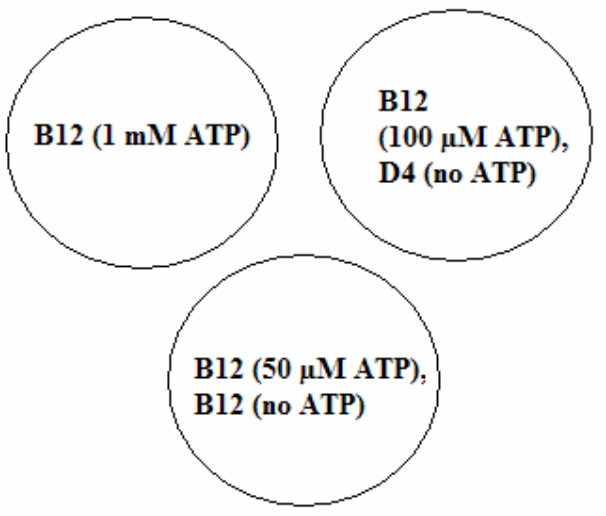

Quantitation of mitochondria

A standard curve of absorbance against BSA concentration was plotted using Microsoft® Windows® Excel 2003 software. A best-fit line in the form of the equation '$y = mx + b$' (where y = absorbance at 595 nm and x = protein concentration) was drawn. This equation was used to calculate the concentration of the protein sample based on the measured absorbance.